Title: mRNA therapy corrects defective glutathione metabolism and restores ureagenesis in argininosuccinic aciduria

Authors: Sonam Gurung[1*], Oskar V. Timmermand[2*], Dany Perocheau[1*], Ana Luisa Gil-Martinez[1], Magdalena Minnion[3,4], Loukia Touramanidou[1], Sherry Fang[5], Martina Messina[5], Youssef Khalil[1], Justyna Spiewak[1], Abigail R. Barber[2], Richard S. Edwards[2], Patricia Lipari Pinto[6], Patrick F. Finn[7], Alex Cavedon[7], Summar Siddiqui[7], Lisa Rice[7], Paolo G.V. Martini[7], Deborah Ridout[1], Wendy Heywood[1], Ian Hargreaves[8], Simon Heales[1,5], Philippa B. Mills[1], Simon N. Waddington[9,10], Paul Gissen[1,5 11], Simon Eaton[1], Mina Ryten[1], Martin Feelisch[3,4], Andrea Frassetto[7], Timothy H. Witney[2ǂ], Julien Baruteau[1,5,11ǂ]

Institutions: [1] Great Ormond Street Institute of Child Health, University College London, London, UK, [2] School of Biomedical Engineering and Imaging Sciences, King's College London, UK, [3] Clinical and Experimental Sciences, Faculty of Medicine, University of Southampton, UK, [4] Southampton NIHR Biomedical Research Centre, University Hospital Southampton NHS Foundation Trust, UK, [5] Great Ormond Street Hospital for Children NHS Foundation Trust, London, UK, [6] Santa Maria's Hospital, Lisbon North University Hospital Center, Lisbon, Portugal, [7] Moderna Inc., Cambridge, MA, USA, [8] Pharmacy and Biomolecular Sciences, Liverpool John Moore University, Liverpool, UK, [9] EGA Institute for Women's Health, University College London, London, UK, [10] Wits/SAMRC Antiviral Gene Therapy Research Unit, Faculty of Health Sciences, University of Witswatersrand, Johannesburg, South Africa, [11] National Institute of Health Research Great Ormond Street Biomedical Research Centre, London WC1N 1EH, UK,

Corresponding author: Dr Julien Baruteau

Genetics & Genomic Medicine Department

Great Ormond Street Institute of Child Health

University College London

30 Guildford Street

WC1N 1EH. London,

+44 (0) 20 7242 9789

j.baruteau@ucl.ac.uk

* Shared first authorship, ǂ Shared senior authorship

Abstract

The urea cycle enzyme argininosuccinate lyase (ASL) enables the clearance of neurotoxic ammonia and the biosynthesis of arginine. ASL-deficient patients present with argininosuccinic aciduria, an inherited metabolic disease with hyperammonaemia and a systemic phenotype coinciding with neurocognitive impairment and chronic liver disease. Here, we describe the dysregulation of glutathione biosynthesis and upstream cysteine utilization in ASL-deficient patients and mice using targeted metabolomics and *in vivo* positron emission tomography (PET) imaging using (*S*)-4-(3-^{18}F-fluoropropyl)-L-glutamate ([^{18}F]FSPG). Upregulation of cysteine metabolism contrasted with glutathione depletion and down-regulated antioxidant pathways. To assess hepatic glutathione dysregulation and liver disease, we present [^{18}F]FSPG PET as a non-invasive diagnostic tool, which monitors therapeutic response in argininosuccinic aciduria. *hASL* mRNA encapsulated in lipid nanoparticles improved glutathione metabolism and chronic liver disease, whilst correcting and rescuing the neonatal and adult Asl-deficient mouse phenotypes, respectively, enhancing ureagenesis. These findings provide new mechanistic insights in liver glutathione metabolism and support clinical translation of mRNA therapy for argininosuccinic aciduria.

One-sentence summary: Argininosuccinic aciduria causes defective glutathione metabolism, which can be monitored by positron emission tomography and corrected by liver targeting mRNA therapy.

Introduction

Urea cycle defects (UCDs) are inborn errors of metabolism causing dysfunction in ammonia detoxification and endogenous arginine synthesis. Argininosuccinic aciduria (ASA) (OMIM 207900) is the second most common UCD, occurring ~1 in every 100,000 live births (*1*). ASA is caused by deficiency in argininosuccinate lyase (ASL), a cytosolic urea cycle enzyme, which catalyses the conversion of argininosuccinate into arginine and fumarate, thereby enabling the removal of excess nitrogen (*2, 3*). ASL is also involved in the citrulline-nitric oxide (NO) cycle to produce NO through the channelling of extracellular L-arginine to nitric oxide synthase (NOS) (*4, 5*).

ASA patients display acute hyperammonaemia and/or chronic phenotype of neurocognitive impairment and liver disease (*3*). The aims of the current therapeutic guidelines for ASA are to normalise ammonia and arginine levels through a low protein diet, ammonia scavenging drugs, and arginine supplementation. Liver transplantation is used in cases of progressive liver disease or recurrent hyperammonaemic crises despite conventional treatment. The proposed experimental treatments include antioxidants, autophagy enhancers, creatinine supplementation, and gene therapies (*2, 6-12*).

Chronic liver dysfunction causes morbidity in all UCD subtypes (*13, 14*) but is reported with higher frequency and severity in ASA (*1, 11, 13, 15*). This liver disease commonly manifests with hepatomegaly and transaminitis, can progress to liver failure, and, eventually, hepatocellular carcinoma (*11, 14-19*). The liver pathology progresses despite appropriate ammonia control, suggesting hyperammonaemia is not the sole cause (*14*). Other suggested mechanisms include arginine deficiency, argininosuccinate toxicity, NO deficiency and oxidative stress (*15, 16, 20*). There are no reliable biomarkers that predict the degree of liver disease in ASA (*16*) and the underlying processes that trigger liver disease are unclear. More detailed mechanistic insight into liver pathophysiology will be crucial to identifying optimal diagnostic markers for better assessment of disease severity, prediction of disease progression and assessment of response to therapy.

The *Asl*$^{Neo/Neo}$ mouse model recapitulates much of human ASA, with reports of hepatomegaly, elevated transaminases, aberrant hepatic glycogen accumulation, and variable fibrosis (*2, 6, 9, 11, 12*). In this

study, we describe the dysregulation of liver glutathione metabolism as a newly-described feature of the chronic liver disease in both ASA patients and *Asl*$^{Neo/Neo}$ mice. We show that decreased liver glutathione in ASA is a consequence of downregulation of the rate-limiting biosynthetic enzyme, glutamate cysteine ligase (GCL), increased glutathione recycling by increased γ-glutamyltranspeptidase (GGT) activity and decreased glutathionuria. We also found hepatic upregulation of the antiporter system x_C^-, which promotes glutathione synthesis to counteract oxidative stress in health and disease (*21*). System x_C^- activity was traceable with the positron emission tomography (PET) radiotracer (*S*)-4-(3-^{18}F-fluoropropyl)-L-glutamate ([^{18}F]FSPG) where it was used both as a diagnostic and to assess the progression of liver disease in ASA. We show proof of concept that mRNA therapy can treat neonatal and rescue adult *Asl*$^{Neo/Neo}$ mice by correcting both glutathione metabolism and ureagenesis *in vivo*, thereby demonstrating this strategy as a promising therapy for ASA.

Results

ASL-deficient patients and *Asl*$^{Neo/Neo}$ mice show downregulation of glutathione biosynthesis despite limited evidence of oxidative stress.

Compared to other UCD, previous publications have highlighted the role of oxidative stress in the pathophysiology of ASL deficiency (*5, 9, 22*). To better understand the cellular response to this oxidative stress, we explored the role of glutathione, the body's primary antioxidant, and its regulation in ASA including its close interaction with the transsulfuration pathway (Figure 1A). We compared the plasma concentrations of total homocysteine, glycine, glutamate in patients from Great Ormond Street Hospital for Children, London, UK affected by one of the 3 main urea cycle defects: ornithine transcarbamylase deficiency (OTCD; n=10), argininosuccinate synthase deficiency (ASSD; n=10) and argininosuccinate lyase deficiency (ASLD; n=13). Two liver-transplanted OTCD patients were excluded due to normalised ureagenesis. Compared to OTCD and ASSD, patients with ASLD had significantly higher mean plasma levels of the three metabolites contributing to glutathione

104 biosynthesis: homocysteine (Figure 1B), glutamate (Supplementary Figure 1A), and glycine
105 (Supplementary Figure 1B) levels. Plasma total homocysteine did not differ between early- and late-
106 onset ASA patients (Supplementary Figure 1C). Since follow-up, total plasma homocysteine
107 (Supplementary Figure 1D), glycine (Supplementary Figure 1E) and glutamate (Supplementary Figure
108 1F) levels remained significantly elevated for all ASLD patients compared to OTCD and ASSD
109 patients.

110 Interestingly, no sex difference was observed for plasma homocysteine and glycine (Supplementary
111 Table 1). Glutamate levels, however, were significantly elevated in OTCD and ASLD females
112 compared to males (Supplementary Table 1). Glutamate and glycine plasma levels are easily influenced
113 by diet, medications, metabolic control and delayed analytical processing. Clinical information
114 regarding these OTCD, ASSD and ASLD patients are presented in Supplementary Table 2. Samples
115 collected during hyperammonemic episodes were excluded from data collection. Patients with average
116 total homocysteine above the normal upper range limit were not screened for methyltetrahydrofolate
117 (*MTHFR*) polymorphism, which may contribute to the differences observed here between patient types.
118 No vitamin B12 deficiency was observed in the patients (Supplementary Figure 1G).

119 We then measured the metabolites of the glutathione pathway in the hypomorphic $Asl^{Neo/Neo}$ mouse
120 model, which recapitulates much of the human phenotype of ASLD (*4*, *9*). As sulfur-containing amino
121 acids (and H_2S) exist in different forms (*23*), we measured both total and reduced free thiol form (R-
122 SH) to determine any compromise to the cellular antioxidant buffering capacity. Corroborating human
123 data, plasma total (Figure 1C) and free (Supplementary Figure 2A) homocysteine levels in 2-week old
124 $Asl^{Neo/Neo}$ mice were significantly elevated compared to WT littermates. Other plasma metabolites of the
125 glutathione biosynthesis pathway, total (Figure 1D) and free (Supplementary Figure 2B) cysteine, total
126 γ-glutamyl-cysteine (Figure 1E) were also significantly increased in $Asl^{Neo/Neo}$ mice compared to WT.
127 Free γ-glutamyl-cysteine showed no difference (Supplementary Figure 2C). In contrast, plasma total
128 glutathione was significantly decreased (Figure 1F). Most of the glutathione released in the
129 bloodstream is synthesised in the liver (*24*). Similar to plasma, liver concentrations of total (Figure 1G)
130 and free (Supplementary Figure 2D) homocysteine, total (Figure 1H) and free (Supplementary Figure

2E) cysteine, and total (Figure 1I) γ-glutamyl-cysteine showed a significant increase in *Asl*$^{Neo/Neo}$ mice compared to WT. Liver free γ-glutamyl-cysteine (Supplementary Figure 2F) showed no difference. As in the plasma, total glutathione levels in the liver were significantly decreased but to a far greater extent (Figure 1J).

Total glutathione is degraded by GGT at the external surface of epithelial cells (*25*). GGT activity and expression in liver showed a significant 5-fold increase in *Asl*$^{Neo/Neo}$ mice compared to WT (Figure 1K and Supplementary Figure 2G). Total (Supplementary Figure 2H) and free (Supplementary Figure 2I) cysteine-glycine synthesised from glutathione catabolism by GGT was also increased in liver. *Asl*$^{Neo/Neo}$ mice (*4*) and ASA patients (*26, 27*) may present chronic kidney disease and renal failure. Supporting this, urine glutathione levels were significantly increased in *Asl*$^{Neo/Neo}$ mice compared to WT, suggesting defective renal glutathione reabsorption (Supplementary Figure 2J). Urine cysteine and cysteine-glycine were also significantly increased in *Asl*$^{Neo/Neo}$ mice compared to WT (Supplementary Figure 2K and 2L), in line with an elevation of these metabolites in the plasma and livers, a consequence which is partially explained by increased GGT activity.

The increase of free thiols metabolites suggested that the persisting buffering capacity and protective role against oxidative stress of free thiols (*23, 28*) was maintained both systemically and in the liver. To better characterise the oxidative stress in ASA, we assessed the ratio of reduced (GSH) versus oxidised glutathione (GSSG), which reduction is a common marker of oxidative stress (*29*). Here the liver GSH:GSSG ratio did not differ between *Asl*$^{Neo/Neo}$ and WT littermates, indicating that the reduction of total glutathione pool in *Asl*$^{Neo/Neo}$ mice was not associated with increased glutathione oxidation (Supplementary Figure 2M). The comparison of the different steady-state concentrations of the precursors and breakdown products of glutathione suggested that precursors accumulate due to a bottleneck in one of the rate-limiting steps of glutathione biosynthesis, while glutathione catabolism by GGT is enhanced, explaining the lower glutathione levels in both the circulation and in the liver of *Asl*$^{Neo/Neo}$ mice.

To determine whether oxidative stress might further contribute to the lower levels of total glutathione in plasma and liver of *Asl*$^{Neo/Neo}$ mice, we measured lipid peroxidation products in the liver using the

158 thiobarbituric acid reactive substances (TBARS) assay. Lipid peroxidation was moderately increased
159 in *Asl*$^{Neo/Neo}$ mice versus WT (Figure 1L). The steady-state concentration of the oxidative breakdown
160 products of NO, nitrite (NO_2^-) and nitrate (NO_3^-), were significantly lower in plasma (Supplementary
161 Figure 2N) and liver (Figure 1M), as previously reported in this disorder (*4*, *5*). Supporting NO
162 deficiency, decreasing trend in nitroso-species were observed in *Asl*$^{Neo/Neo}$ livers versus WT
163 (Supplementary Figure 2O). The lack of difference in nitrotyrosine levels by western blot in *Asl*$^{Neo/Neo}$
164 livers versus WT confirmed the absence of nitro-oxidative stress (Figure 1N, Supplementary Figure
165 2P). The nuclear factor erythroid 2-related factor 2 (Nrf2) is a transcriptional factor regulating
166 antioxidant response against oxidative stress. Nrf2 protein levels didn't differ between WT and *Asl*$^{Neo/Neo}$
167 livers (Supplementary Figure 2Q). Taken together, upstream precursors of glutathione biosynthesis
168 accumulate, coinciding with reduced total glutathione, compromised NO production, moderate
169 oxidative stress and persisting antioxidant capacity in ASA.

170 Glutathione biosynthesis relies on 2 enzymatic steps: (i) the rate limiting glutamate cysteine ligase
171 (GCL) catalyses the conversion of glutamate and cysteine to γ-glutamyl-cysteine then (ii) glutathione
172 synthase (GS) catalyses the conversion of γ-glutamyl-cysteine and glycine to glutathione (Figure 1A).
173 GCL is a heterodimer with a heavy catalytic subunit (GCLC) and a light or modifier subunit (GCLM)
174 (*25*). We hypothesised that reduced glutathione was not a consequence of increased oxidative stress,
175 but an effect of deficiencies in the enzymes involved in its biosynthesis. Indeed, *Asl*$^{Neo/Neo}$ mice had
176 decreased gene expression of GCLC (Figure 1O) and GCLM (Figure 1P) compared to WT, whereas
177 GS expression showed a decreased trend (Figure 1Q). Supporting this, untargeted proteomics
178 comparing WT and *Asl*$^{Neo/Neo}$ livers highlighted glutathione functions to be one of the major
179 physiological functions to be downregulated (Figure 1R, Supplementary Figure 3A-C, Supplementary
180 Table 3).

181

182 **A non-invasive marker confirms the impaired glutathione metabolism in *Asl*$^{Neo/Neo}$ mice**

The biosynthesis of glutathione is dependent on cellular import of cystine in exchange for glutamate efflux via the cystine/glutamate antiporter system x_C^-, a transmembrane transport system (Figure 2A) (31). Cystine is subsequently reduced to cysteine for *de novo* glutathione biosynthesis (*25*). Metabolic reprogramming in cancer cells generate oxidative stress, which is balanced by increased glutathione biosynthesis via enhanced x_C^- mediated cystine import (*30*). Using positron emission tomography (PET), the radiolabelled glutamate analogue [^{18}F]FSPG provides an *in vivo* functional readout of *de novo* glutathione biosynthesis and has been used both in the clinic for cancer diagnosis (*31*-*33*), and preclinically to assess cancer drug resistance (*34*) and disease progression in multiple sclerosis (*35*).

In order to functionally assess alterations in the glutathione biosynthetic pathway, [^{18}F]FSPG was administered intravenously (IV) to 2-3 weeks-old *Asl*$^{Neo/Neo}$ mice and WT littermates, with radiotracer retention dynamically imaged by PET. In all mice, typical healthy tissue [^{18}F]FSPG retention was observed in the salivary glands, thymus, and pancreas, accompanied by renal elimination. Liver [^{18}F]FSPG retention for *Asl*$^{Neo/Neo}$ mice was 14 ± 4% injected dose (ID)/g, which was 3-fold higher (p=0.002) than that of WT mice (5.2 ± 1.5 %ID/g). In PET images of WT mice, [^{18}F]FSPG retention in the liver was just above background, with images dominated by radiotracer retention in the pancreas and kidney. Conversely, it was challenging to distinguish between pancreatic and liver [^{18}F]FSPG retention in *Asl*$^{Neo/Neo}$ mice (Figures 2B, 2C, Supplementary Figure 4A). We confirmed that the protein expression of xCT in 2 week-old *Asl*$^{Neo/Neo}$ mice liver was substantially increased than that of the WT littermates, which had low baseline expression (Figures 2D). Unexpectedly, high [^{18}F]FSPG retention was also present in the skin of *Asl*$^{Neo/Neo}$ mice (13 ± 1.8 %ID/g) which was not the case in WT littermates (5.3 ± 2.3 %ID/g; Figure 2B, 2E; p=0.002; Supplementary Figure 4B). Increased [^{18}F]FSPG skin retention accompanied gross changes to tissue structure, as shown by hematoxylin and eosin (H&E) staining (Figure 2F). [^{18}F]FSPG is therefore a useful non-invasive marker of aberrant glutathione metabolism in the liver and skin of *Asl*$^{Neo/Neo}$ mice, mediated at least in-part through the upregulated expression of the xCT antiporter.

Single intravenous administration of *hASL* mRNA corrects ureagenesis up to 7 days in adult *Asl*$^{Neo/Neo}$ mice

The promising therapeutic effects of mRNA technology have been demonstrated recently in multiple liver inherited metabolic conditions (*36, 37*). Specifically engineered *hASL* mRNA encapsulated in lipid nanoparticles restored ASL expression and activity in ASL-deficient fibroblasts from patients compared to a *Luciferase (Luc)* mRNA control lipid nanoparticle (Supplementary Figures 5A-C). mRNA therapy has transient efficacy and requires re-administration to enable a sustained effect. Thus, we conducted a pharmacokinetic study of *hASL* mRNA in *Asl*$^{Neo/Neo}$ mice to assess the efficacy and duration of effect on the urea cycle. Three-week-old *Asl*$^{Neo/Neo}$ mice received a single IV injection of either *hASL* or *Luc* mRNA at 1 mg mRNA/kg body weight and were sacrificed at 2h, 24h, 72h or 7 days (Figure 3A). Due to the severity of the phenotype, the experimental design did not include any longitudinal assessment of biomarkers to avoid additional stress, which could precipitate the animal's death. Specific cohorts of animals received mRNA therapy at T0 and harvested at the selected time point. A marked reduction of plasma ammonia (Figure 3B), argininosuccinic acid (Figure 3C) and citrulline (Figure 3D) in dried blood spots, and urine orotate (Figure 3E) was observed within 24h of administration in *hASL* mRNA treated *Asl*$^{Neo/Neo}$ mice compared to control (*Luc* mRNA) treated group. This effect was sustained over seven days. Importantly, the levels of these metabolites post *hASL* mRNA treatment in *Asl*$^{Neo/Neo}$ mice were comparable to the physiological levels in WT mice. Interestingly, plasma ammonia, argininosuccinic acid and citrulline in dried blood spots were elevated at 2 hours post-injection in the *hASL* mRNA versus *Luc* mRNA treated group (Figure 3A-C), raising the question of a risk of acute impairment of the urea cycle. No effect on arginine levels were observed (Supplementary Figure 6A). Western blot and immunohistochemistry data in liver showed restored ASL protein expression at physiological levels at 24h post-administration of *hASL* mRNA (Figures 3F-I, Supplementary Figure 6B-D). ASL levels were consistently higher in *hASL* versus the *Luc* mRNA treated group over this seven-day time course. Liver ASL activity was also restored to physiological levels at 24h and 72h in *hASL* compared to the *Luc* mRNA treated group but began to decline by seven days (Figure 3J).

hASL mRNA therapy from birth normalises the phenotype of *Asl*$^{Neo/Neo}$ mice

Pharmacodynamic data showed a single mRNA dose to be efficacious for up to seven days. To better understand the value of this treatment, we initiated a survival study with repeated administration of *hASL* mRNA versus *Luc* mRNA in neonatal *Asl*$^{Neo/Neo}$ pups. Mice received systemic administration of mRNA constructs every seven days with the first IV dose administered at day 1 of life. Due to difficulties injecting young pups, an intraperitoneal (IP) dose of 2 mg/kg at day 8 of life was performed. This twice higher dose was based on liver biodistribution between IV and IP routes, which showed that a two-fold higher IP dose has a similar liver biodistribution as a single IV dose (Supplementary Figures 7A, 7B). Mice were treated for seven weeks and harvested 48 h following the last injection (Figure 4A). The macroscopic phenotype of *Asl*$^{Neo/Neo}$ mice was restored to that of WT littermates in the *hASL* mRNA treatment group, with normalisation of survival (Figure 4B, p=0.002), growth (Figure 4C, Supplementary Figure 8A), fur (Figure 4D) and hepatomegaly (Supplementary Figure 8B). One *hASL* mRNA treated mutant was culled at 24 days of age due to malocclusion, a complication unrelated to the ASL phenotype or mRNA therapy, and was excluded from the analysis. In contrast, *Luc* mRNA treated *Asl*$^{Neo/Neo}$ littermates showed abnormal fur, impaired growth, and early death within 2 weeks of life (Figures 4B-D).

Animals which survived seven weeks were culled 48 h after the last mRNA injection. Analysis showed normalization of ammonaemia (Figure 4E), argininosuccinic acid (Figure 4F) and citrulline (Figure 4G) levels in dried blood spots, and urinary orotate levels (Figure 4H) in *hASL* mRNA treated *Asl*$^{Neo/Neo}$ mice. No significant differences in arginine levels in dried blood spots between WT or *Luc* mRNA or *hASL* mRNA treated *Asl*$^{Neo/Neo}$ mice were observed (Supplementary Figure 8C). Elevated plasma amino transferase (ALT) was normalized in the *hASL* mRNA treated *Asl*$^{Neo/Neo}$ mice (Supplementary Figure 8D). Longitudinal analysis of plasma ammonia levels (Supplementary Figure 8E), argininosuccinic acid (Supplementary Figure 8F) and citrulline (Supplementary Figure 8G) levels in dried blood spots, and urinary orotate levels (Supplementary Figure 8H) in *hASL* mRNA treated *Asl*$^{Neo/Neo}$ mice showed sustained therapeutic benefit over time. Next, functional assessment of urea cycle *in vivo* was measured by quantifying labelled urea in the plasma following the systemic injection of the ^{13}C labelled sodium

acetate stable isotope 30 minutes pre-harvest. ^{13}C labelling showed restored ureagenesis in the *hASL* treated *Asl*$^{Neo/Neo}$ mice (Figure 4I). ASL levels in liver assessed by western blot (Figures 4J, 4K) and immunohistochemistry (Figures 4L, 4M) were restored to physiological levels and physiological pattern following *hASL* mRNA therapy. Similar to single-dose short-term therapy, ASL activity in liver was restored to WT physiological levels following *hASL* mRNA therapy in *Asl*$^{Neo/Neo}$ mice at this late time-point (Figure 4N). Gender analysis showed that there were no sex-related differences in the different efficacy endpoints in the *hASL* mRNA treated group (Supplementary Table 4).

hASL mRNA therapy partially rescues the adult phenotype in *Asl*$^{Neo/Neo}$ mice

As untreated *Asl*$^{Neo/Neo}$ mice start dying from 2-3 weeks of age (*4*), we next wanted to assess whether it was possible to rescue of the severe phenotype of *Asl*$^{Neo/Neo}$ mice following late initiation of *hASL* mRNA therapy. *Asl*$^{Neo/Neo}$ mice received their first IV *hASL* mRNA dose in early adulthood at day 21 of life followed by weekly mRNA administration for up to 8 weeks (Figure 5A). All but one treated mouse survived to the end of the study which died after two injections at day 31 of life. In contrast, *Luc* mRNA treated mice only survived up to day 37 of life, with most animals dying before day 30 (Figure 5B, p=0.002). *hASL* mRNA treated *Asl*$^{Neo/Neo}$ mice showed significantly improved growth compared to *Luc* mRNA *Asl*$^{Neo/Neo}$ littermates, however the body weight remained significantly lower than WT littermates (Figure 5C, Supplementary Figure 9A). The full recovery of hair growth in *hASL* mRNA treated *Asl*$^{Neo/Neo}$ mice was observed with similar fur pattern compared to WT (Figure 5D). Liver to body weight ratio remained significantly elevated in both *Asl*$^{Neo/Neo}$ mice groups (Supplementary Figure 9B). Plasma ammonia (Figure 5E), argininosuccinic acid (Figure 5F) and citrulline (Figure 5G) in dried blood spots and urinary orotic acid levels (Figure 5H) were significantly reduced following *hASL* mRNA therapy to physiological WT levels. As shown in pups treated soon after birth, ^{13}C ureagenesis revealed restored *in vivo* urea cycle function compared to that of WT in *hASL* mRNA treated *Asl*$^{Neo/Neo}$ mice (Figure 5I) compared to *Luc* mRNA treated *Asl*$^{Neo/Neo}$ littermates. An increasing trend was observed in arginine levels between *Luc* mRNA compared to the *hASL* mRNA treated *Asl*$^{Neo/Neo}$ group (Supplementary Figure 9C). ALT levels indicated an absence of liver toxicity in the *hASL* mRNA

treated *Asl*$^{Neo/Neo}$ mice compared to the WT littermates (Supplementary Figure 9D). ASL levels in the liver, assessed by western blot (Figures 5J, 5K), were restored to physiological levels following *hASL* mRNA therapy compared to WT. Liver ASL activity was also significantly improved following *hASL* mRNA compared to *Luc* mRNA in *Asl*$^{Neo/Neo}$ mice (Figure 5L). Gender analysis could not determine any sex differences between the different efficacy endpoints in the *hASL* mRNA treated group (Supplementary Figure 10 and Supplementary Table 5).

[^{18}F]FSPG-PET provides a sensitive pharmacodynamic marker of *hASL* mRNA treatment

To investigate the potential of [^{18}F]FSPG PET as a non-invasive tool of therapeutic efficacy, [^{18}F]FSPG was administered IV to 2 weeks-old untreated and *hASL* mRNA treated *Asl*$^{Neo/Neo}$ mice (IV administration of 1 mg/kg *hASL* mRNA at birth followed by weekly IP administration of 2 mg/kg mRNA before imaging at 2 weeks of age). Supporting our functional and metabolic data, [^{18}F]FSPG retention was halved in *hASL* mRNA treated (11 ± 2.0 %ID/g) versus untreated *Asl*$^{Neo/Neo}$ mice (22 ± 2.3 % ID/g; p = 0.026; Figures 6A, 6B, Supplementary Figure 11A). At the treatment time-point, however, [^{18}F]FSPG retention was not completely restored to baseline levels from WT livers (5.0 ± 2.8 %ID/g). In line with lowered [^{18}F]FSPG retention, the expression of cystine/glutamate antiporter system x_C^- was greatly reduced in livers from *hASL* mRNA treated versus *Asl*$^{Neo/Neo}$ mice (Figure 7C). In these animals, glutathione metabolism was corrected, with restoration of hepatic liver glutathione in both neonatal and adult treated *Asl*$^{Neo/Neo}$ mice similar to that of WT levels (Figure 7D). This restoration of glutathione levels was associated with a significant reduction of total homocysteine ratio compared to WT in livers from *hASL* mRNA treated versus untreated *Asl*$^{Neo/Neo}$ mice (Figure 7E). Conversely, skin [^{18}F]FSPG retention was not affected by mRNA therapy. [^{18}F]FSPG skin retention was 4.2 ± 3.4 %ID/g in WT mice, compared to 15 ± 3.7 %ID/g and 15 ± 4.2 %ID/g in untreated and *hASL* mRNA treated *Asl*$^{Neo/Neo}$ mice, respectively (Supplementary Figures 11B, 11C).

hASL mRNA therapy corrects the metabolic dysfunction and liver pathophysiology in *Asl*$^{Neo/Neo}$ mice

We wanted to determine the extent of the correction of liver metabolic dysfunction following *hASL* mRNA treatment in *Asl*$^{Neo/Neo}$ mice. To do this, we used RNA-sequencing (RNA-seq) transcriptomic analysis and visualised the overall variation in gene expression across WT and *Asl*$^{Neo/Neo}$ mice treated at birth with either *hASL* mRNA or *Luc* mRNA therapy. Principal component analysis showed clustering of the *hASL* mRNA treated and WT liver samples, suggesting a similar profile of gene expression in both groups. In contrast, *Luc* mRNA treated *Asl*$^{Neo/Neo}$ mice clustered separately (Figure 7A). Next, we analysed differential gene expression identifying all genes with a log2-fold change of >0.1 or < -0.1 and passing an FDR cut off of <0.05. Comparing WT vs *Luc* mRNA *Asl*$^{Neo/Neo}$ groups, we found 2,705 genes to be significantly up- (1,257 genes) or down-regulated (1,448 genes; Figure 7B). Remarkably, only 7 genes (1 upregulated and 6 downregulated) were differentially expressed between WT vs *hASL* mRNA *Asl*$^{Neo/Neo}$ mice livers, thereby demonstrating the efficacy of mRNA therapy in correcting liver dysfunction (Figure 7C). No pathway correlation was observed between these genes, which have different localisation and function (Supplementary Table 6). This interpretation of the data was supported by the analysis of differential gene expression between *Luc* mRNA and *hASL* mRNA *Asl*$^{Neo/Neo}$. Similar to the WT vs *Luc* mRNA *Asl*$^{Neo/Neo}$ comparison (Figure 7D), we identified a large number of differentially expressed genes (4,297 genes) with 1,962 genes being significantly upregulated (log2-fold change > 0.1 and FDR < 0.05) and 2,335 being significantly downregulated (log2-fold change < -0.1 and FDR < 0.05).

To further study the dysregulation of glutathione function, the analysis of pathways affecting glutathione metabolism was performed on the RNA-seq data. Our analysis highlighted downregulation of multiple genes involved in glutathione biosynthesis and metabolism alongside alterations of genes of the methionine cycle, transsulfuration and antioxidant pathways between *Luc* mRNA *Asl*$^{Neo/Neo}$ mice and WT livers (Figure 7E). These findings additionally support disruption of glutathione metabolism in *Asl*$^{Neo/Neo}$ mice, including the downregulation of *Gclc*. Importantly, these pathways were corrected

post *hASL* mRNA treatment as shown by post pathways analysis comparison between *hASL* mRNA and *Luc* mRNA treated $Asl^{Neo/Neo}$ mice (Figure 7E)**.**

NO deficiency is a hallmark of ASA (*4*, *5*). Previous reports have shown that NO donors can upregulate the rate limiting enzyme of glutathione biosynthesis GCL in vascular smooth muscle cells (*38*) and endothelial cells (*39*). To test the role of NO on glutathione, we incubated human hepatocellular carcinoma derived Huh7 cells with NO donor S-nitroso-N-acetylpenicillamine (SNAP) versus vehicle (DMSO) control and observed a significant increase in mRNA expression of both GCL subunits, GCLC (Figure 7F) and GCLM (Figure 7G). This suggests that the normalisation of ASL expression corrects hepatic glutathione metabolism by restoring the NO availability and thereby GCL upregulation (Figure 7H).

Discussion

Glutathione is a master antioxidant, a mitochondrial protectant, and regulator of multiple redox processes (*40*, *41*). Glutathione depletion is a well-identified feature of common chronic liver diseases, *e.g.* non-alcoholic fatty liver disease, alcoholic liver disease and cholestasis (*42*). Generally, raised production of reactive oxygen species causes sustained oxidative stress and scavenges glutathione, although occasionally, compromised glutathione biosynthesis or increased glutathione recycling have been observed (*25*).

Here we observed glutathione depletion as a key feature of the chronic liver disease in ASA. Glutathione depletion is likely to be multifactorial, with various mechanistic explanations identified in this work, such as decreased biosynthesis, increased degradation and increased urinary excretion. Although it has been shown that glutathionuria can cause systemic glutathione depletion (*43*), the normalisation of liver glutathione levels after *hASL* mRNA therapy shows the importance of dysregulated glutathione biosynthesis in the liver. In particular, we observed downregulation of the rate-limiting enzyme of glutathione biosynthesis, GCL, affecting both the catalytic and modifier subunits. The upregulation of the xCT transporter in the liver suggests a feedback mechanism to alleviate the consequences of

glutathione depletion. This mechanism has been shown in cancer cells to promote glutathione biosynthesis and thereby cell survival from an increase of the intracellular cysteine pool, and can be observed as well in monogenic liver diseases (*21*, *44*).

These findings contrast with only moderate evidence of oxidative stress and downregulation of genes involved in antioxidant pathways. In ASA livers, the main glutathione-dependent functions and related pathways involved in antioxidant activity and endogenous and xenobiotics detoxification were downregulated. Increased oxidative stress is common in ASA and has been described systemically (*5*), and in neuronal (*9*) or endothelial (*22*) cells. Direct toxicity from argininosuccinate and conjugates (*7, 20, 45*), and NO deficiency are two pro-oxidant mechanisms. NO deficiency is caused by arginine depletion and subsequent NOS uncoupling (*4, 5, 9*). NOS uncoupling alters physiological NO synthesis and promotes synthesis of the reactive oxygen species superoxide ion (O_2^-). Additionally, at physiological levels, NO can act as a chain-breaking antioxidant capable of attenuating lipid peroxidation (*46*). In our study however, the $Asl^{Neo/Neo}$ mouse presents only moderate evidence of hepatic oxidative stress despite evidence of systemic and hepatic NO deficiency.

ASL is the final enzyme required for arginine synthesis in mammals. Arginine is the precursor of NO and consequently, ASA is also a model of inherited NO deficiency. Various clinical symptoms in ASA such as arterial hypertension (*5*), colitis (*47*), epilepsy (*48*) and motor disorder (*49*) are directly caused by NO deficiency and subsequent downregulation of key physiological processes or metabolic enzymes. NO can upregulate GCL via a non-canonical pathway independent from cGMP in vascular smooth muscle cells (*38*) and endothelial cells (*39*). We observed NO-induced GCL mRNA upregulation in human hepatocytes providing a potential mechanistic link between liver NO deficiency and glutathione depletion, however further studies are required to confirm this link. ASS1 and ASL are both part of the same multiprotein complex jointly with NO synthase. ASL plays a key structural role in maintaining this complex (*4*). ASLD patients have a systemic phenotype, presumably caused partly by systemic NO deficiency (*15*), which ASSD patients do not have. Various symptoms affecting the ASLD brain, cardiovascular system, gastrointestinal tract, bone physiology have a pathophysiological

explanation based on NO deficiency (*9*, *22*, *47-51*). Therefore, the clinical, pathophysiological and molecular evidences of NO deficiency in ASLD are firmly established whereas evidence of NO deficiency in ASSD remains limited. The potential extrapolation of ASLD glutathione dysregulation in ASSD remains to be proven.

Glutathione dysregulation and ureagenesis defect are two distinct pathways affected by ASA. Ureagenesis can be assessed with multiple biomarkers such as ammonia, amino acids, orotic acid, stable isotopes but this does not inform on the status of glutathione biosynthesis and poorly correlates with the chronic liver disease (*16*). To assess glutathione dysregulation, plasma biomarkers could be assessed, such as homocysteine, cysteine, glutathione, glycine and glutamate. This study, however, highlights the potential of exploiting defective glutathione biosynthesis with non-invasive [^{18}F]FSPG-PET imaging as a sensitive diagnostic tool to assess the liver disease in ASA. The use of [^{18}F]FSPG-PET imaging is rapidly expanding for clinical cancer imaging (*34*, *52*). While the use of PET radiotracers in monogenic diseases is a new application, especially in liver indications, we believe this tool will be of interest to academic teams or companies actively developing liver replacement therapies for ASA such as cell or gene (*i.e.* viral (*9*, *12*) or non viral) therapies. The ability to track the effective correction of impaired glutathione metabolism in the ASA liver provides substantial benefits over other more invasive techniques. Dysregulation of glutathione metabolism and antioxidant pathways were fully corrected following mRNA therapy, as observed in liver transcriptomics and liver glutathione levels. The liver [^{18}F]FSPG retention in neonatally-treated animals was halved compared to untreated mice, however radiotracer retention was not completely normalised to WT levels. This could be due to the experimental design, which included a short 2-week period of therapy to achieve age-matched comparison with untreated control *Asl*$^{Neo/Neo}$ animals. Interestingly, the correction was limited to the liver, with no benefit observed in the skin, demonstrating the preferential liver-targeting effect of mRNA therapy, as previously described (*53*).

The lack of effective therapies for both ureagenesis and the chronic liver disease in ASA has promoted the development of various experimental therapies. The autophagy enhancer Tat-Beclin-1 (TB-1)

peptide has shown improved ureagenesis along with reduction in hepatocellular injury and glycogen accumulation that may prevent long-term hepatotoxicity (*6*). Restoration of ureagenesis was achieved using liver-targeting viral-mediated gene therapies using adenoviral (*5, 11*), adeno-associated viral (AAV) (*9, 12*), or lentiviral vectors (*10*). For viral vector-mediated gene delivery, there are ongoing concerns over capsid immunogenicity and toxicity. There have been recent reports of serious hepatotoxicity following AAV gene delivery in X-linked myotubular myopathy and spinal muscular atrophy (*54-57*). In parallel, mRNA encapsulated in lipid nanoparticles is emerging as a promising therapy for liver monogenic diseases (*58-60*). This technology enables the delivery of a functional therapeutic protein to target cells with comparatively longer half-life and lower costs than protein replacement therapies. The absence of acute immunogenicity and integration in the host genome enables safe repeating administration to compensate for mRNA degradation and transient efficacy, becoming a viable alternative to viral vectors (*61, 62*). Proof of concept mRNA therapy in liver inherited metabolic diseases has increased in frequency in recent years (*36, 37, 63, 64*), supporting data for early phase clinical trials for ornithine transcarbamylase (NCT04442347), propionic acidemia (NCT04899310), methylmalonic acidemia (NCT04159103) and glycogen storage disease type 1A (NTC05095727). Based on previous proof of concept studies performed in another UCD, arginase deficiency, (*65, 66*), the therapeutic dose of 1 mg/kg of *hASL* mRNA delivered weekly through systemic routes of administration was tested in the $Asl^{Neo/Neo}$ mouse. The treatment of animals from birth showed remarkable effects by normalising the macroscopic phenotype, metabolic biomarkers, *in vivo* ureagenesis, liver ASL expression and activity to physiological levels. Comparatively, induction of therapy in early adulthood showed partial but still very effective phenotypic rescue. The observation that arginine levels were unable to be rescued, however, remains unexplained. Overall, this study showed proof of concept that mRNA therapy is both safe and efficacious for both early-onset and rescue therapy in a hypomorphic mouse model of ASA with severe phenotype and paves the way for clinical translation. A knock-out mouse model of ASA has previously been described (*67*) but is no longer available for comparison with our model. Previous translational work in methylmalonic acidaemia has shown similar efficacy of mRNA therapy at same dose and pattern of administration in both severe hypomorphic and knock-out mouse models (*63*), supporting our findings.

Limitations in our study include the small animal number per group, which limited the statistical power of some efficacy endpoints. Despite the small sample sizes, however, biochemical and phenotypic differences between WT and *Asl*$^{Neo/Neo}$ mice were extensive, as was the rescue effect of mRNA treatment. Small group sizes, however, limited our ability to assess the sex differences of thiol metabolites in urea cycle defect patients and mRNA treated *Asl*$^{Neo/Neo}$ mice. Additionally, mRNA therapy was studied up to 7 and 9 weeks in neonatally- and adult-treated *Asl*$^{Neo/Neo}$ mice, respectively. We cannot exclude that an extended duration of mRNA therapy in ASA might have revealed only partial sustained efficacy due to a single organ correction, *i.e.* the liver, in this systemic disease. Due to the study design, long-term LNP-related toxicity, a critical aspect for clinical translation, was not studied, although this type of toxicity has not been shown in other LNP-mRNA studies in other murine models of liver inherited metabolic diseases (*36*, *37*).

In conclusion, our study shows dysfunction of glutathione metabolism in both ASL-deficient patients and *Asl*$^{Neo/Neo}$ mouse model, whilst mRNA-LNP therapy corrected both glutathione metabolism and ureagenesis *in vivo*. Preliminary data suggests that glutathione biosynthesis in the liver is regulated by NO availability. Furthermore, we demonstrated the potential of [^{18}F]FSPG-PET as a companion diagnostic to assess the liver disease and therapeutic efficacy in ASA. These new insights into the liver pathophysiology of ASA provide new perspectives for targeted therapies, which would change the outcome of patients affected by this rare disease with currently high unmet needs and limited therapeutic options.

Materials and Methods

Study design: This study was designed to investigate hepatic glutathione metabolism and its role in the chronic liver disease in ASA. To assess glutathione metabolism in ASA, we first measured thiol metabolites in plasma of ASL-deficient patients. To investigate the cause of dysregulated glutathione metabolism in ASA, we measured plasma and liver thiol metabolites in *Asl*$^{Neo/Neo}$ mouse model and performed liver untargeted proteomics. Next, we monitored this redox changes in ASL-deficient murine

liver using [^{18}F]FSPG-PET. We then investigated the therapeutic potential of *hASL* mRNA in correcting dysregulated glutathione metabolism. We first assessed *hASL* mRNA efficacy by ASL supraphysiological overexpression and correction in human derived liver cell line and ASL-deficient fibroblasts, respectively. To evaluate this, we designed pharmacokinetic studies after systemic administration in *Asl*$^{Neo/Neo}$ animals of *hASL* mRNA or *Luc* mRNA. Untreated WT littermates were used as controls. *Asl*$^{Neo/Neo}$ mice were administered IV at 3-weeks of age and harvested at different timepoints, 2, 24, 72 h or 7 days. We then designed two survival studies for *Asl*$^{Neo/Neo}$ animals treated from birth and early adulthood. We initially assessed whether ureagenesis, the main cause of mortality in these *Asl*$^{Neo/Neo}$ mice, was corrected. In the first study, neonatal pups at day 1 were administered mRNA systemically weekly up to 7-weeks of age. In the second survival study of animals treated from early adulthood, mice were given weekly IV administration from day 21 onwards up to 9-weeks of age. Efficacy endpoints were survival, growth, fur pattern, plasma ammonia and urea-cycle related amino acids measured in dried blood spot, urine orotic acid, ^{13}C ureagenesis, liver western blot, immunostaining and enzyme activity for ASL. All harvests were performed 48 h following the last injection. Mutant mice were assigned randomly to study groups. All animals were monitored and weighted daily. After assessment of the therapeutic effect on ureagenesis, we assessed the therapeutic effect of *hASL* mRNA on dysregulated glutathione metabolism using [^{18}F]FSPG-PET and thiol metabolites. Analysis was performed blindly to genotype. We assessed liver transcriptomics in control and treated *Asl*$^{Neo/Neo}$ mice. We investigated the expression of glutathione synthetic enzymes in vitro in the presence of NO donor. *n=3* independent experiments were conducted for each *in vitro* experiment of the study. Animal procedures were approved by institutional ethical review and performed per UK home office licenses PP9223137, 70/14300 and PEFC6ABF1.

Statistical analysis: Data was analysed and represented using Graphpad Prism 9.0 software (San Diego, CA, USA). Figures shown mean +/- standard deviation. Kaplan-Meier survival curves were analysed using log-rank test. Student's t-test was performed to compare two groups. Simple linear regression analysis comparing average slopes per group was performed to compare growth curves. Due to early death of *Luc*-mRNA treated *Asl*$^{Neo/Neo}$ mice, the analysis comparing this cohort was performed

for the duration of the survival of these animals. For adult treated animals, analysis was performed using data from the timepoint of the first injection of LNP-mRNA. One-way ANOVA with Tukey's post-hoc test comparison or two-way ANOVA with Šídák's post-hoc test comparison was used to compare more than 2 groups. Log transformation was used to compare groups lacking normal distribution. All statistical results for figures 1-7 are summarised in Supplementary table 7A-G.

Supplementary Materials

Materials and Methods

Figs. S1 to S11

Tables S1 to S7

Data File S1

References 68-78

References

1. M. L. Summar, S. Koelker, D. Freedenberg, C. Le Mons, J. Haberle, H. S. Lee, B. Kirmse, The incidence of urea cycle disorders. *Mol Genet Metab* **110**, 179-180 (2013).
2. J. Baruteau, C. Diez-Fernandez, S. Lerner, G. Ranucci, P. Gissen, C. Dionisi-Vici, S. Nagamani, A. Erez, J. Häberle, Argininosuccinic aciduria: Recent pathophysiological insights and therapeutic prospects. *J Inherit Metab Dis* **42**, 1147-1161 (2019).
3. A. Erez, Argininosuccinic aciduria: from a monogenic to a complex disorder. *Genet Med* **15**, 251-257 (2013).
4. A. Erez, S. C. Nagamani, O. A. Shchelochkov, M. H. Premkumar, P. M. Campeau, Y. Chen, H. K. Garg, L. Li, A. Mian, T. K. Bertin, J. O. Black, H. Zeng, Y. Tang, A. K. Reddy, M. Summar, W. E. O'Brien, D. G. Harrison, W. E. Mitch, J. C. Marini, J. L. Aschner, N. S. Bryan, B. Lee, Requirement of argininosuccinate lyase for systemic nitric oxide production. *Nat Med* **17**, 1619-1626 (2011).
5. S. C. Nagamani, P. M. Campeau, O. A. Shchelochkov, M. H. Premkumar, K. Guse, N. Brunetti-Pierri, Y. Chen, Q. Sun, Y. Tang, D. Palmer, A. K. Reddy, L. Li, T. C. Slesnick, D. I. Feig, S. Caudle, D. Harrison, L. Salviati, J. C. Marini, N. S. Bryan, A. Erez, B. Lee, Nitric-oxide supplementation for treatment of long-term complications in argininosuccinic aciduria. *Am J Hum Genet* **90**, 836-846 (2012).
6. L. R. Soria, S. Gurung, G. De Sabbata, D. P. Perocheau, A. De Angelis, G. Bruno, E. Polishchuk, D. Paris, P. Cuomo, A. Motta, M. Orford, Y. Khalil, S. Eaton, P. B. Mills, S. N. Waddington, C. Settembre, A. F. Muro, J. Baruteau, N. Brunetti-Pierri, Beclin-1-mediated

activation of autophagy improves proximal and distal urea cycle disorders. *EMBO Mol Med* **13**, e13158 (2021).
7. B. Seminotti, J. C. da Silva, R. T. Ribeiro, G. Leipnitz, M. Wajner, Free Radical Scavengers Prevent Argininosuccinic Acid-Induced Oxidative Stress in the Brain of Developing Rats: a New Adjuvant Therapy for Argininosuccinate Lyase Deficiency? *Mol Neurobiol* **57**, 1233-1244 (2020).
8. S. C. Nagamani, A. Erez, B. Lee, Argininosuccinate lyase deficiency. *Genet Med* **14**, 501-507 (2012).
9. J. Baruteau, D. P. Perocheau, J. Hanley, M. Lorvellec, E. Rocha-Ferreira, R. Karda, J. Ng, N. Suff, J. A. Diaz, A. A. Rahim, M. P. Hughes, B. Banushi, H. Prunty, M. Hristova, D. A. Ridout, A. Virasami, S. Heales, S. J. Howe, S. M. K. Buckley, P. B. Mills, P. Gissen, S. N. Waddington, Argininosuccinic aciduria fosters neuronal nitrosative stress reversed by Asl gene transfer. *Nat Commun* **9**, 3505 (2018).
10. L. Touramanidou, D. Perocheau, S. Gurung, A. C. Cozmescu, S. N. Waddington, J. R. Counsell, P. Gissen, J. Baruteau, European Society of Gene and Cell Therapy (ESGCT), Virtual Congress, 2021.
11. L. C. Burrage, S. Madan, X. Li, S. Ali, M. Mohammad, B. M. Stroup, M. M. Jiang, R. Cela, T. Bertin, Z. Jin, J. Dai, D. Guffey, M. Finegold, S. Nagamani, C. G. Minard, J. Marini, P. Masand, D. Schady, B. L. Shneider, D. H. Leung, D. Bali, B. Lee, Chronic liver disease and impaired hepatic glycogen metabolism in argininosuccinate lyase deficiency. *JCI Insight* **5**, (2020).
12. S. N. Ashley, J. M. L. Nordin, E. L. Buza, J. A. Greig, J. M. Wilson, Adeno-associated viral gene therapy corrects a mouse model of argininosuccinic aciduria. *Mol Genet Metab* **125**, 241-250 (2018).
13. G. Ranucci, M. Rigoldi, G. Cotugno, S. M. Bernabei, A. Liguori, S. Gasperini, B. M. Goffredo, D. Martinelli, L. Monti, P. Francalanci, M. Candusso, R. Parini, C. Dionisi-Vici, Chronic liver involvement in urea cycle disorders. *J Inherit Metab Dis* **42**, 1118-1127 (2019).
14. A. Bigot, M. C. Tchan, B. Thoreau, H. Blasco, F. Maillot, Liver involvement in urea cycle disorders: a review of the literature. *Journal of inherited metabolic disease* **40**, 757-769 (2017).
15. J. Baruteau, E. Jameson, A. A. Morris, A. Chakrapani, S. Santra, S. Vijay, H. Kocadag, C. E. Beesley, S. Grunewald, E. Murphy, M. Cleary, H. Mundy, L. Abulhoul, A. Broomfield, R. Lachmann, Y. Rahman, P. H. Robinson, L. MacPherson, K. Foster, W. K. Chong, D. A. Ridout, K. M. Bounford, S. N. Waddington, P. B. Mills, P. Gissen, J. E. Davison, Expanding the phenotype in argininosuccinic aciduria: need for new therapies. *J Inherit Metab Dis* **40**, 357-368 (2017).
16. S. C. S. Nagamani, S. Ali, R. Izem, D. Schady, P. Masand, B. L. Shneider, D. H. Leung, L. C. Burrage, Biomarkers for liver disease in urea cycle disorders. *Mol Genet Metab* **133**, 148-156 (2021).
17. M. Tuchman, B. Lee, U. Lichter-Konecki, M. L. Summar, M. Yudkoff, S. D. Cederbaum, D. S. Kerr, G. A. Diaz, M. R. Seashore, H. S. Lee, R. J. McCarter, J. P. Krischer, M. L. Batshaw, Cross-sectional multicenter study of patients with urea cycle disorders in the United States. *Mol Genet Metab* **94**, 397-402 (2008).
18. M. Marble, R. R. McGoey, E. Mannick, B. Keats, S. S. Ng, S. Deputy, H. Gereighty, E. Schmidt-Sommerfeld, Living related liver transplant in a patient with argininosuccinic aciduria and cirrhosis: metabolic follow-up. *J Pediatr Gastroenterol Nutr* **46**, 453-456 (2008).
19. A. Zimmermann, C. Bachmann, R. Baumgartner, Severe liver fibrosis in argininosuccinic aciduria. *Arch Pathol Lab Med* **110**, 136-140 (1986).
20. S. C. Nagamani, O. A. Shchelochkov, M. A. Mullins, S. Carter, B. C. Lanpher, Q. Sun, S. Kleppe, A. Erez, E. O'Brian Smith, J. C. Marini, B. Lee, A randomized controlled trial to evaluate the effects of high-dose versus low-dose of arginine therapy on hepatic function tests in argininosuccinic aciduria. *Mol Genet Metab* **107**, 315-321 (2012).
21. J. Liu, X. Xia, P. Huang, xCT: A Critical Molecule That Links Cancer Metabolism to Redox Signaling. *Mol Ther* **28**, 2358-2366 (2020).
22. J. Kho, X. Tian, W. T. Wong, T. Bertin, M. M. Jiang, S. Chen, Z. Jin, O. A. Shchelochkov, L. C. Burrage, A. K. Reddy, H. Jiang, R. Abo-Zahrah, S. Ma, P. Zhang, K. D. Bissig, J. J. Kim, S. Devaraj, G. G. Rodney, A. Erez, N. S. Bryan, S. C. S. Nagamani, B. H. Lee,

Argininosuccinate Lyase Deficiency Causes an Endothelial-Dependent Form of Hypertension. *Am J Hum Genet* **103**, 276-287 (2018).
23. M. M. Cortese-Krott, A. Koning, G. G. C. Kuhnle, P. Nagy, C. L. Bianco, A. Pasch, D. A. Wink, J. M. Fukuto, A. A. Jackson, H. van Goor, K. R. Olson, M. Feelisch, The Reactive Species Interactome: Evolutionary Emergence, Biological Significance, and Opportunities for Redox Metabolomics and Personalized Medicine. *Antioxid Redox Signal* **27**, 684-712 (2017).
24. X. Jiang, Q. Zhou, B. Du, S. Li, Y. Huang, Z. Chi, W. M. Lee, M. Yu, J. Zheng, Noninvasive monitoring of hepatic glutathione depletion through fluorescence imaging and blood testing. *Sci Adv* **7**, (2021).
25. S. C. Lu, Regulation of glutathione synthesis. *Mol Aspects Med* **30**, 42-59 (2009).
26. J. Baruteau, C. Diez-Fernandez, S. Lerner, G. Ranucci, P. Gissen, C. Dionisi-Vici, S. Nagamani, A. Erez, J. Haberle, Argininosuccinic aciduria: Recent pathophysiological insights and therapeutic prospects. *J Inherit Metab Dis* **42**, 1147-1162 (2019).
27. S. Kolker, V. Valayannopoulos, A. B. Burlina, J. Sykut-Cegielska, F. A. Wijburg, E. L. Teles, J. Zeman, C. Dionisi-Vici, I. Baric, D. Karall, J. B. Arnoux, P. Avram, M. R. Baumgartner, J. Blasco-Alonso, S. P. Boy, M. B. Rasmussen, P. Burgard, B. Chabrol, A. Chakrapani, K. Chapman, I. S. E. Cortes, M. L. Couce, L. de Meirleir, D. Dobbelaere, F. Furlan, F. Gleich, M. J. Gonzalez, W. Gradowska, S. Grunewald, T. Honzik, F. Horster, H. Ioannou, A. Jalan, J. Haberle, G. Haege, E. Langereis, P. de Lonlay, D. Martinelli, S. Matsumoto, C. Muhlhausen, E. Murphy, H. O. de Baulny, C. Ortez, C. C. Pedron, G. Pintos-Morell, L. Pena-Quintana, D. P. Ramadza, E. Rodrigues, S. Scholl-Burgi, E. Sokal, M. L. Summar, N. Thompson, R. Vara, I. V. Pinera, J. H. Walter, M. Williams, A. M. Lund, A. Garcia Cazorla, The phenotypic spectrum of organic acidurias and urea cycle disorders. Part 2: the evolving clinical phenotype. *J Inherit Metab Dis* **38**, 1059-1074 (2015).
28. A. E. Abdulle, A. M. van Roon, A. J. Smit, A. Pasch, M. van Meurs, H. Bootsma, S. J. L. Bakker, M. Y. Said, B. O. Fernandez, M. Feelisch, H. van Goor, D. J. Mulder, Rapid free thiol rebound is a physiological response following cold-induced vasoconstriction in healthy humans, primary Raynaud and systemic sclerosis. *Physiol Rep* **7**, e14017 (2019).
29. J. B. Owen, D. A. Butterfield, Measurement of oxidized/reduced glutathione ratio. *Methods Mol Biol* **648**, 269-277 (2010).
30. P. Koppula, Y. Zhang, L. Zhuang, B. Gan, Amino acid transporter SLC7A11/xCT at the crossroads of regulating redox homeostasis and nutrient dependency of cancer. *Cancer Commun (Lond)* **38**, 12 (2018).
31. P. N. McCormick, H. E. Greenwood, M. Glaser, O. D. K. Maddocks, T. Gendron, K. Sander, G. Gowrishankar, A. Hoehne, T. Zhang, A. J. Shuhendler, D. Y. Lewis, M. Berndt, N. Koglin, M. F. Lythgoe, S. S. Gambhir, E. Arstad, T. H. Witney, Assessment of Tumor Redox Status through (S)-4-(3-[(18)F]fluoropropyl)-L-Glutamic Acid PET Imaging of System xc (-) Activity. *Cancer Res* **79**, 853-863 (2019).
32. H. E. Greenwood, P. N. McCormick, T. Gendron, M. Glaser, R. Pereira, O. D. K. Maddocks, K. Sander, T. Zhang, N. Koglin, M. F. Lythgoe, E. Arstad, D. Hochhauser, T. H. Witney, Measurement of Tumor Antioxidant Capacity and Prediction of Chemotherapy Resistance in Preclinical Models of Ovarian Cancer by Positron Emission Tomography. *Clin Cancer Res* **25**, 2471-2482 (2019).
33. H. E. Greenwood, R. Edwards, N. Koglin, M. Berndt, F. Baark, J. Kim, G. Firth, E. Khalil, A. Mueller, T. H. Witney, Radiotracer stereochemistry affects substrate affinity and kinetics for improved imaging of system xC (-) in tumors. *Theranostics* **12**, 1921-1936 (2022).
34. S. Baek, C. M. Choi, S. H. Ahn, J. W. Lee, G. Gong, J. S. Ryu, S. J. Oh, C. Bacher-Stier, L. Fels, N. Koglin, C. Hultsch, C. A. Schatz, L. M. Dinkelborg, E. S. Mittra, S. S. Gambhir, D. H. Moon, Exploratory clinical trial of (4S)-4-(3-[18F]fluoropropyl)-L-glutamate for imaging xC-transporter using positron emission tomography in patients with non-small cell lung or breast cancer. *Clin Cancer Res* **18**, 5427-5437 (2012).
35. A. Hoehne, M. L. James, I. S. Alam, J. A. Ronald, B. Schneider, A. D'Souza, T. H. Witney, L. E. Andrews, H. C. Cropper, D. Behera, G. Gowrishankar, Z. Ding, T. Wyss-Coray, F. T. Chin, S. Biswal, S. S. Gambhir, [(18)F]FSPG-PET reveals increased cystine/glutamate antiporter (xc-) activity in a mouse model of multiple sclerosis. *J Neuroinflammation* **15**, 55 (2018).

36. D. An, J. L. Schneller, A. Frassetto, S. Liang, X. Zhu, J. S. Park, M. Theisen, S. J. Hong, J. Zhou, R. Rajendran, B. Levy, R. Howell, G. Besin, V. Presnyak, S. Sabnis, K. E. Murphy-Benenato, E. S. Kumarasinghe, T. Salerno, C. Mihai, C. M. Lukacs, R. J. Chandler, L. T. Guey, C. P. Venditti, P. G. V. Martini, Systemic Messenger RNA Therapy as a Treatment for Methylmalonic Acidemia. *Cell Rep* **21**, 3548-3558 (2017).
37. L. Jiang, J. S. Park, L. Yin, R. Laureano, E. Jacquinet, J. Yang, S. Liang, A. Frassetto, J. Zhuo, X. Yan, X. Zhu, S. Fortucci, K. Hoar, C. Mihai, C. Tunkey, V. Presnyak, K. E. Benenato, C. M. Lukacs, P. G. V. Martini, L. T. Guey, Dual mRNA therapy restores metabolic function in long-term studies in mice with propionic acidemia. *Nat Commun* **11**, 5339 (2020).
38. D. Moellering, J. McAndrew, R. P. Patel, T. Cornwell, T. Lincoln, X. Cao, J. L. Messina, H. J. Forman, H. Jo, V. M. Darley-Usmar, Nitric oxide-dependent induction of glutathione synthesis through increased expression of gamma-glutamylcysteine synthetase. *Arch Biochem Biophys* **358**, 74-82 (1998).
39. D. Moellering, J. Mc Andrew, R. P. Patel, H. J. Forman, R. T. Mulcahy, H. Jo, V. M. Darley-Usmar, The induction of GSH synthesis by nanomolar concentrations of NO in endothelial cells: a role for gamma-glutamylcysteine synthetase and gamma-glutamyl transpeptidase. *FEBS Lett* **448**, 292-296 (1999).
40. M. Feelisch, M. M. Cortese-Krott, J. Santolini, S. A. Wootton, A. A. Jackson, Systems redox biology in health and disease. *EXCLI J* **21**, 623-646 (2022).
41. A. Meister, Glutathione metabolism. *Methods Enzymol* **251**, 3-7 (1995).
42. M. Vairetti, L. G. Di Pasqua, M. Cagna, P. Richelmi, A. Ferrigno, C. Berardo, Changes in Glutathione Content in Liver Diseases: An Update. *Antioxidants (Basel)* **10**, (2021).
43. M. W. Lieberman, A. L. Wiseman, Z. Z. Shi, B. Z. Carter, R. Barrios, C. N. Ou, P. Chevez-Barrios, Y. Wang, G. M. Habib, J. C. Goodman, S. L. Huang, R. M. Lebovitz, M. M. Matzuk, Growth retardation and cysteine deficiency in gamma-glutamyl transpeptidase-deficient mice. *Proc Natl Acad Sci U S A* **93**, 7923-7926 (1996).
44. X. Liu, Y. Zhang, L. Zhuang, K. Olszewski, B. Gan, NADPH debt drives redox bankruptcy: SLC7A11/xCT-mediated cystine uptake as a double-edged sword in cellular redox regulation. *Genes Dis* **8**, 731-745 (2021).
45. K. Aoyagi, S. Nagase, M. Gotoh, K. Akiyama, M. Satoh, A. Hirayama, A. Koyama, Role of reactive oxygen and argininosuccinate in guanidinosuccinate synthesis in isolated rat hepatocytes. *Enzyme Protein* **49**, 205-211 (1996).
46. D. A. Wink, K. M. Miranda, M. G. Espey, R. M. Pluta, S. J. Hewett, C. Colton, M. Vitek, M. Feelisch, M. B. Grisham, Mechanisms of the antioxidant effects of nitric oxide. *Antioxid Redox Signal* **3**, 203-213 (2001).
47. N. Stettner, C. Rosen, B. Bernshtein, S. Gur-Cohen, J. Frug, A. Silberman, A. Sarver, N. N. Carmel-Neiderman, R. Eilam, I. Biton, M. Pevsner-Fischer, N. Zmora, A. Brandis, K. Bahar Halpern, R. Mazkereth, D. di Bernardo, N. Brunetti-Pierri, M. H. Premkumar, G. Dank, S. C. S. Nagamani, S. Jung, A. Harmelin, A. Erez, Induction of Nitric-Oxide Metabolism in Enterocytes Alleviates Colitis and Inflammation-Associated Colon Cancer. *Cell Rep* **23**, 1962-1976 (2018).
48. S. Lerner, E. Anderzhanova, S. Verbitsky, R. Eilam, Y. Kuperman, M. Tsoory, Y. Kuznetsov, A. Brandis, T. Mehlman, R. Mazkereth, U. Neuropsychologists, R. McCarter, M. Segal, S. C. S. Nagamani, A. Chen, A. Erez, ASL Metabolically Regulates Tyrosine Hydroxylase in the Nucleus Locus Coeruleus. *Cell Rep* **29**, 2144-2153 e2147 (2019).
49. S. Lerner, R. Eilam, L. Adler, J. Baruteau, T. Kreiser, M. Tsoory, A. Brandis, T. Mehlman, M. Ryten, J. A. Botia, S. G. Ruiz, A. C. Garcia, C. Dionisi-Vici, G. Ranucci, M. Spada, R. Mazkereth, R. McCarter, R. Izem, T. J. Balmat, R. Richesson, U. Members of the, E. Gazit, S. C. S. Nagamani, A. Erez, ASL expression in ALDH1A1(+) neurons in the substantia nigra metabolically contributes to neurodegenerative phenotype. *Hum Genet* **140**, 1471-1485 (2021).
50. M. H. Premkumar, G. Sule, S. C. Nagamani, S. Chakkalakal, A. Nordin, M. Jain, M. Z. Ruan, T. Bertin, B. Dawson, J. Zhang, D. Schady, N. S. Bryan, P. M. Campeau, A. Erez, B. Lee, Argininosuccinate lyase in enterocytes protects from development of necrotizing enterocolitis. *Am J Physiol Gastrointest Liver Physiol* **307**, G347-354 (2014).

51. Z. Jin, J. Kho, B. Dawson, M. M. Jiang, Y. Chen, S. Ali, L. C. Burrage, M. Grover, D. J. Palmer, D. L. Turner, P. Ng, S. C. Nagamani, B. Lee, Nitric oxide modulates bone anabolism through regulation of osteoblast glycolysis and differentiation. *J Clin Invest* **131**, (2021).
52. G. Kavanaugh, J. Williams, A. S. Morris, M. L. Nickels, R. Walker, N. Koglin, A. W. Stephens, M. K. Washington, S. K. Geevarghese, Q. Liu, D. Ayers, Y. Shyr, H. C. Manning, Utility of [(18)F]FSPG PET to Image Hepatocellular Carcinoma: First Clinical Evaluation in a US Population. *Mol Imaging Biol* **18**, 924-934 (2016).
53. L. Jiang, P. Berraondo, D. Jerico, L. T. Guey, A. Sampedro, A. Frassetto, K. E. Benenato, K. Burke, E. Santamaria, M. Alegre, A. Pejenaute, M. Kalariya, W. Butcher, J. S. Park, X. Zhu, S. Sabnis, E. S. Kumarasinghe, T. Salerno, M. Kenney, C. M. Lukacs, M. A. Avila, P. G. V. Martini, A. Fontanellas, Systemic messenger RNA as an etiological treatment for acute intermittent porphyria. *Nat Med* **24**, 1899-1909 (2018).
54. J. Baruteau, S. N. Waddington, I. E. Alexander, P. Gissen, Gene therapy for monogenic liver diseases: clinical successes, current challenges and future prospects. *J Inherit Metab Dis* **40**, 497-517 (2017).
55. J. M. Wilson, T. R. Flotte, Moving Forward After Two Deaths in a Gene Therapy Trial of Myotubular Myopathy. *Human gene therapy* **31**, 695-696 (2020).
56. A. Philippidis, Fourth Boy Dies in Clinical Trial of Astellas' AT132. *Hum Gene Ther* **32**, 1008-1010 (2021).
57. J. Guillou, A. de Pellegars, F. Porcheret, V. Fremeaux-Bacchi, E. Allain-Launay, C. Debord, M. Denis, Y. Pereon, C. Barnerias, I. Desguerre, G. Roussey, S. Mercier, Fatal thrombotic microangiopathy case following adeno-associated viral SMN gene therapy. *Blood Adv* **6**, 4266-4270 (2022).
58. U. Sahin, K. Karikó, Ö. Türeci, mRNA-based therapeutics--developing a new class of drugs. *Nat Rev Drug Discov* **13**, 759-780 (2014).
59. P. Berraondo, P. G. V. Martini, M. A. Avila, A. Fontanellas, Messenger RNA therapy for rare genetic metabolic diseases. *Gut* **68**, 1323-1330 (2019).
60. K. M. Córdoba, D. Jericó, A. Sampedro, L. Jiang, M. J. Iraburu, P. G. V. Martini, P. Berraondo, M. A. Avila, A. Fontanellas, Messenger RNA as a personalized therapy: The moment of truth for rare metabolic diseases. *Int Rev Cell Mol Biol* **372**, 55-96 (2022).
61. X. Hou, T. Zaks, R. Langer, Y. Dong, Lipid nanoparticles for mRNA delivery. *Nat Rev Mater* **6**, 1078-1094 (2021).
62. T. R. Damase, R. Sukhovershin, C. Boada, F. Taraballi, R. I. Pettigrew, J. P. Cooke, The Limitless Future of RNA Therapeutics. *Front Bioeng Biotechnol* **9**, 628137 (2021).
63. D. An, A. Frassetto, E. Jacquinet, M. Eybye, J. Milano, C. DeAntonis, V. Nguyen, R. Laureano, J. Milton, S. Sabnis, C. M. Lukacs, L. T. Guey, Long-term efficacy and safety of mRNA therapy in two murine models of methylmalonic acidemia. *EBioMedicine* **45**, 519-528 (2019).
64. H. Yu, E. Brewer, M. Shields, M. Crowder, C. Sacchetti, B. Soontornniyomkij, D. Dou, B. Clemente, M. Sablad, P. Chivukula, S. Hughes, S. Roberts, K. Rajappan, S. Tannis, R. Sekulovich, S. Parker, P. Limphong, Restoring ornithine transcarbamylase (OTC) activity in an OTC-deficient mouse model using LUNAR-OTC mRNA. *Clinical and Translational Discovery* **2**, e33 (2022).
65. S. Khoja, X. B. Liu, B. Truong, M. Nitzahn, J. Lambert, A. Eliav, E. Nasser, E. Randolph, K. E. Burke, R. White, X. Zhu, P. G. V. Martini, I. Nissim, S. D. Cederbaum, G. S. Lipshutz, Intermittent lipid nanoparticle mRNA administration prevents cortical dysmyelination associated with arginase deficiency. *Mol Ther Nucleic Acids* **28**, 859-874 (2022).
66. B. Truong, G. Allegri, X. B. Liu, K. E. Burke, X. Zhu, S. D. Cederbaum, J. Häberle, P. G. V. Martini, G. S. Lipshutz, Lipid nanoparticle-targeted mRNA therapy as a treatment for the inherited metabolic liver disorder arginase deficiency. *Proc Natl Acad Sci U S A* **116**, 21150-21159 (2019).
67. V. Reid Sutton, Y. Pan, E. C. Davis, W. J. Craigen, A mouse model of argininosuccinic aciduria: biochemical characterization. *Mol Genet Metab* **78**, 11-16 (2003).
68. J. Nelson, E. W. Sorensen, S. Mintri, A. E. Rabideau, W. Zheng, G. Besin, N. Khatwani, S. V. Su, E. J. Miracco, W. J. Issa, S. Hoge, M. G. Stanton, J. L. Joyal, Impact of mRNA chemistry and manufacturing process on innate immune activation. *Sci Adv* **6**, eaaz6893 (2020).

69. R. Edwards. H. E. Greenwood, G. McRobbie, I. Khan, T. H. Witney, Robust and Facile Automated Radiosynthesis of [(18)F]FSPG on the GE FASTlab. *Mol Imaging Biol* **23,** 854-864 (2021)
70. H. E. Greenwood, Z. Nyitrai, G. Mocsai, S. Hobor, T. H. Witney, High-Throughput PET/CT Imaging Using a Multiple-Mouse Imaging System. *J Nucl Med* **61**, 292-297 (2020).
71. H. Prinsen, B. G. M. Schiebergen-Bronkhorst, M. W. Roeleveld, J. J. M. Jans, M. G. M. de Sain-van der Velden, G. Visser, P. M. van Hasselt, N. M. Verhoeven-Duif, Rapid quantification of underivatized amino acids in plasma by hydrophilic interaction liquid chromatography (HILIC) coupled with tandem mass-spectrometry. *J Inherit Metab Dis* **39**, 651-660 (2016).
72. D. R. Janero, N. S. Bryan, F. Saijo, V. Dhawan, D. J. Schwalb, M. C. Warren, M. Feelisch, Differential nitros(yl)ation of blood and tissue constituents during glyceryl trinitrate biotransformation in vivo. *Pro Natl Acad Sci U S A* **101**, 16958-16963 (2004).
73. H. T. McKenna, K. A. O'Brien, B. O. Fernandez, M. Minnion, A. Tod, B. D. McNally, J. A. West, J. L. Griffin, M. P. Grocott, M. G. Mythen, M. Feelisch, A. J. Murray, D. S. Martin, Divergent trajectories of cellular bioenergetics, intermediary metabolism and systemic redox status in survivors and non-survivors of critical illness. *Redox Biol* **41**, 101907 (2021).
74. T. R. Sutton, M. Minnion, F. Barbarino, G. Koster, B. O. Fernandez, A. F. Cumpstey, P. Wischmann, M. Madhani, M. P. Frenneaux, A. D. Postle, M. M. Cortese-Krott, M. Feelisch, A robust and versatile mass spectrometry platform for comprehensive assessment of the thiol redox metabolome. *Redox Biol* **16**, 359-380 (2018).
75. C. Y. Kok, S. C. Cunningham, K. H. Carpenter, A. P. Dane, S. M. Siew, G. J. Logan, P. W. Kuchel, I. E. Alexander, Adeno-associated virus-mediated rescue of neonatal lethality in argininosuccinate synthetase-deficient mice. *Mol Ther* **21**, 1823-1831 (2013).
76. M. I. Love, W. Huber, S. Anders, Moderated estimation of fold change and dispersion for RNA-seq data with DESeq2. *Genome Biol* **15**, 550 (2014).
77. H. Wickham, ggplot2: Elegant Graphics for Data Analysis. *Springer-Verlag New York. ISBN 978-3-319-24277-4* https://ggplot2.tidyverse.org**.**, (2016).
78. E. Bliss, W. E. Heywood, M. Benatti, N. J. Sebire, K. Mills, An optimised method for the proteomic profiling of full thickness human skin. *Biol Proced Online* **18**, 15 (2016).

Acknowledgements

The authors would like to thank Eman Khalil for assistance with xCT western blotting, Phil Blower, Kavitha Sunassee, Jana Kim, Floyd Laniyan, Samantha Richards, Rebecca Towns, Katherine Howett, Mirabela Bandol and the staff from Biological services for help with PPL licence, breeding and maintenance of the ASL colony at King's College London and University College London. We are grateful to the patients, families and metabolic physicians (Dr Spyros Batzios, Dr Clare Beesley, Dr Alexander Broomfield, Dr Anupam Chakrapani, Dr Maureen Cleary, Dr Dr James Davison, Emma Footitt, Dr Stephanie Grunewald, Dr Karin Tuschl, Dr Mildrid Yeo) from Great Ormond Street Hospital for Children in London, UK for anonymously sharing data for this study. Some graphical illustrations were created with Biorender.com. **Funding:** This work was supported by funding from Moderna Inc.,

the United Kingdom Medical Research Council Clinician Scientist Fellowship MR/T008024/1 (JB), London Advanced Therapy Confidence in Collaboration in Advanced Therapies award (2CiC017) (JB, THW), a Wellcome Trust Senior Fellowship 220221/Z/20/Z (THW), the CRUK City of London Centre Award C7893/A26233 (THW), and the NIHR Great Ormond Street Hospital Biomedical Research Centre (JB, PG, PBM, SE). The views expressed are those of the author(s) and not necessarily those of the NHS, the NIHR or the Department of Health. **Author Contributions:** JB and THW designed the study. SG, OVT and DP conducted most of the experimental work. LT, YK, ARB, RSE, PBM, SNW and PG contributed to technical assistance in experimental work. ALGM and MR analysed the transcriptomics data. MM and MF analysed the thiol reactome data. SF and MM collected patients' data. SE analysed the ureagenesis with stable isotope. PFF, AC, SS, LR, PGVM, AF provided the *Luc* and *hASL* mRNA constructs. SG wrote the manuscript. DR provided assistance with statistical analysis. All authors contributed to review/editing and approved the final submission. **Competing interests**: JB reports research funding from Moderna Inc. PFF, AC, SS, LR, PGVM, AF are employees of Moderna Inc. and may hold equities from the company. AF and LR are inventors of patent application no. PCT/US23/17573 "Lipid nanoparticles and polynucleotides encoding arginosuccinate lyase for the treatment of argininosuccinic aciduria". The other authors declare no competing interests. **Data and material availability:** All data associated with this study are present in the paper or the Supplementary Materials. Requests for data should be addressed to JB or THW. The transcriptomic dataset is available on NCBI Gene Expression Omnibus, accession number GSE222874.

MAIN FIGURES LEGENDS

Figure 1. ASL-deficient patients and mouse model *Asl*$^{Neo/Neo}$ show dysfunction of glutathione metabolism despite limited evidence of oxidative stress.

(**A**) Glutathione biosynthesis requires precursor metabolites glutamate, glycine and cysteine, the latter being an intermediary metabolite from the transsulfuration pathway. Glutathione is degraded into cysteine-glycine by γ-glutamyl transferase through the γ-glutamyl cycle. (**B**) Mean of plasma total homocysteine in patients with OTCD, ASSD and ASLD. Plasma (**C**) total homocysteine, (**D**) cysteine, (**E**) γ-glutamyl-cysteine and (**F**) total glutathione levels, Liver (**G**) homocysteine, (**H**) cysteine, (**I**) γ-glutamyl-cysteine total thiols and (**J**) total glutathione levels in 2-week old *Asl*$^{Neo/Neo}$ mice and WT littermates. (**K**) GGT activity measured in the liver in 2-week old *Asl*$^{Neo/Neo}$ mice and WT littermates. (**L**) Lipid peroxidation measured by thiobarbituric acid reactive substances in *Asl*$^{Neo/Neo}$ mice and WT littermates. (**M**) Nitric oxide metabolites (nitrite and nitrate) in liver samples of *Asl*$^{Neo/Neo}$ mice and WT littermates. (**N**) Quantification of liver nitrotyrosine levels by western blot between *Asl*$^{Neo/Neo}$ mice and WT. mRNA expression of GCL subunits (**O**) GCLC, (**P**) GCLM and (**Q**) GS in liver of *Asl*$^{Neo/Neo}$ mice compared to WT littermates. Urea cycle dysfunction is shown by purple arrows. (**R**) Ingenuity pathway analysis of liver untargeted proteomics in *Asl*$^{Neo/Neo}$ mice compared to WT littermates, highlighting downregulation of the main glutathione functions, detoxification of xenobiotic and endogenous compounds (black arrows), antioxidant activity (red arrows). (**B**) One-way ANOVA with Tukey's post-hoc test. (**B)** Unpaired two-tailed Student's t test performed on log-transformed data. Graph displays not transformed data. (**C-Q**) Unpaired two-tailed Student's t test; * $p<0.05$, ** $p<0.01$, *** $p<0.001$, ns not significant. **(B)**: OTCD n=11-13, ASSD n=10, ASLD n=13. ASSD: argininosuccinate synthase deficiency; ASLD: argininosuccinate lyase deficiency; CyS: cysteine; GCLC: glutamylcysteine ligase catalytic subunit; GCLM: glutamylcysteine ligase modifier subunit; GS: glutathione synthase; GGT:

Gamma-glutamyl transferase; GSH: glutathione; HcyS: homocysteine; MDA: malondialdehyde; OTCD: ornithine transcarbamylase deficiency. Graphs show means ±SD.

Figure 2: A non-invasive marker confirms the impaired glutathione metabolism in *Asl*$^{Neo/Neo}$ mice.

(A) Schematic overview of system x_C^- function, shuttling cystine, glutamate and [^{18}F]FSPG (red) across the cell membrane. Reduced cystine, cysteine, and glutamate are precursors for glutathione biosynthesis. **(B)** Representative PET/CT images of [^{18}F]FSPG distribution (%ID/g), in the coronal and axial plane, of 2 week old WT littermates and *Asl*$^{Neo/Neo}$ mice with increased [^{18}F]FSPG retention present in the liver and skin of *Asl*$^{Neo/Neo}$ mice. **(C)** Quantified [^{18}F]FSPG retention in the liver. **(D)** Western blot of liver xCT expression, xCT is upregulated in the liver of *Asl*$^{Neo/Neo}$ mice. **(E)** Quantified [^{18}F]FSPG retention in the skin of WT and *Asl*$^{Neo/Neo}$ mice. (**F**) H&E stain from skin of Asl$^{Neo/Neo}$ and WT mice showing architectural differences highlighting the skin abnormality observed in ASL deficiency. (**B**) P= pancreas, B=bladder, K=kidney. (**C, E**) Unpaired 2-tailed Student's t test; **p<0.01, Graph shows mean ±SD. Scale bar is 100 μm.

Figure 3: Single intravenous administration of *hASL* mRNA corrects ureagenesis up to 7 days in adult *Asl*$^{Neo/Neo}$ mice

(A) Schematic illustration of experimental plan. Three-week old *Asl*$^{Neo/Neo}$ mice received a single intravenous (IV) injection of either *hASL* or *Luc* mRNA at 1mg/kg body weight and were sacrificed at 2h, 24h, 72h or 7 days. **(B**) Average ammonia levels from plasma and average (**C**) argininosuccinic acid (**D**) citrulline levels from dried blood spots at 2, 24, 72 hours and 7 days. (**E**) Urine orotic acid levels normalised to creatinine at 24 hours. (**F**) ASL liver western blot at 24 hours, 72 hours and 7 days. (**G**) Quantification of ASL immunoblot normalised to GAPDH (**H**) Representative images of liver ASL immunostaining at 24 hours post mRNA administration and (**I**) Quantification. Scale bar= 100µM. (**J**) Liver ASL activity at 2, 24, 72 hours and 7 days. Values normalised against WT control. (**B, D, G, J**) Two-way ANOVA with Šídák's post-hoc test per timepoint. (**C**) Two-way ANOVA with Šídák's post-

hoc test per timepoint post log transformation, (**E**) One-way ANOVA post Tukey's post-hoc test comparison post log-transformation (**I**) One-way ANOVA post Tukey's post-hoc test comparison, ns=not significant, *p<0.05, **p<0.01, ***p<0.005, ****p<0.0001. (**B-D, G, J**) Grey dotted line represents mean WT values. Graph shows mean ±SD.

Figure 4: *hASL* mRNA therapy from birth normalises the phenotype of *Asl*$^{Neo/Neo}$ mice.

(**A**) Schematic illustration of experimental plan. *Asl*$^{Neo/Neo}$ mice were given weekly intravenous (IV) dose of 1mg/kg of either *hASL* or *Luc* mRNA from birth up to 7 weeks, except for week 1 where the mice were administered intraperitoneally with dose of 2mg/kg. Harvest was performed 48 hours post the last injection. (**B**) Kaplan-Meier survival curve of *hASL* and *Luc*-mRNA treated *Asl*$^{Neo/Neo}$ mice. (**C**) Average growth curve of WT, *hASL* and *Luc*-mRNA treated *Asl*$^{Neo/Neo}$ mice. (**D**) Representative images of wild-type (blue asterisk), *hASL* (red asterisk) and *Luc* mRNA (black asterisk) treated *Asl*$^{Neo/Neo}$ mice at harvest. (**E**) Average plasma ammonia concentration, (**F**) argininosuccinic acid (**G**) and citrulline concentrations from dried blood spots, (**H**) urine orotic acid and (**I**) C13 ureagenesis from WT, *hASL* and *Luc*-mRNA treated *Asl*$^{Neo/Neo}$ mice. (**J**) ASL western blot of WT, *hASL* and *Luc*-mRNA treated *Asl*$^{Neo/Neo}$ mice and (**K**) quantification. (**L**) Representative images of ASL immunostaining in livers of WT, *hASL* and *Luc*-mRNA treated *Asl*$^{Neo/Neo}$ mice and (**M**) quantification. (**N**) Liver ASL activity from WT, *hASL* and *Luc*-mRNA treated *Asl*$^{Neo/Neo}$ mice livers (**D**) Scale bar=2cm. (**L**) Scale bar= 100µM. (**B**) Log-rank (Mantel-Cox) (**C**) Simple linear regression analysis comparing average slopes per group. (**D**) Scale bar=2cm. (**E, G-I, K, M, N**) One-way ANOVA with Tukey's post-hoc test analysis, (**F**) One-way ANOVA post Tukey's post-hoc test comparison on log-transformed values, ns=not significant, *p<0.05, **p<0.01, ***p<0.005, ****p<0.0001. **(C-H, M, N)**. Graph shows mean ±SD.

Figure 5: *hASL* mRNA therapy partially rescues the adult phenotype in *Asl*$^{Neo/Neo}$ mice.

(**A**) Schematic illustration of experimental plan. *Asl*$^{Neo/Neo}$ mice were given weekly intravenous (IV) dose of 1mg/kg of either *hASL* or *Luc* mRNA from day 21 up to 9 weeks. (**B**) Kaplan-Meier survival

curve of *hASL* and *Luc*-mRNA treated *Asl*$^{Neo/Neo}$ mice. (**C**) Average growth curve of WT, *hASL* and *Luc*-mRNA treated *Asl*$^{Neo/Neo}$ mice. (**D**) Representative images of WT, *hASL* and *Luc* mRNA treated *Asl*$^{Neo/Neo}$ mice at harvest. (**E**) Average plasma ammonia concentration, (**F**) argininosuccinic acid (**G**) and citrulline concentrations from dried blood spots, (**H**) urine orotic acid and (**I**) C13 ureagenesis from WT, *hASL* and *Luc*-mRNA treated *Asl*$^{Neo/Neo}$ mice. (**J**) ASL western blot of WT, *hASL* and *Luc*-mRNA treated *Asl*$^{Neo/Neo}$ mice and (**K**) quantification (**L**) Liver ASL activity from WT, *hASL* and *Luc*-mRNA treated *Asl*$^{Neo/Neo}$ mice livers (**B**) Log-rank (Mantel-Cox), p=0.0025 (**C**) Simple linear regression analysis comparing average slopes per group. (**D**) Scale bar=2cm. (**F-I, K, L**) One-way ANOVA with Tukey's post-hoc test analysis. (**E**) One-way ANOVA with Tukey's post-hoc test analysis on log-transformed values ns=not significant, *p<0.05, **p<0.01, ****p<0.0001. **(C-D, E-H, K, L)** Graph shows mean ±SD.

Figure 6: *hASL* mRNA therapy corrects the dysfunction of glutathione metabolism in *Asl*$^{Neo/Neo}$ mice.

(A) [^{18}F]FSPG distribution (%ID/g) in representative coronal and axial plane PET/CT images of WT, untreated *Asl*$^{Neo/Neo}$ and *hASL* mRNA treated *Asl*$^{Neo/Neo}$ mice. **(B)** [^{18}F]FSPG quantification of the liver in WT, untreated *Asl*$^{Neo/Neo}$ and *hASL* mRNA treated *Asl*$^{Neo/Neo}$ mice**. (C**) Western blot of xCT expression, upregulated xCT in untreated *Asl*$^{Neo/Neo}$ liver is decreased in the liver of *hASL* mRNA treated *Asl*$^{Neo/Neo}$ mice. **(D)** Total glutathione levels from liver in WT, Luc mRNA treated *Asl*$^{Neo/Neo}$ mice and *hASL* mRNA treated *Asl*$^{Neo/Neo}$ mice from neonatal or adulthood. **(E)** Liver total homocysteine concentrations expressed as ratio out of WT levels (shown as dotted line) from untreated versus *hASL* mRNA treated *Asl*$^{Neo/Neo}$ mice in adulthood. Graph shows mean ±SD. (**A**) K= Kidney, P= Pancreas. (**B, D**) One-way ANOVA with Tukey's post-hoc test; (**E**): Unpaired 2-tailed Student's t test; ns=not significant, **p<0.01, ***p<0.001, ****p<0.0001.

Figure 7: *hASL* mRNA therapy corrects the metabolic dysfunction and liver pathophysiology in *Asl*$^{Neo/Neo}$ mice.

(A) Principal component analysis plots comparing treatment applied (untreated WT, *hASL* or *Luc* mRNA) and mouse genotype (WT or *Asl*$^{Neo/Neo}$) with percentage of variance associated with each axis. (**B**) Volcano plots showing differential gene expression (DEG) analysis of *Luc* mRNA vs WT, (**C**) *hASL* mRNA vs WT and (**D**) *hASL* mRNA vs *Luc* mRNA. Scatter plots show log transformed adjusted p-values (<0.05) on the y-axis against log2 fold change (>0.10) values on the x-axis. Blue and red dots represent genes that are significantly downregulated and upregulated respectively between groups. Grey dots represent genes that are not significantly altered. (**E**) Pathway analysis highlighting genes of interest significantly altered in DEG analysis organised with their associated pathways when comparing *Luc* mRNA vs WT and *hASL* mRNA vs *Luc* mRNA groups. mRNA expression of **(F)** GCLC and **(G)** GCLM with NO donor SNAP at 200µM versus control DMSO in Huh7 cells. (**H**) Schematic highlighting the ureagenesis defect, NO deficiency, subsequent downregulation of glutathione biosynthesis and increased glutathione recycling in the liver caused by ASL deficiency. All these pathways are corrected by mRNA therapy. (**F, G**): Unpaired 2-tailed Student's t test; ns=not significant, ***p<0.001, ****p<0.0001. (**F, G**): average values from 3 independent experiments. Each dot represents one experiment.

FIGURES

Figure 1

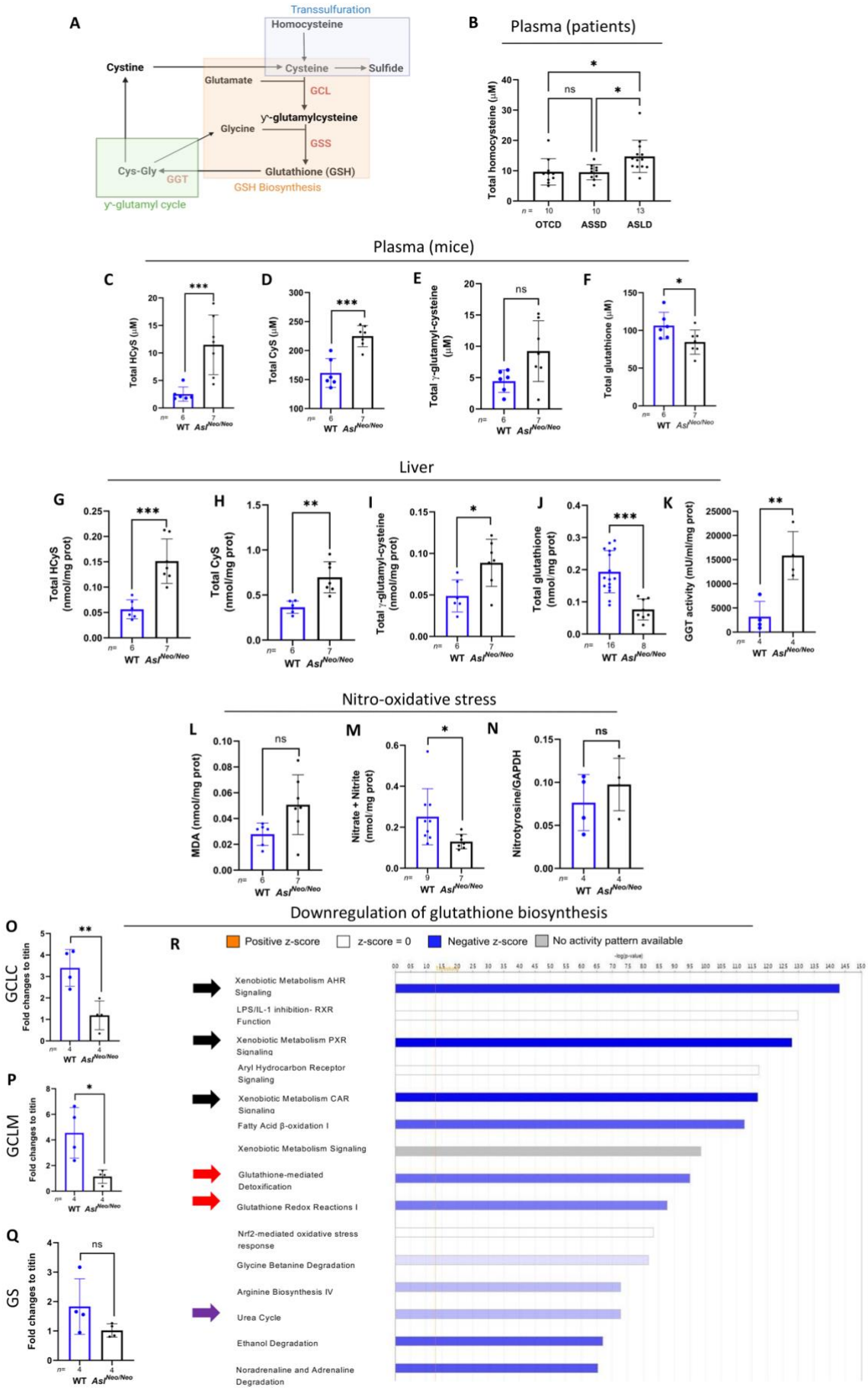
A
Transsulfuration
Homocysteine
Cystine
Cysteine
Sulfide
Glutamate
GCL
γ-glutamylcysteine
Glycine
GSS
Cys-Gly
GGT
Glutathione (GSH)
GSH Biosynthesis
γ-glutamyl cycle
B
Plasma (patients)
Total homocysteine (µM)
ns
OTCD
ASSD
ASLD
Plasma (mice)
C
Total HCyS (µM)
D
Total CyS (µM)
E
Total γ-glutamyl-cysteine (µM)
F
Total glutathione (µM)
WT
Asl Neo/Neo
Liver
G
Total HCyS (nmol/mg prot)
H
Total CyS (nmol/mg prot)
I
Total γ-glutamyl-cysteine (nmol/mg prot)
J
Total glutathione (nmol/mg prot)
K
GGT activity (mU/ml/mg prot)
Nitro-oxidative stress
L
MDA (nmol/mg prot)
M
Nitrate + Nitrite (nmol/mg prot)
N
Nitrotyrosine/GAPDH
Downregulation of glutathione biosynthesis
O
GCLC
Fold changes to titin
P
GCLM
Q
GS
R
Positive z-score
z-score = 0
Negative z-score
No activity pattern available
Xenobiotic Metabolism AHR Signaling
LPS/IL-1 inhibition- RXR Function
Xenobiotic Metabolism PXR Signaling
Aryl Hydrocarbon Receptor Signaling
Xenobiotic Metabolism CAR Signaling
Fatty Acid β-oxidation I
Xenobiotic Metabolism Signaling
Glutathione-mediated Detoxification
Glutathione Redox Reactions I
Nrf2-mediated oxidative stress response
Glycine Betanine Degradation
Arginine Biosynthesis IV
Urea Cycle
Ethanol Degradation
Noradrenaline and Adrenaline Degradation

Figure 2

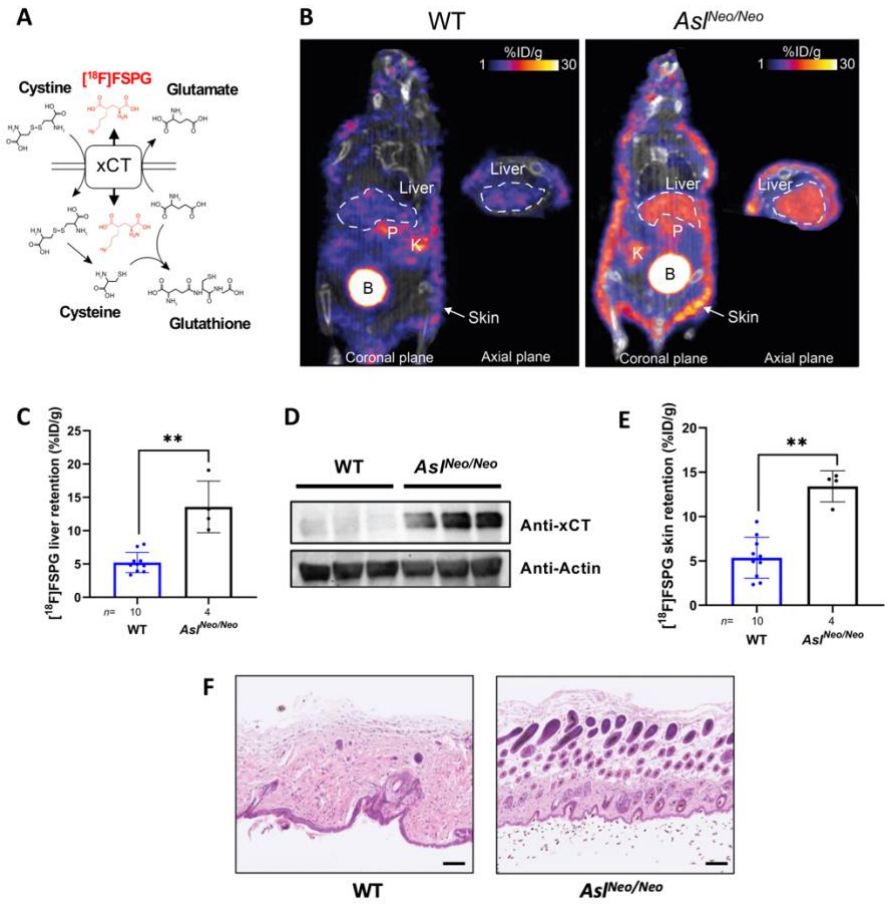
A
Cystine
[18F]FSPG
Glutamate
xCT
Cysteine
Glutathione
B
WT
Asl Neo/Neo
%ID/g
1
30
Liver
P
K
B
Skin
Coronal plane
Axial plane
C
[18F]FSPG liver retention (%ID/g)
**
n= 10 4
WT
Asl Neo/Neo
D
WT
Asl Neo/Neo
Anti-xCT
Anti-Actin
E
[18F]FSPG skin retention (%ID/g)
**
n= 10 4
WT
Asl Neo/Neo
F
WT
Asl Neo/Neo

Figure 3

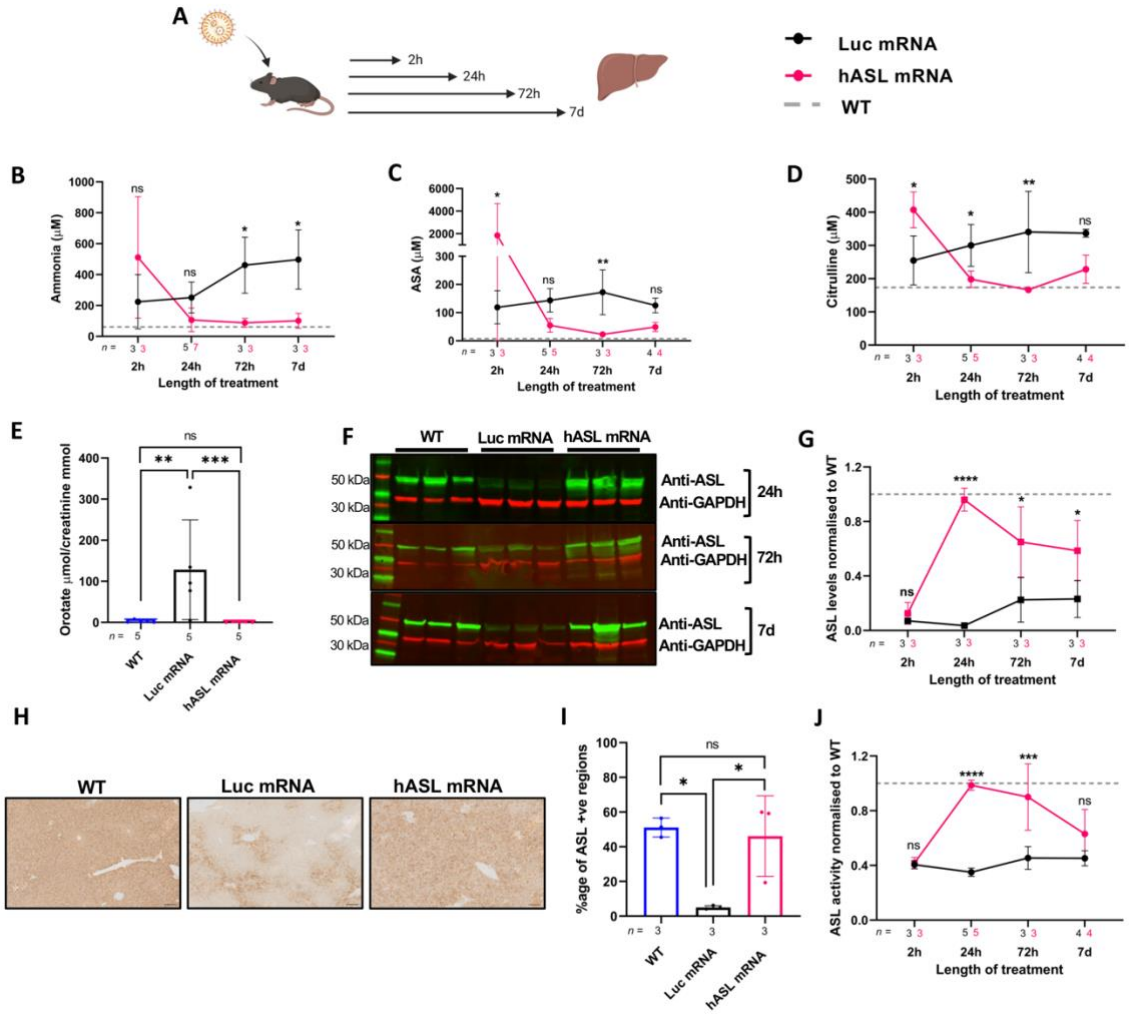
A
2h
24h
72h
7d
Luc mRNA
hASL mRNA
WT
B
Ammonia (μM)
Length of treatment
C
ASA (μM)
Length of treatment
D
Citrulline (μM)
Length of treatment
E
Orotate μmol/creatinine mmol
WT
Luc mRNA
hASL mRNA
F
WT
Luc mRNA
hASL mRNA
50 kDa
30 kDa
Anti-ASL
Anti-GAPDH
24h
72h
7d
G
ASL levels normalised to WT
Length of treatment
H
WT
Luc mRNA
hASL mRNA
I
%age of ASL +ve regions
WT
Luc mRNA
hASL mRNA
J
ASL activity normalised to WT
Length of treatment

Figure 4

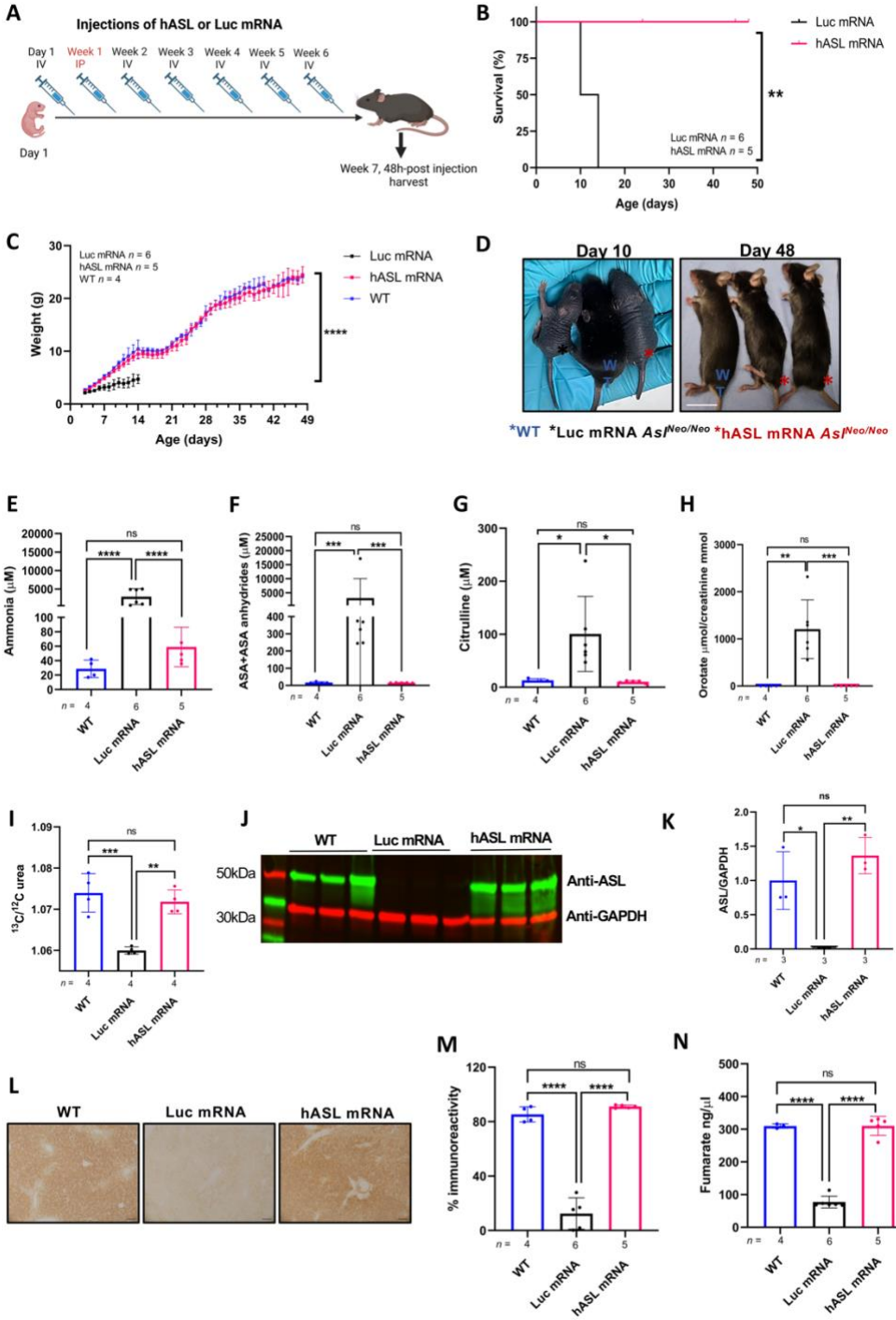
A
Injections of hASL or Luc mRNA
Day 1 IV
Week 1 IP
Week 2 IV
Week 3 IV
Week 4 IV
Week 5 IV
Week 6 IV
Day 1
Week 7, 48h-post injection harvest
B
Survival (%)
Age (days)
Luc mRNA
hASL mRNA
Luc mRNA n = 6
hASL mRNA n = 5
**
C
Weight (g)
Age (days)
Luc mRNA n = 6
hASL mRNA n = 5
WT n = 4
Luc mRNA
hASL mRNA
WT
****
D
Day 10
Day 48
*WT *Luc mRNA Asl Neo/Neo *hASL mRNA Asl Neo/Neo
E
Ammonia (μM)
F
ASA+ASA anhydrides (μM)
G
Citrulline (μM)
H
Orotate μmol/creatinine mmol
I
13C/12C urea
J
WT
Luc mRNA
hASL mRNA
50kDa
30kDa
Anti-ASL
Anti-GAPDH
K
ASL/GAPDH
L
WT
Luc mRNA
hASL mRNA
M
% immunoreactivity
N
Fumarate ng/μl
ns

Figure 5

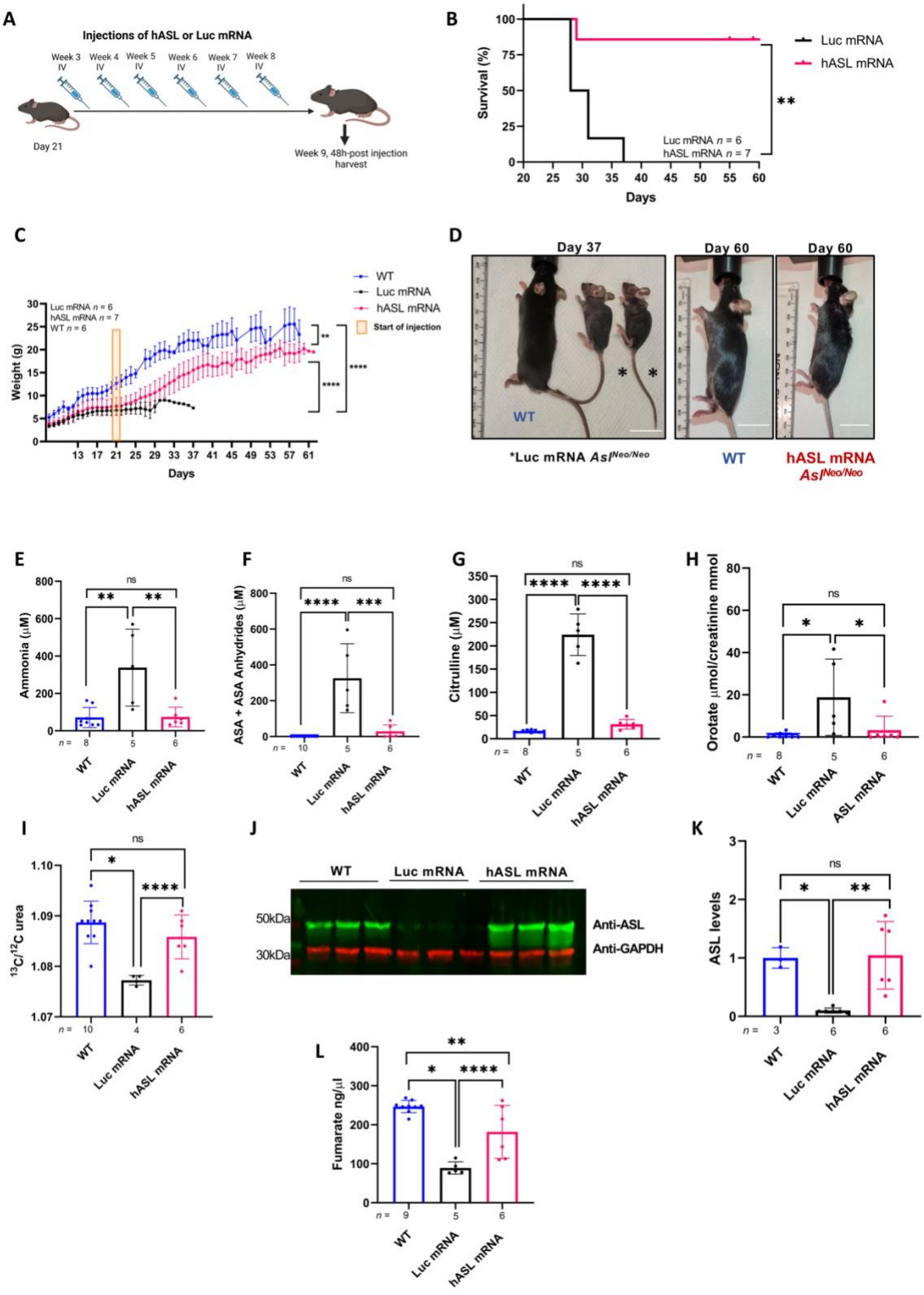

975

976

977 **Figure 6**

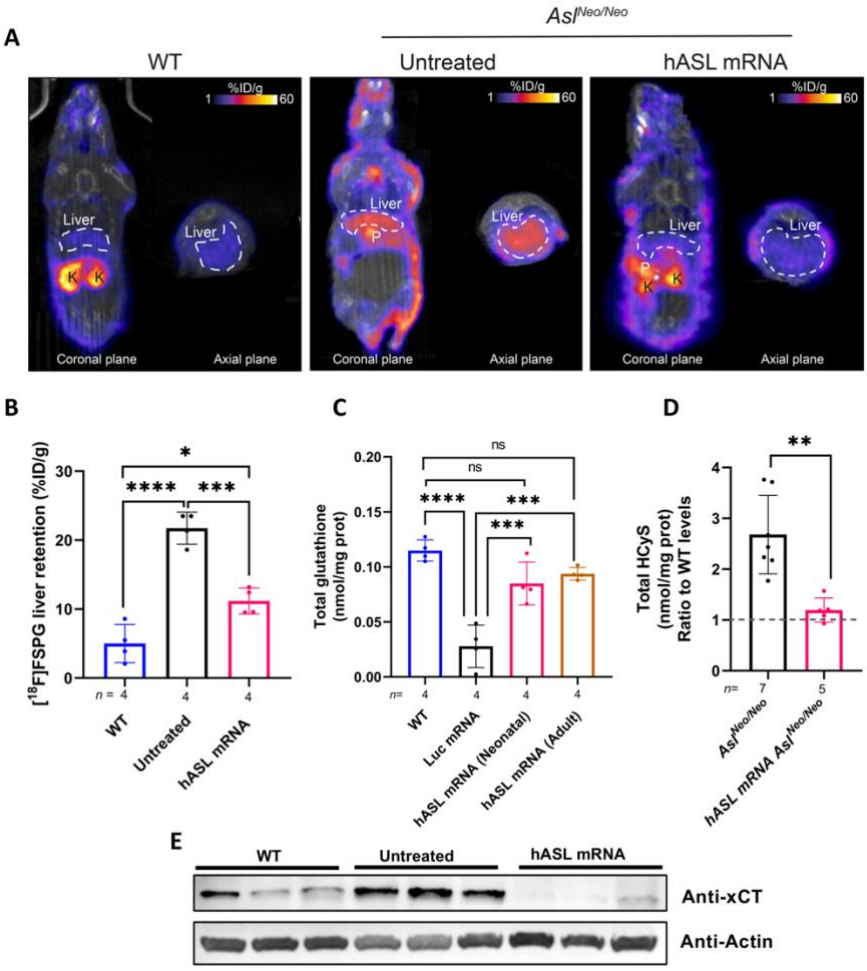

978

979

980

981

982

983

984

985

986

Figure 7

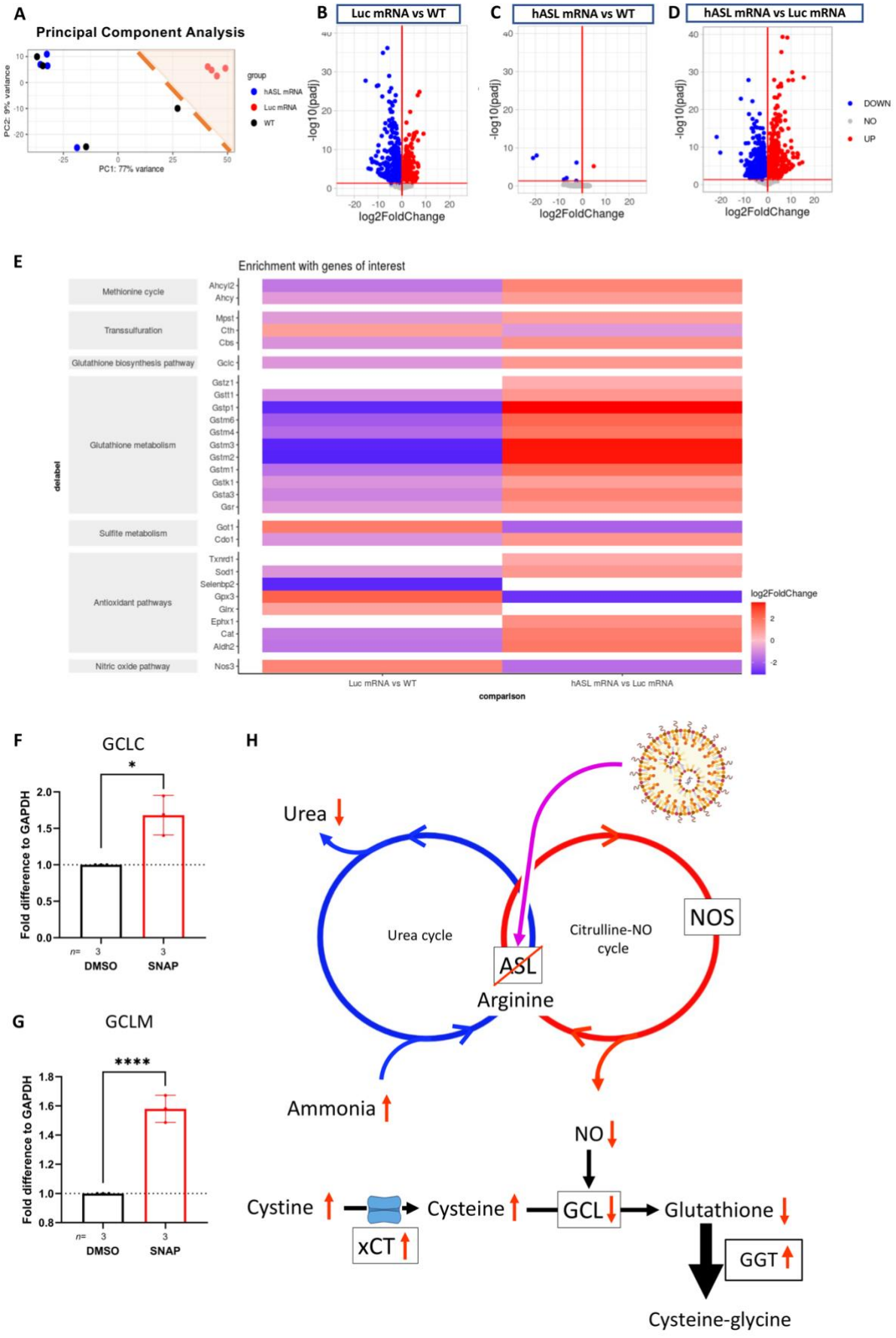
A
Principal Component Analysis
PC2: 9% variance
PC1: 77% variance
group
hASL mRNA
Luc mRNA
WT
B
Luc mRNA vs WT
C
hASL mRNA vs WT
D
hASL mRNA vs Luc mRNA
-log10(padj)
log2FoldChange
DOWN
NO
UP
E
Enrichment with genes of interest
Methionine cycle
Ahcyl2
Ahcy
Transsulfuration
Mpst
Cth
Cbs
Glutathione biosynthesis pathway
Gclc
Glutathione metabolism
Gstz1
Gstt1
Gstp1
Gstm6
Gstm4
Gstm3
Gstm2
Gstm1
Gstk1
Gsta3
Gsr
Sulfite metabolism
Got1
Cdo1
Antioxidant pathways
Txnrd1
Sod1
Selenbp2
Gpx3
Glrx
Ephx1
Cat
Aldh2
Nitric oxide pathway
Nos3
delabel
log2FoldChange
Luc mRNA vs WT
hASL mRNA vs Luc mRNA
comparison
F
GCLC
Fold difference to GAPDH
n= 3 3
DMSO
SNAP
G
GCLM
Fold difference to GAPDH
n= 3 3
DMSO
SNAP
H
Urea
Urea cycle
Citrulline-NO cycle
NOS
ASL
Arginine
Ammonia
NO
Cystine
xCT
Cysteine
GCL
Glutathione
GGT
Cysteine-glycine

Supplementary Materials

This word file includes:

- Material and Methods
- Figs. S1 to S11
- Tables S1 to S7
- Data File S1
- References 68-78

Materials and Methods

mRNA formulation: *hASL* and Luciferase (*Luc*) encoding mRNA encapsulated in Lipid Nanoparticles (LNPs) were provided by Moderna Inc. using their proprietary technology. Codon optimized mRNA encoding *hASL* was synthesized in vitro by T7 RNA polymerase-mediated transcription. The mRNA initiated with a cap, followed by a 5' untranslated region (UTR), an open reading frame (ORF) encoding *hASL*, a 3' UTR and a polyadenylated tail. Uridine was globally replaced with N1-methylpseudouridine, previously described (*68*). For in vivo intravenous delivery, LNP formulations were generated. Briefly, mRNA was mixed with lipids at a molar ratio of 3:1 (mRNA:lipid), previously described (*36*). mRNA-loaded nanoparticles were exchanged into final storage buffer and had particle sizes of 80 – 100 nm, >80% encapsulation of the mRNA by RiboGreen assay, and <10 EU/mL endotoxin levels.

Patient Sample Study: Patients with ornithine transcarbamylase deficiency (OTCD), argininosuccinate synthase deficiency (ASSD) and argininosuccinate lyase deficiency (ASLD) followed at Great Ormond Street Hospital for Children NHS Foundation Trust, London, UK were asked to join a study with research ethics consent 13/LO/0168 issue by the Health Research Authority. Biological data were analysed anonymously.

Animals: Animal procedures were approved by institutional ethical review and performed per UK home office licenses PP9223137, 70/14300 and PEFC6ABF1. *Asl*$^{Neo/Neo}$ mice (B6.129S7-*Asl*^{tm1Brle}/J) were purchased from Jackson Laboratory (strain #018830; Bar Harbor, ME), and maintained on standard rodent chow (Harlan 2018, Teklab Diets, Madison, WI) with free access to water in a 12-hour light / 12 hours dark environment. WT littermates were used as controls and housed in the same cages. Genotyping was performed using DNA extracted from tail clips as previously described (*9*). In-life blood collection for longitudinal analysis was performed via tail-bleed and terminal blood collection via cardiac puncture, followed by cervical dislocation for harvest. Urine samples were collected longitudinally and post-harvest on Whatman filter paper. Animals were culled either at the stated endpoint or at the occurrence of >15% body weight loss and/or reaching severity limit.

Pharmacokinetics and survival studies: *Asl*$^{Neo/Neo}$ animals were given systemic administration of *hASL* mRNA or *Luc* mRNA at dose of 1mg/kg or 2mg/kg for IV and IP injections, respectively. Untreated WT littermates were used as controls. For pharmacokinetics experiment, *Asl*$^{Neo/Neo}$ mice were administered IV via tail-vein at 3-weeks of age and harvested at either 2, 24, 72 h or 7 days. In survival study for animals treated from birth, neonate pups at day 1 were administered mRNA intravenously through the temporal superficial vein, followed by intraperitoneal IP administration at day 7 at dose of 2 mg/kg and IV administration via tail-vein weekly from day 14 onwards up to 7-weeks of age. In survival study of animals treated from early adulthood, mice were given weekly IV administration through tail-vein from day 21 onwards up to 9-weeks of age. All harvests were performed 48 h following the last injection. Mutant mice were assigned randomly to study groups. All animals were monitored and weighted daily. In-life blood collection for longitudinal analysis was performed via tail-bleed and terminal blood collection via cardiac puncture, followed by cervical dislocation for harvest. Urine samples were collected longitudinally and post-harvest on Whatman filter paper. Animals were culled either at the stated endpoint or at the occurrence of >15% body weight loss and/or reaching severity limit.

[^{18}F]FSPG PET imaging: [^{18}F]FSPG was synthesized using a GE FASTlab automated synthesis module and quality control performed as previously reported (*69*). Anaesthetized (1.5-2% isoflurane in

O_2) 2-3 week old *Asl*$^{Neo/Neo}$ mice with age-matched WT littermates were imaged following IV injection of 1-3 MBq of radiotracer. For rescue experiment with mRNA therapy, *Asl*$^{Neo/Neo}$ mice were given 1 mg/kg IV dose of *hASL* mRNA dose at day 1 of birth followed with weekly 2 mg/kg IP injection. Age-matched control untreated *Asl*$^{Neo/Neo}$ and WT littermates were included. For all animals, dynamic PET scans were acquired between 40 and 90 min post-injection on a Mediso NanoScan PET/CT system (1-5 coincidence mode; 3D reconstruction; CT attenuation-corrected; scatter corrected) using a four-bed mouse hotel (Mediso) (*70*). CT images were acquired for anatomical visualization (360 projections; helical acquisition; 55 kVp; 600 ms exposure time). A dynamic iterative reconstruction algorithm, Tera-Tomo 3D ($0.4 \times 0.4 \times 0.4$ mm^3 voxel size), was used with attenuation, scatter, and random coincidences correction. Radiotracer concentration was quantified using VivoQuant software (v 2.5, Invicro Ltd), with volumes of interest drawn manually using the CT image as reference. Data were expressed as percent injected dose per gram of tissue (% ID/g). Following [^{18}F]FSPG PET, mice were culled by cervical dislocation and liver, skin and other tissue was collected, snap frozen and moved to a -80°C freezer for later *ex vivo* analysis.

Ammonia and ALT measurement: To obtain plasma samples, whole blood was collected in EDTA tube (Sarstedt, Germany) and centrifuged immediately at 13,000 rpm for 5 min at room temperature. Supernatant was then transferred into a microcentrifuge tube and stored at -80^{o}C. Ammonia and ALT reads were obtained from Fujifilm NX600 machine using ammonia and ALT cartridges respectively (Fujifilm, Japan) using 10µl plasma volume (diluted vol:vol 1:3 in PBS).

Amino acid analysis: Liquid chromatography-Mass spectrometry (LC-MS/MS) was used for amino acid measurements (argininosuccinic acid and L-citrulline) from dried bloodspots as described previously (*6*) using the hydrophilic interaction liquid chromatography (HILIC) separation of metabolites, method adapted from (*71*). Briefly, 40µl of whole blood was spotted on Guthrie blood spot card, dried at room temperature for 24h and stored in -20^{o}C in a foil bag with desiccant. 3mm blood spot punch was extracted in 100µl methanol containing stable isotopes (2nmol/l, L-citrulline-d7, CDN isotopes, Pomite-Claire, Quebec), used as internal standards, for 15 min in sonicating waterbath at room temperature. The supernatant was collected and dried using Eppendorf® Concentrator Plus and

resuspended in 80µl of 0.05M HCl, topped with 280µl of Solvent A (10mM ammonium formiate+85% Acetonitrile (ACN)+0.15%Formic acid (FA)), centrifuged at 16,000rpm for 5 min and supernatant taken for analysis.

Acquity UltraPure Liquid Chromatography (UPLC)-system (Waters, Manchester, UK) using Acquity UPLC BEH Amide column (2.1x100mm, 1.7µm particle size) and Van Guard™ UPLC BEH Amide pre-column (2.1x5mm, 1.7µm particle size) (Waters Limited, UK) was used for amino acid chromatography. The mobile phases were (A) 10mM ammonium formiate in 85% ACN and 0.15% FA and (B) 15mM ammonium formiate containing 0.15% formic acid, pH 3.0. Detection was performed using a tandem mass spectrometer Xevo TQ-S (Waters, Manchester, UK) using multiple reaction monitoring in positive ion mode. The dwell time was set automatically with MRM-transition of 291.2>70.2, 273.2>70.2 and 176.1>159 respectively for ASA, ASA-anhydrides and L-citrulline. L-Citrulline-d7 (183.15>166.05) was used as internal standard control. Argininosuccinate data were analysed using Masslynx 4.2 software (Micromass UK Ltd, Cheshire, UK) and TargetLynx™ application manager used for subsequent batch analysis.

Nitric oxide metabolites: Plasma samples were pre-treated with N-ethylmaleimide (NEM) and deproteinised by precipitation with methanol (v:v 1:1), followed by centrifugation at 16,000 ×g for 20 min. Liver samples were diluted 1:3 (w/v) with homogenisation solution (10mM PBS supplemented with 10mM NEM and 2.5mM EDTA) and homogenised on ice using an all-glass Kimble tissue grinder in combination with a GlasCol GT Series stirrer (8 up-and down strokes). Tissue homogenates were deproteinized in the same manner as plasma. Deproteinized samples were analysed for nitrate (NO_3^-) and nitrite (NO_2^-) using a dedicated high-performance liquid chromatography analyser (ENO20, Eicom) as described (*72*).

Tissue homogenates were analysed for content of total nitrosation products (RXNO) by gas-phase chemiluminescence of bound NO following reductive denitrosation. Nitrite was removed from sample aliquots by addition of 10% (v:v) of a reaction solution comprising 5% sulfanilamide in 1 M HCl and reaction for 15 min prior to injection into an acidic triiodide-containing reduction chamber. The amount

of NO liberated from low-molecular weight and protein nitroso-species was quantified by a gas-phase chemiluminesence analyser (CLD 77 am sp, EcoPhysics), as previously described (*72*).

Oxidative stress marker and thiol redox status: Circulating lipid peroxidation products in plasma were evaluated by measuring the thiobarbituric acid reactive substances (TBARS) essentially as described elsewhere (*73*). Malondialdehyde (MDA), a major breakdown product of the peroxidation of unsaturated fatty acids, in plasma or liver homogenate reacts with thiobarbituric acid, at high temperature and acidic conditions, to form a coloured adduct with maximum absorption at 532 nm. After subtraction of background coloration, the resultant absorbance at 532 nm in the sample is then compared to that of a standard curve of solutions of known concentrations of MDA.

Thiol redox status in plasma and liver homogenates was measured using ultra-high performance liquid chromatography tandem mass spectrometry (UPLC-MS/MS) following derivatization with the thiol alkylans NEM, as described in detail elsewhere (*74*). The LC-MS system was used to separate and quantify the biological aminothiols including total glutathione (GSH and GSSG), cysteine (CyS), cystine (CySS), homocysteine (HCyS), homocystine (HCySS), glutamyl-cysteine, cysteinylglycine as well as sulfide. In addition to the free thiols in the sample, their total concentrations (free + protein-bound forms and disulfides) were determined after sample pre-processing with dithiothreitol (DTT). For this purpose, aliquots of plasma and tissue homogenates already reacted with NEM were subjected to reduction by addition of 50mM DTT (1:1 v:v). Following incubation for 30 min at room temperature for complete reduction, excess NEM (100mM; 1:10, v:v) was added for derivatization of the liberated thiols and samples were processed as before. NEM-derivatized sample aliquots were spiked with stable-isotope labelled internal standards, subjected to ultrafiltration for protein removal and diluted in 10 mM ammonium phosphate buffer before analysis by LC-MS/MS.

ASL enzyme activity: For liver ASL activity, 20-30mg of liver was homogenised in 400µl of cold homogenising buffer (50mM phosphate buffer pH 7.5 and 1x Roche EDTA-free protease inhibitor (Roche, Switzerland)) using Precellys homogeniser tube (VWR, UK) and Precellys 24 tissue homogeniser (Bertin Instruments, France), centrifuged at 10000g for 20 min at 4^{o}C and protein levels measured from the supernatant using BCA kit (ThermoFisher Scientific, Rockford, IL, USA). 60µg of

protein lysate was incubated with 3.6mM ASA in final volume of 50µl, incubated at 37ºC for 1h followed by reaction termination at 80ºC for 20 min. The mixture was centrifuged at 10000g for 5 min and 5µl of the supernatant was used to measure fumarate levels per instruction from the commercial fumarate kit (Abcam, Cambridge, UK).

For ASL enzymatic assay in fibroblasts, 800,000 cells were plated 24h before in a 6cm tissue culture grade dish. 2.5µg of hASL mRNA-LNPs or Luc mRNA-LNPs were transfected and incubated for 48h. Cells were harvested in 250µl of assay buffer provided in fumarate kit. 60µg of protein per samples was incubated with 300µM of ASA in final volume of 100µl, incubated for 15 min at 37ºC followed by reaction termination at 80ºC for 15 min. Samples were then centrifuged at room temperature for 5 min at maximum speed on benchtop centrifuge. 50µl of supernatant was used for fumarate reaction to determine fumarate reaction per the kit instructions.

Orotate measurement: Urine was spotted on a Whatman filter paper and dried over 24h room temperature and stored in -20ºC in a foil bag with desiccant, method adapted from (*75*). For extraction, a 3mm punch of the urine was eluted in 150µl of ddH_2O containing 40µM labelled orotic acid (stable isotope 1,3-15N2 orotic acid, Cambridge isotopes, Andover, MA) and creatinine-D3 (N-Methyl-D3, CDN isotopes) at room temperature for 3h. Orotic acid was analysed in negative ion mode using LC-MS/MS on waters Xevo-TQ-S with MRM transitions (155.1>111.1 and 157.1>113.1) respectively for labelled and unlabelled orotic acid. An isocratic method was used with sample eluted at flow rate of 0.25ml/min with 40% solvent A (water +0.1% FA) and 60% ACN for 1.5 min followed by wash with 100% ACN for 0.5 min and 0.5 min of initial starting condition. Creatinine was used as control to normalise orotic acid levels from the same extracted sample. Creatinine was measured in positive ion mode with MRM transitions (113.95>43.85 and 116.95>46.85) for unlabelled and labelled creatinine respectively with same LC-MS/MS conditions as orotic acid.

Cell culture: Huh7 cells were obtained from Creative Bioarray (CSC-C9441L). Fibroblasts cells were maintained in Dulbecco's modified Eagle medium (ThermoFisher Scientific, 41965062) supplemented with 10% (vol/vol) Fetal Bovine Serum (Sigma-Aldrich, F9665) and 50 units of Penicillin and Streptomycin (ThermoScientific, P4458) and maintained at 37ºC in a humidified 5% CO_2-air

atmosphere. Healthy control fibroblast line was obtained commercially (Lonza, CC-2511). ASL deficient patient fibroblasts were obtained from 2 patients who joint a study with research ethics consent 13/LO/0171 issue by the Health Research Authority. The genotype of patient 1 was c.437G>A / c.437G>A; R146Q / R146Q. The genotype of patient 2 was c.719-2A>G / c.857A>G; ? / GlN286Arg.

In-cell western: Fibroblasts were plated at a density of 5,000 cells per well in a 96 well plate (CellBind 96 well microplates, 66025-626). The next day cells were transfected with 0.2µg of *hASL* mRNA or *Luc* mRNA per well for 24 hours after which the cells were fixed in ice-cold methanol for 15 minutes. Rest of the procedure was performed in room temperature. Following 3 quick washes with 1xPBS, the wells were blocked with Licor blocking buffer (927-40000, Licor, Cambridge, UK) for 90 minutes followed by incubation with Anti-ASL antibody (Abcam) for 2 hours. The wells were washed 3x with 1xPBS, incubated with anti-rabbit secondary (IRDye® 800CW Goat anti-Rabbit IgG 1:1000, 926-32210, Licor) and cell dye (CellTag700, 1:1000, 926-41091, Licor) for 1h and washed 3x with 1xPBS for 5 minutes after. Post final wash, PBS was removed, plates dried and read on Licor Odyssey CLx (settings: 4mm focus offset, lowest setting quality, resolution 169µM, 700 and 800 channel). Acquisition and analysis were performed in the Licor ImageStudio Lite software (Licor, Cambridge, UK).

***Ex vivo* total glutathione quantification:** Frozen liver and skin tissue was thawed on ice and 25-50 mg of tissue was added to prechilled Lysing Matrix D tube (MP Biomedicals) containing ice cold 400 µL 1X passive lysis buffer (Promega; E1941). The tissue was then lysed at 4 °C on a Precellys Evolution (Bertin Technologies, Montigny-le-Bretonneux, France); samples run for five 30s cycles at 6700 RPM. Lysates were centrifuged at 15,000 × *g* for 10 min at 4°C and the supernatant taken for analysis. Total intracellular glutathione was determined using the luminescent-based GSH/GSSG-Glo Assay Kit (Promega; V6611) according to manufacturer's instructions in a white 96-well plate prepared with 5 µL of sample supernatant (neat or 1:10 diluted) along with 5 µL of GSH standards (1-100 µM). Results were normalized to protein concentration, determined using the Pierce™ BCA Protein Assay Kit (ThermoFisher Scientific, Rockford, IL, USA) as per the manufacturer's instructions.

Western blot: Western blot analysis for was carried out using the iBind Flex system (ThermoFisher Scientific, Rockford, IL, USA), a previously published method (*33*), for antibody immunoblotting. To produce lysates frozen liver and skin tissue was processed and the protein concentration determined as above, except, the prechilled ice cold 400 µL RIPA buffer, with 1% Proteinase and phosphatase inhibitors (HALT) was used instead of 1X passive lysis buffer.

Membranes were probed using rabbit polyclonal anti-xCT (1:500; Novus Biologicals; NB300-318). Actin was used as a loading control for all experiments (1:1000; Cell Signaling Technology; 4967). HRP-linked anti-rabbit IgG (1:200, Cell Signalling Technology; 7074) was used as secondary antibody.

Protein bands were visualized using ECL Prime Western Blotting Detection Reagent (Cytiva; RPN2236) as per the manufacturer's instructions and the iBright™ Imaging System (ThermoFisher Scientific, Rockford, IL, USA). Image analysis and band quantification was performed using the iBright™ Analysis Software (ThermoFisher Scientific, Rockford, IL, USA). xCT protein signal per sample was normalised against actin which was used as a loading control.

For ASL and nitrotyrosine levels analysis in liver, 30mg of liver was homogenised in ice-cold 1x RIPA buffer (Cell Signalling) using Precellys homogenising tube and homogeniser, centrifuged at 10000g for 20 min at 4ºC and protein levels measured from the supernatant using BCA kit. 40µg of protein per sample was diluted 1:1 with 2x Laemmli sample buffer (containing 10% 2-β-mercaptoethanol (β-ME)) at final volume of 40µl, vortexed and heated to 95ºC for 10 min. SDS-PAGE was used to separate the proteins at 100V for 1h followed by wet transfer of proteins into an immobilin PVDF membrane at 400mA for 1h. The membrane was blocked in 5% non-fat milk powder in PBS-T (1xPBS with 0.1% tween-20) followed by overnight incubation at 4ºC with primary antibodies (Anti-ASL, Abcam ab97370, 1:1000; Anti-GAPDH mouse, Abcam ab8245, 1:10,000; Anti-nitrotyrosine, Merck 05-233, 1:100; Anti-GAPDH rabbit, Abcam ab9485, 1:1000), 3x 5-min washes with PBS-T, 1h incubation with fluorescent secondary antibodies (IRDye® 800CW Goat anti-Rabbit IgG 1:1000, 926-32210 and IRDye® 680RD Donkey anti-Mouse IgG, 923-68072, Licor) and 3x 5 min washes with PBS-T. Image acquisition and analysis was performed using Licor Odyssey and image analysed using Licor

ImageStudio Lite software. ASL protein signal per sample was normalised against GAPDH which was used as a loading control.

Histology: At harvest, liver was fixed in 10% formalin solution, left at room temperature for 48h before transferring and storing in 70% ethanol. The liver was paraffin embedded and sectioned at 5µM thickness. Sections were dewaxed in histoclear, hydrated through graded ethanol solution to water followed by incubated in 1% H_2O_2 to remove blood stains. Antigen retrieval was performed in boiling 0.01M citrate buffer for 20 min and then cooled to rt. The slides were blocked in 15% goat-serum and TBST-T for 30 min in rt then incubated overnight with primary antibody 9Anti-ASL, ab97370, Abcam, 1:1000) in 10% goat serum and washed 3x with TBST-T. DAB staining was performed using Polink-2 Plus HRP Polymer and AP Polymer detection for Rb antibody kit (D39-18, Origene) following the manufacturer's instructions. The slides were then dehydrated with increasing gradient of ethanol to water and histoclear. The slides were mounted using non-aqueous mounting media – Microscopy DPX (Merck) and dried overnight.

The slides were imaged under Zeiss Axioplan Histology scope at UCL Great Ormond Street Institute of Child Health Imaging Facility. Ten images per condition was taken in random and averaged. Images were analysed using Fiji software using macro written by Dr. Dale Moulding from UCL Great Ormond Street Institute of Child Health Imaging Facility. The macro utilises colour deconvolution to quantify DAB percentage coverage to calculate percentage of ASL positive regions.

Hematoxylin & Eosin (H&E) staining: The paraffin embedded sections were dewaxed in histoclear solution (Scientific Laboratory Supplies, HS-200) for 5 minutes. Sections were then dehydrated through 3 changes of ethanol (100%, 95% to 75%) for 5 minutes each and rinsed in water for 5 min. This was followed by staining in haematoxylin solution (Vector Laboratories, H3401) for 10 minutes and rinsing in running tap water for at least 5 minutes. Staining in working 0.5 % eosin Y solution (Merck, 109844) for 2 minutes was performed and followed by a water wash for 1 min. Dehydration of the samples was finally done through 3 changes of ethanol (from 75%, 95% to 100% ethanol) for 5 minutes each. Clearing of the samples was done using into histoclear. Finally, a drop of DPX mount (Merck, 1.00579.0500) was placed on each tissue and a coverslip added.

GGT Activity: GGT activity was measured using colorimetric Abcam kit (ab241029, Abcam, Cambridge). 10-20mg of frozen liver sample was homogenised in 200µl of GGT Assay Buffer provided in the kit, then centrifuged (13,000g for 10 min) to remove insoluble material. 10µl per sample was used for the assay following kit instructions. The GGT activity was normalised to protein levels per sample.

^{13}C ureagenesis: 30 min pre-harvest animals were given intraperitoneal (IP) administration of 1% body weight labelled sodium acetate (1,2-$^{13}C_2$, 99%, CLM-440-1, CK Isotopes). Plasma was harvested as before and stored at -80^{o}C until analysis. Samples were processed and analysed using isotope-ratio mass spectrometry. Mouse plasma (25 µL) was deproteinized by addition of 25µL of 60% perchloric acid and 0.5 mL 5mM urea (added as unlabelled carrier), sample vortexed, and centrifuged at 21,130g for 5 minutes to remove precipitated protein. The tube was then left uncapped for 30 minutes at room temperature to facilitate evaporation of CO_2. The supernatant was transferred to a new microcentrifuge tube and 100µl 0.5M potassium phosphate added. The pH was adjusted to 4 –7 with 1M KOH solution using pH strips. Sample centrifuged at 21,130g for 5 minutes to remove the precipitated potassium perchlorate. The supernatant was added to an ion exchange column (1ml Dowex-1 1X8-200 resin in empty polypropylene SPE Tube), and eluant collected into a 12ml Exetainer (Labco. UK Ltd). The ion exchange column was washed with 2mL 10 mM HCl, and the eluant combined with the earlier fraction in the Exetainer. Samples were dried under N_2 at 80°C. Dried samples were left uncapped in sealed dessicator for 18 hours with gauze soaked in 1M NaOH to absorb any residual trace of bicarbonate/CO_2.. The tube was sealed with a cap, and flushfilled with 75ml/min helium for 5 minutes per tube. Meanwhile, 8ml 0.5 M potassium phosphate, pH 6.0 was heated to boil for 5 minutes to remove dissolved gas, then cooled. After cooling, 60mg urease dissolved in buffer by very gentle vortexing. 400 µL urease in potassium phosphate buffer injected through the septum of each vial using a gastight syringe, avoiding introduction of any air bubbles. Samples incubated for 60 minutes at 25°C and 100µL 20% phosphoric acid through the septum, using a gastight syringe, avoiding introduction of any air bubbles. Samples incubated for a further 60 minutes at 25°C to allow full release of CO_2. Samples analysed by Thermo-Finnigan DeltaPlus XP Plus isotope ratio-mass spectrometer (ThermoFisher

Scientific, Rockford, IL, USA) with Gasbench sample Introduction unit and CTC GC-PAL autosampler, with 10 technical replicates (final 10 of 15 sample injections of 100µL). Urea production was calculated from the $^{13}CO_2/^{12}CO_2$ ratio, taking into account the initial dilution by carrier urea, and the concentration of urea in the plasma samples.

Bioluminescence imaging: Animals were anesthetized with isoflurane (Abbott Laboratories, Illinois, US), injected intraperitoneally with D-luciferin firefly (15mg/ml in PBS) (L-123-10, Gold Biotechnology, Olivette, US) at a dose of 150mg/kg and imaged 5 min later with a cooled charge-coupled device (CCD) camera in the IVIS® Spectrum in vivo imaging system (IVIS; PerkinElmer, Waltham, US). Grey-scale photographs were acquired with a 24-cm field of view and then a bioluminescence image was obtained using a binning resolution factor of 4, a 1.2/f stop and open filter. Regions of interest (ROIs) were defined manually using a standard area for the mouse liver. Signal intensities were calculated with Living Image software (Perkin Elmer, Waltham, US) and expressed as photons per second per cm^2 per steradian. At each timepoint, bioluminescence imaging was carried out with PBS injected control rodents to establish a median baseline; data points were expressed as fold-change over this internal standard for each individual animal.

Transcriptomics: RNA was extracted from liver samples using Qiagen RNeasy kits (74004) following kit instructions. Liver samples from the WT, Luc mRNA and hASL mRNA neonatal treated group of $Asl^{Neo/Neo}$ mutants were analysed. In all cases, cDNA libraries were prepared using the Kapa mRNA Hyper Prep kit (KapaBiosystem, Pleasanton, CA, USA) according to the manufacturer's instructions, and sequenced on an Illumina NextSeq 1000/2000 to generate ~16 million 50-bp paired end reads per sample (UCL Genomics). Fastp was used for adapter trimming, read filtering and base correction. Processed reads were mapped to the GRCm38 mouse reference genome via STAR using gene annotations from GENODE M29. Normalization and differential gene expression analyses were carried out using the DESeq2 R package (v2.12) (*76*) with differentially expressed genes (DEGs) defined on the basis of a log2-fold change > 0.1 or < -0.1, and an FDR-corrected p-value of < 0.05. Volcano plots were generated to visualize the results of analyses between *Luc* mRNA against WT, *hASL* mRNA against WT, and *hASL* mRNA against *Luc* mRNA. The differential expression of specific genes of

interest was plotted in a heatmap with their respective molecular pathways. The data were visualized using ggplot2R R package (v3.3.5) (*77*). The dataset is available on NCBI Gene Expression Omnibus, accession number GSE222874.

Label Free Proteomics: Excised mouse liver tissue was homogenised on ice in 500 µl of 50 mM Ambic buffer, 2% ASB-14 using the TissueRuptor mechanical homogeniser (Qiagen). After sonication, protein concentration was assessed using the bicinchoninic acid protein assay kit (ThermoFisher Scientific, Rockford, IL, USA). 300 µg of protein for each individual sample was aliquoted for individual analyses. samples then underwent acetone precipitation. The protein pellets were subjected to in-solution digestion as described previously (*78*). Briefly samples were resuspended and reduced using dithioerythritol then subsequently carboamindomethylated using iodoacetamide and digested using 1 µg of sequence grade trypsin gold (Promega). Label free proteomic analysis was performed using a nanoAquity coupled to a Synapt-G2-Si mass spectrometer with high-definition ion mobility capability (Waters, UK) as previously described (*78*). Raw data were analysed using Progenesis LC–MS (Nonlinear Dynamics Limited, Newcastle, UK) raw data was processed as described previously with the Uniprot mouse reference proteome database. Peptide search settings were performed at a 1% false discovery rate with fixed modification for carboamidomethylation of cysteines and variable oxidation of methionine. Protein identifications with a confidence score > 20 and more than one unique peptide were exported for further analysis along with P values and fold changes values determined by Progeneis QI.

Bioinformatics: Ingenuity Pathway Analysis software (Qiagen) was used to perform in depth canonical pathway analysis and determine biological functions altered in the datasets

RT-PCR of GCL and GS: Liver samples were stored frozen at −80 °C before RNA extraction with the RNeasy kit (QIAgen, Crawley, UK) according to the manufacturer's instructions. cDNA was amplified using High-Capacity RNA-to-cDNA™ Kit (Applied Biosystems, Rockford, IL, USA). The GCLC sequence was amplified using the following primers: 5′-ACACCTGGATGATGCCAACGAG-3′ (forward) and 5′-CCTCCATTGGTCGGAACTCTAC-3′ (reverse), the GCLM sequence was

amplified using the following primers: 5′-TCCTGCTGTGTGATGCCACCAG-3′ (forward) and 5′-GCTTCCTGGAAACTTGCCTCAG -3′ (reverse) and the GS sequence was amplified using the following primers: 5′-CCAGGAAGTTGCTGTGGTGTAC-3′ (forward) and 5′-GCTGTATGGCAATGTCTGGACAC-3′ (reverse). Amplification was detected and normalised against Titin which was amplified using the following primers: 5′-AAAACGAGCAGTGACGTGAGC-3′ (forward) and 5′-TTCAGTCATGCTGCTAGCGC-3′ (reverse). Amplification reactions were carried out using 5 µl of sample, 2.5 µmol.l^{-1} of each primer, and SYBR green master mix using the Luna universal qPCR master mix (New England Biolabs, Ipswich, USA) for a 25 µl reaction. The amplification conditions were 95 °C for 10 min followed by 40 cycles of 95°C for 15s, 60°C for 45s. Data were processed with StepOne^{TM} software (ThermoFisher Scientific, Rockford, IL, USA).

For nitric oxide (NO) donor experiment, HuH7 cells were plated at density of 500,000 cells per 6-well TC dish (657 160, Cellstar). The next day cells were treated with NO donor S-nitroso-N-acetylpenicillamine (SNAP) (AB120014, Abcam) at 200µM (dissolved in DMSO (D2438, Sigma-Aldrich)) or vehicle (DMSO) control at the same volume as SNAP for 24 hours. RNA extraction and cDNA synthesis was performed as above. Human GCLC sequence was amplified using the following primers: 5′- GGAAGTGGATGTGGACACCAGA-3′ (forward) and 5′-GCTTGTAGTCAGGATGGTTTGCG-3′ (reverse), the human GCLM sequence was amplified using the following primers: 5′- TCTTGCCTCCTGCTGTGTGATG-3′ (forward) and 5′-TTGGAAACTTGCTTCAGAAAGCAG -3′ (reverse). Amplification was detected and normalised against GAPDH which was amplified using the following primers: 5′-GAAGGTGAAGGTCGGAGTCA-3′ (forward) and 5′- TTGAGGTCAATGAAGGGGTC-3′ (reverse). Amplification reaction was carried out as above.

Reagents and antibodies: Full list of antibodies provided in **Table 1**, reagents in **Table 2** and instruments in **Table 3**.

Table 1: List of primary and secondary antibodies

Antibodies	Host	Company	Catalog num	Dilution used
Anti-ACSL4 [F-4]	Rabbit	Santa Cruz Biotechnology	Sc-365230	1:200 WB
Anti-Actin	Rabbit	Cell Signalling	4967	1:1000 WB
Anti-ASL	Rabbit	Abcam	Ab97370	1:1000 WB and histology
Anti-GAPDH	Mouse	Abcam	Ab97370	1:10000 WB
Anti-GPX4	Rabbit	Abcam	Ab125066	1:500 WB
Anti-Nrf2 (fibroblast)	Rabbit	ThermoFisher	**PA5-27882**	1:500 WB
Anti-Nrf2 (liver)	Rabbit	Abcam	Ab62352	1:500 WB
Anti-GAPDH	Mouse	Abcam	Ab97370	1:10000 WB
Anti-xCT	Rabbit	Novus Biologicals	NB300-318	1:500 WB
Anti-Nitrotyrosine	Mouse	Merck Millipore	05-233 clone 1A6	1:100 WB
Anti-GAPDH	Rabbit	Abcam	Ab9485	1:1000 WB
IRDye® 800CW goat anti-rabbit IgG		Licor	926-32210	1:1000 in-cell 1:10,000 WB
IRDye® 680RD Donkey anti-mouse IgG		Licor	923-68072	1:10,000 WB
CellTag™ 700		Licor	926-41091	1:1000
HRP-linked anti-rabbit IgG		Cell Signalling	7074	1:200 WB

Table 2: List of materials and reagents

Name	Company	Catalog number
1,1,3,3-Tetramethoxypropane (MDBMA)	Sigma-Aldrich	108383-100ML
2,3,4,5,6-Pentafluorobenzyl bromide (PFBBr)	Sigma-Aldrich	101052-5G
2-β-mercaptoethanol (β-ME),	Bio-rad	1610710
4x Laemmli sample buffer	Bio-Rad	1610747
Ammonium Formiate	Sigma-Aldrich	156264
Argininosuccinic Acid disodium salt hydrate	Sigma	A5707
BCA Kit	ThermoFisher	23227
CellBind 96 well microplates	VWR	66025-626
Chameleon® Duo Pre-stained Protein Ladder	Licor	928-60000
D-luciferin firefly	Gold Biotechnology	L-123-10
Dichloromethane	VWR Chemicals	23366.293
DMEM	ThermoFisher	41965-039
DPBS, no calcium, no magnesium-10 x 500 mL	ThermoFisher	14190169
EDTA-free proteinase inhibitor cocktail	Roche	11836170001
ECL Prime Western Blotting Detection Reagent	Cytiva	RPN2236
FBS (Heat-Inactivated)	Sigma	F9665
Fumarate kit	Abcam	Ab102516
Formic Acid 99% Optima™ LC/MS grade	Fisher chemical	A117-50
FUJI DRI-CHEM SLIDE NH3-PIIS	Fujifilm	15809633
FUJI DRI-CHEM SLIDE ALT/GPT-PIIS	Fujifilm	16654035
Gamma glutamyl transferase (GGT) Assay Kit (Colorimetric)	Abcam	Ab241029
Hexane	Sigma-Aldrich	34859-2.5L
HPLC grade Acetonitrile	Fisher Chemical	10660131

HPLC grade Methanol	Fisher chemical	10675112
Hydrochloric acid	BDH	101254H
Licor Blocking buffer	Licor	927-40000
Luminescent-based GSH/GSSG-Glo Assay Kit	Promega	V6611
Lysing Matrix D tube	MP Biomedicals	
Phosphate Buffer Solution 1M pH 7.4	Sigma-Aldrich	P3619-1GA
Polink-2 Plus HRP Polymer and AP Polymer detection for Rb antibody kit	Origene	D39-18
Potassium dihydrogen phosphate	VWR Chemicals	153184U
Precellys ceramic-kit 1.4/2.8 mm 2ml	VWR International	431-0710
PVDF membrane 0.45um	GE healthcare	15259894
Tetrabutylammonium bisulphate (TBA)	Sigma-Aldrich	86868-25G
Qiagen RNeasy kits	Qiagen	74004
L-Arginine	Sigma-Aldrich	A5006
Argininosuccinic Acid (ASA)	Sigma-Aldrich	A5707
L-Citrulline	Sigma-Aldrich	C7629
L-Glutamic Acid	Sigma-Aldrich	G1251
L-Glutamine	Sigma-Aldrich	G3126
Ornithine	Sigma-Aldrich	O2375
Creatinine	Sigma	C4255
Orotic Acid	Sigma	O2750
Urea-^{13}C	Sigma-Aldrich	299359-1G
L-Arginine-13C6	CK Isotopes, Ibstock	CLM-2265-H
L-Citrulline-d7	CDN Isotopes, Pointe-Claire, Quebec	D-7306
L-Glutamic Acid-d5	CDN Isotopes	D-0899

L-Glutamine-13C2	CK Isotopes	CLM-2001
L-Ornithine-d7 HCl	CDN Isotopes	D-7319
1,3-15N2 orotic acid	Cambridge Isotope laboratories	NLM-1048-PK
Creatinine (N-Methyl-D3, 98%)	CDN Isotopes	D-3689
Urea-^{13}C	Sigma-Aldrich	299359-1G
Creatinine (N-Methyl-D3, 98%)	CDN Isotopes	D-3689
Urea-^{13}C	Sigma-Aldrich	299359-1G
Acquity UPLC BEH Amide column (2.1x100mm, 1.7µm particle size)	Waters, UK	186004801
Van Guard™ UPLC BEH Amide pre-column (2.1x5mm, 1.7µm particle size)	Waters, UK	186004799
ACQUITY UPLC BEH C18 Column, 130Å, 1.7 µm, 2.1 mm X 50 mm, 1/pk	Waters, UK	186002350

Table 3: List of instruments

Instrument name	**Company**
Capintech dose calibrator	Mirion medical
Concentrator plus	Eppendorf
DRI-CHEM NX600	Fujifilm
FLUOstar Optima	BMG Labtech
GCMS Instrument	Thermoscientific
iBright™ Imaging System	ThermoFisher Scientific
IVIS® Spectrum In Vivo Imaging System	PerkinElmer, Waltham, US
In cell western Fluorescence Imaging scanner	Licor Odyssey CLx
NanoPET/CT plus system	Mediso

Precellys 24 tissue homogeniser	Bertin instruments
Precellys Evolution	Bertin Technologies
Xevo TQ-S	Waters, UK
Zeiss Axioplan	Zeiss

Supplementary Figures

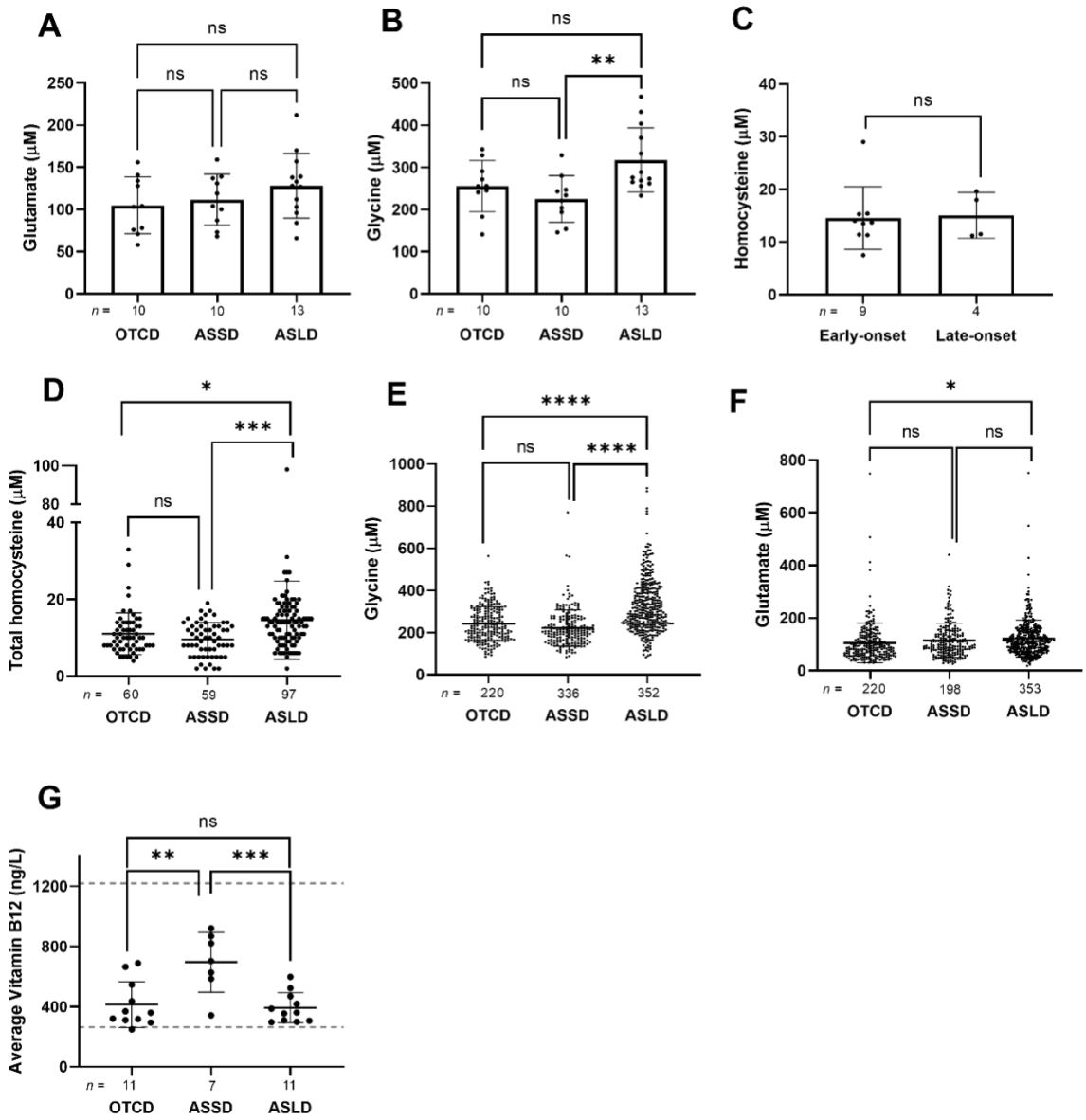

Supplementary Figure 1. Dysfunction of glutathione metabolism in ASL-deficient patients.

Mean of plasma (**A**) glutamate and (**B**) glycine in patients with OTCD, ASSD and ASLD. (**C**) Mean plasma total homocysteine levels between early- and late-onset ASLD. Collated single measurements of plasma (**D**) total homocysteine, (**E**) glycine and (**F**) glutamate (**G**) Plasma vitamin B12 of patients followed for OTCD, ASSD and ASLD, dashed grey lines indicated normal vitamin B12 range. (**A, B, D-F**) One-way ANOVA with Tukey's post-hoc test (**C**) Unpaired two-tailed Student's t test; * $p<0.05$,

*** $p<0.001$, **** $p<0.0001$, ns not significant. (ASSD: argininosuccinate synthase deficiency; ASLD: argininosuccinate lyase deficiency; OTCD: ornithine transcarbamylase deficiency. Graphs show means ±SD.

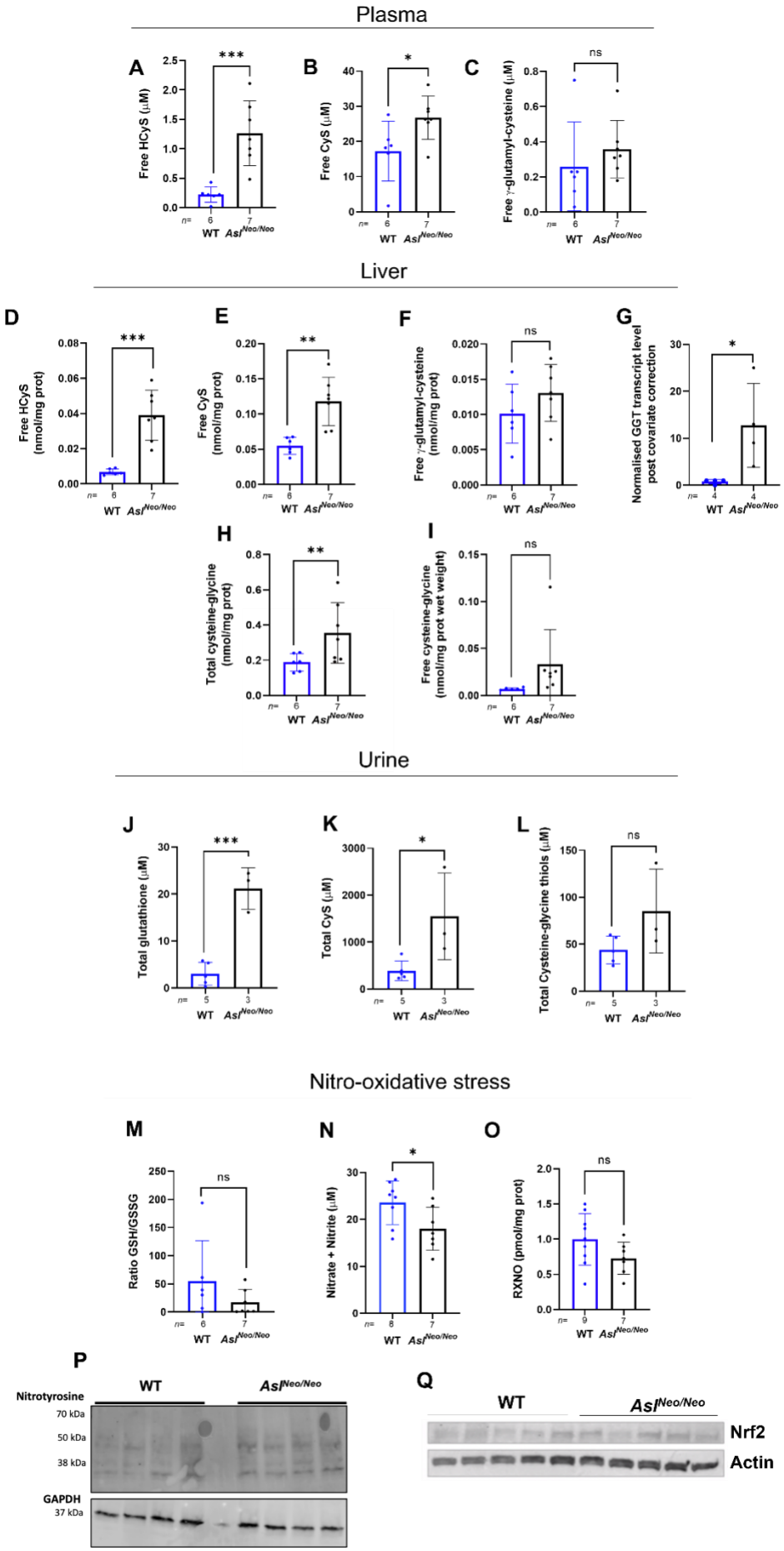
Plasma
A
Free HCyS (μM)
***
B
Free CyS (μM)
*
C
Free γ-glutamyl-cysteine (μM)
ns
Liver
D
Free HCyS (nmol/mg prot)
***
E
Free CyS (nmol/mg prot)
**
F
Free γ-glutamyl-cysteine (nmol/mg prot)
ns
G
Normalised GGT transcript level post covariate correction
*
H
Total cysteine-glycine (nmol/mg prot)
**
I
Free cysteine-glycine (nmol/mg prot wet weight)
ns
Urine
J
Total glutathione (μM)
***
K
Total CyS (μM)
*
L
Total Cysteine-glycine thiols (μM)
ns
Nitro-oxidative stress
M
Ratio GSH/GSSG
ns
N
Nitrate + Nitrite (μM)
*
O
RXNO (pmol/mg prot)
ns
WT
Asl Neo/Neo
P
Nitrotyrosine
70 kDa
50 kDa
38 kDa
GAPDH
37 kDa
Q
Nrf2
Actin

Supplementary Figure 2. Dysfunction of glutathione metabolism in ASL-deficient mouse model *Asl*$^{Neo/Neo}$.

(**A**) Free homocysteine, (**B**) free cysteine and (**C**) free γ-glutamyl-cysteine in plasma of 2-weeks old *Asl*$^{Neo/Neo}$ versus WT littermates. (**D**) Free homocysteine, (**E**) free cysteine and (**F**) liver free γ-glutamyl-cysteine in liver of *Asl*$^{Neo/Neo}$ mice compared to WT littermates. (**G**) Normalised GGT transcript per million post covariate correction level from liver transcriptomics between WT and *Asl*$^{Neo/Neo}$ livers. (**H**) Total cysteine-glycine and (**I**) free cysteine-glycine in livers of 2-weeks old *Asl*$^{Neo/Neo}$ versus WT littermates. (**J**) Total glutathione, (**K**) cysteine and (**L**) cysteine-glycine levels in the urine of *Asl*$^{Neo/Neo}$ mice compared to WT littermates. (**M**) Reduced versus oxidised glutathione ratio in *Asl*$^{Neo/Neo}$ livers versus WT littermates. (**N**) Nitric oxide metabolites (nitrite and nitrate) in plasma samples of *Asl*$^{Neo/Neo}$ mice and WT littermates. (**O**) Decreased trend of nitroso-species (RXNO), including N-nitrosospecies (RNNO) and S-nitrosospecies (RSNO) in *Asl*$^{Neo/Neo}$ livers versus WT littermates. (**P**) Liver nitrotyrosine levels by western blot between *Asl*$^{Neo/Neo}$ mice and WT. (**Q**) Liver Nrf2 levels by western blot between *Asl*$^{Neo/Neo}$ mice and WT. (**A-F, H-O**) Unpaired two-tailed Student's t test; * $p<0.05$, ** $p<0.01$, *** $p<0.001$, ns not significant. (CySS: cystine; GSH: glutathione; HcyS: homocysteine; HcySS: homocystine; Nrf2: nuclear factor erythroid 2-related factor 2. Graphs show means ±SD.

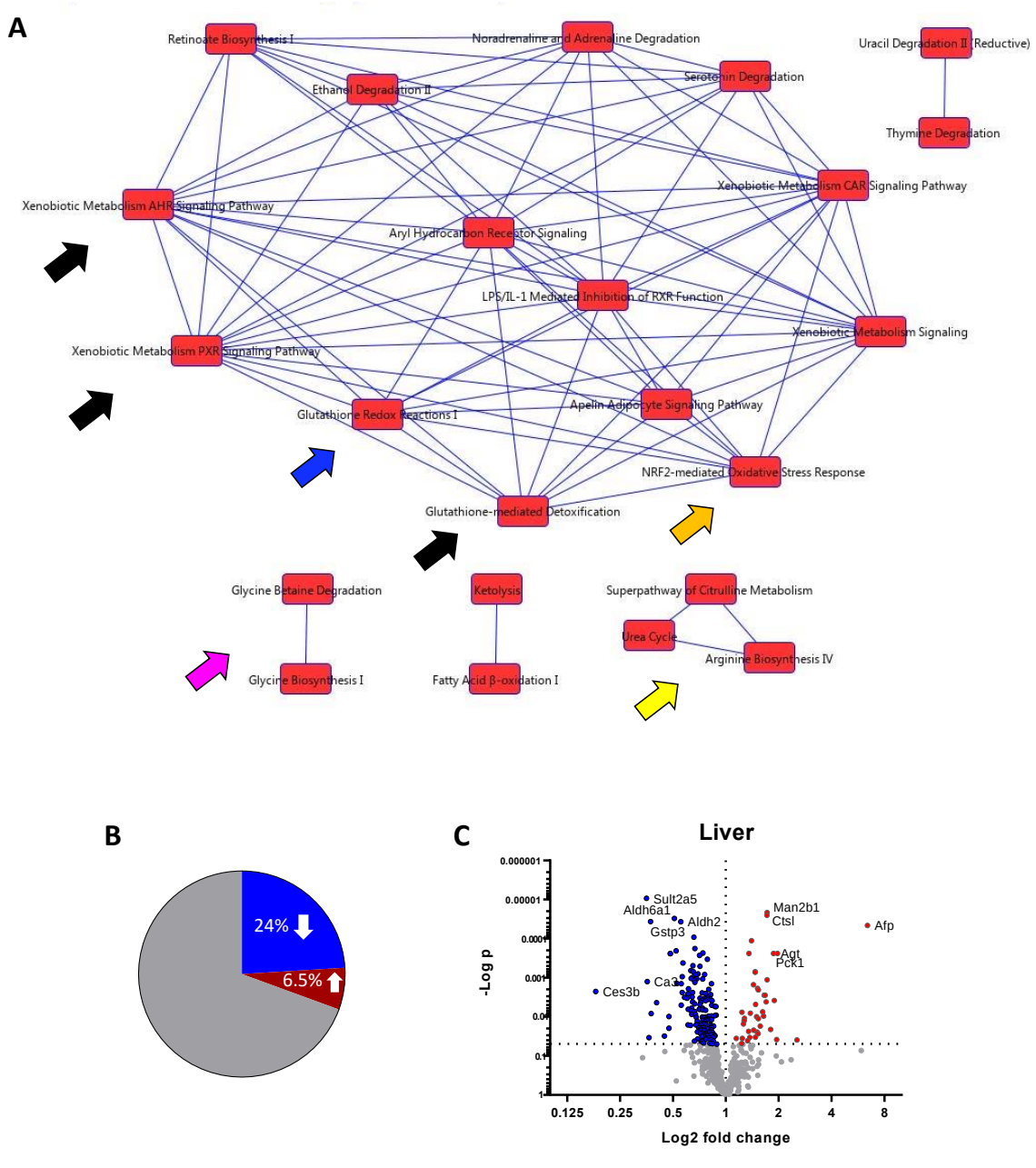

Supplementary Figure 3. Dysregulation of liver metabolism in ASL-deficient mouse model *Asl*$^{Neo/Neo}$.

(**A**) Overlapping canonical pathways showing many major metabolic pathway of the liver are affected: Glutathione antioxidant activity (blue arrow), antioxidant pathways (orange arrow), glutathione-mediated detoxification of endogenous compounds and xenobiotics (black arrows), urea cycle dysregulation (yellow arrow), dysregulation of glycine metabolism (purple arrow). (**B**) Pie chart indicating the percentage effect of the *Asl*^{Neo} allele on the mouse liver tissue proteome with majority of

significant protein downregulated. (**C**) Volcano plot of differentially expressed proteins in the mutant liver proteome. Significance by FDR adjusted *p* value ANOVA WT n=4, *Asl*$^{Neo/Neo}$ n= 5.

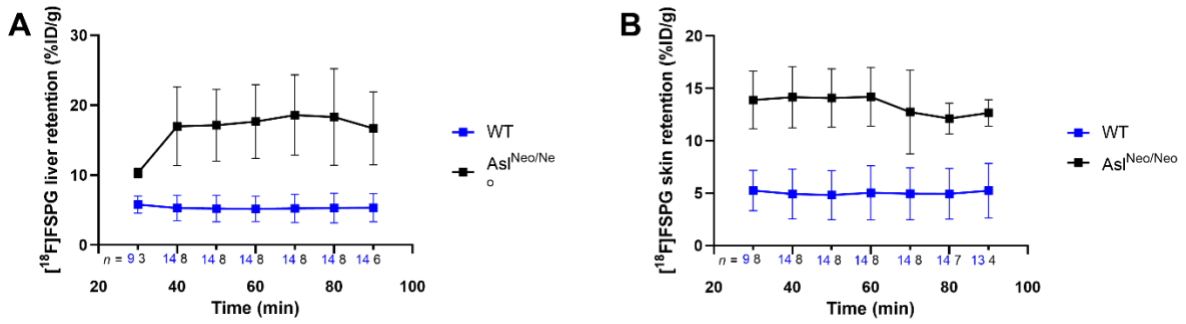

Supplementary Figure 4. [^{18}F] FSPG radiotracer PET scan in *Asl*$^{Neo/Neo}$ mice.

[^{18}F] FSPG PET in Asl$^{Neo/Neo}$ and WT mice showed that **(A)** liver and **(B)** skin [^{18}F] FSPG concentration (%ID/g) was seemingly unchanged between 40 and 90 minutes post injection.

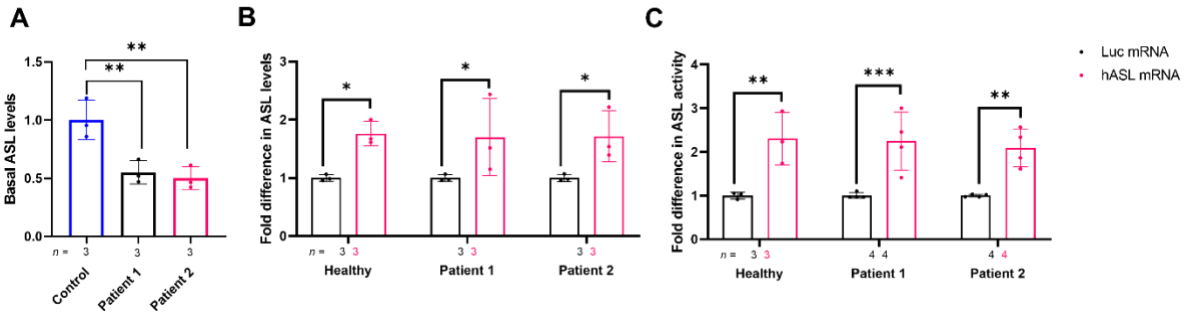

Supplementary Figure 5. *In vitro* efficacy of *hASL* mRNA.

(**A**) Basal expression levels of ASL in fibroblasts from control and two ASA patients. Fold difference in (**B**) ASL levels and (**C**) ASL activity following 24 hours and 48 hours incubation with either *Luc* mRNA or *hASL* mRNA, respectively from 3 independent experiments and normalised to healthy control (**A**) and Luc mRNA treated control (**B, C**). Statistical analysis by One-way ANOVA with Dunnett's multiple comparisons test against healthy control (**A**) and two-way ANOVA with uncorrected Fisher's Least Significant Difference (LSD) (**B, C**), * $p<0.05$, ** $p<0.01$, *** $p<0.001$. Graphs show means ±SD.

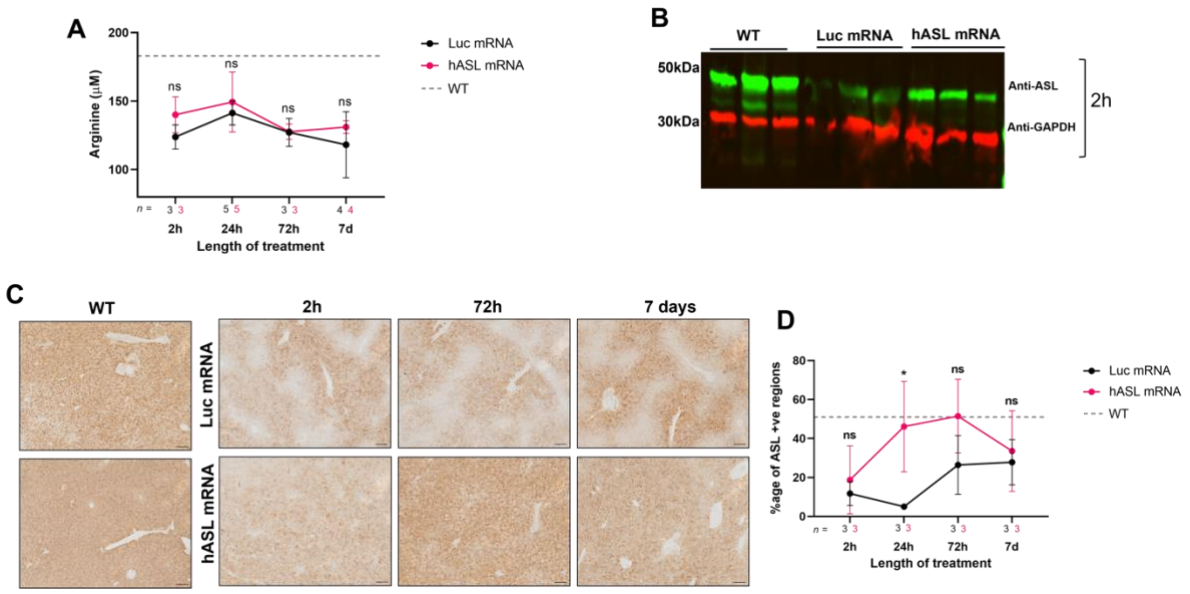

Supplementary Figure 6. Pharmacokinetics of *hASL* mRNA in *Asl*$^{Neo/Neo}$ mice

(**A**) Average arginine levels from plasma from dried blood spots at 2, 24, 72 hours and 7 days. (**B**) ASL western blot at 2 hours post mRNA administration (n=3). (**C**) Representative images of liver ASL immunostaining at 2 hours, 72 hours and 7 days post mRNA administration from WT and *Luc* mRNA or *hASL* mRNA treated *Asl*$^{Neo/Neo}$ mice and (**D**) quantification normalised to WT scaled to 1 (grey dotted line). (**A**) Grey dotted line represents mean WT values (**C**) Scale bar= 100µM. (**A, D**) Two-way ANOVA with Šídák's post-hoc test per group and timepoint, ns=not significant, *p<0.05. Graph show means ±SD.

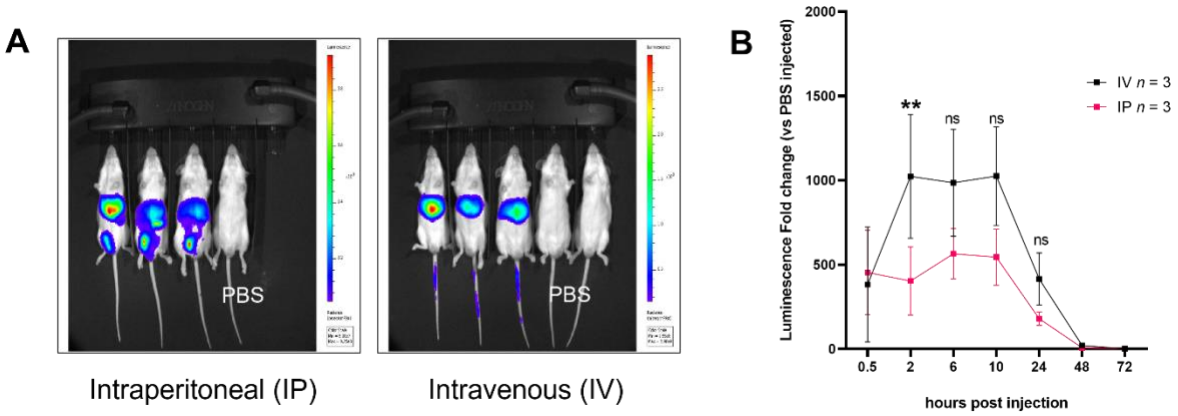

Supplementary Figure 7. Equivalence of liver biodistribution between intravenous and intraperitoneal administration

(A) Representative *in vivo* luminescence image of WT CD1 strain animals injected with either PBS (IP) or *Luc* mRNA either intraperitoneally or intravenously 10 hours post injection. (**B**) Luminescence fold change in liver post 0.5, 2, 6, 10-, 24-, 48- and 72-hours post injection, show two-fold difference in efficacy between IV vs IP. Readings normalised to PBS injected controls. Two-way ANOVA with Šídák's post-hoc test per timepoint, ns= not significant, **p<0.01, IV and IP n=3, PBS n=4. Graph show means ±SD. IV = intravenous, IP= intraperitoneal.

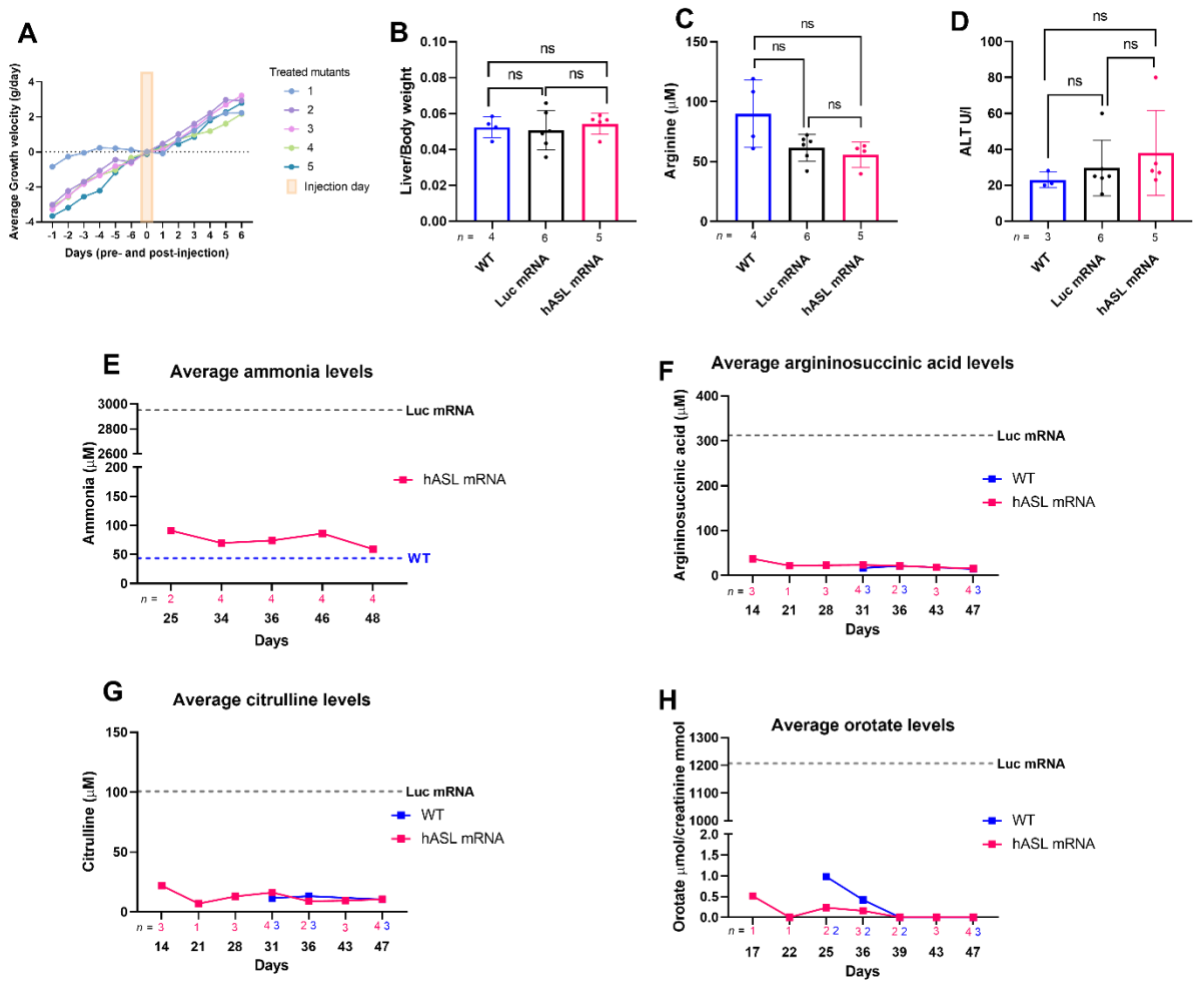

Supplementary Figure 8. *hASL* mRNA therapy from birth corrects the phenotype of *Asl*$^{Neo/Neo}$ mice

(**A**) Average growth velocity per *hASL* treated animals each day pre- and post-injection. (**B**) Liver to body weight ratio at harvest comparing WT against *hASL* mRNA treated *Asl*$^{Neo/Neo}$ mice. (**C**) Plasma arginine levels at harvest from dried blood spots comparing WT against Luc and *hASL* mRNA treated *Asl*$^{Neo/Neo}$ mice. (**D**) Plasma alanine aminotransferase (ALT) levels at harvest comparing WT against *hASL* mRNA treated *Asl*$^{Neo/Neo}$ mice. Longitudinal (**E**) average plasma ammonia concentration, (**F**) argininosuccinic acid (**G**) citrulline from dried blood spots and (H) urine orotate from *hASL* mRNA treated *Asl*$^{Neo/Neo}$ mice. (**B-D**) Unpaired two-tailed t-test per timepoint, ns= not significant. (**E-H**) Grey line indicates average levels from *Luc* mRNA treated *Asl*$^{Neo/Neo}$ mice at harvest (**F**), blue line indicates average WT levels at harvest. (**A**) Graph shows mean per animal. (**B-D**) Graph show means ±SD. (E-H) Graphs show mean per timepoint.

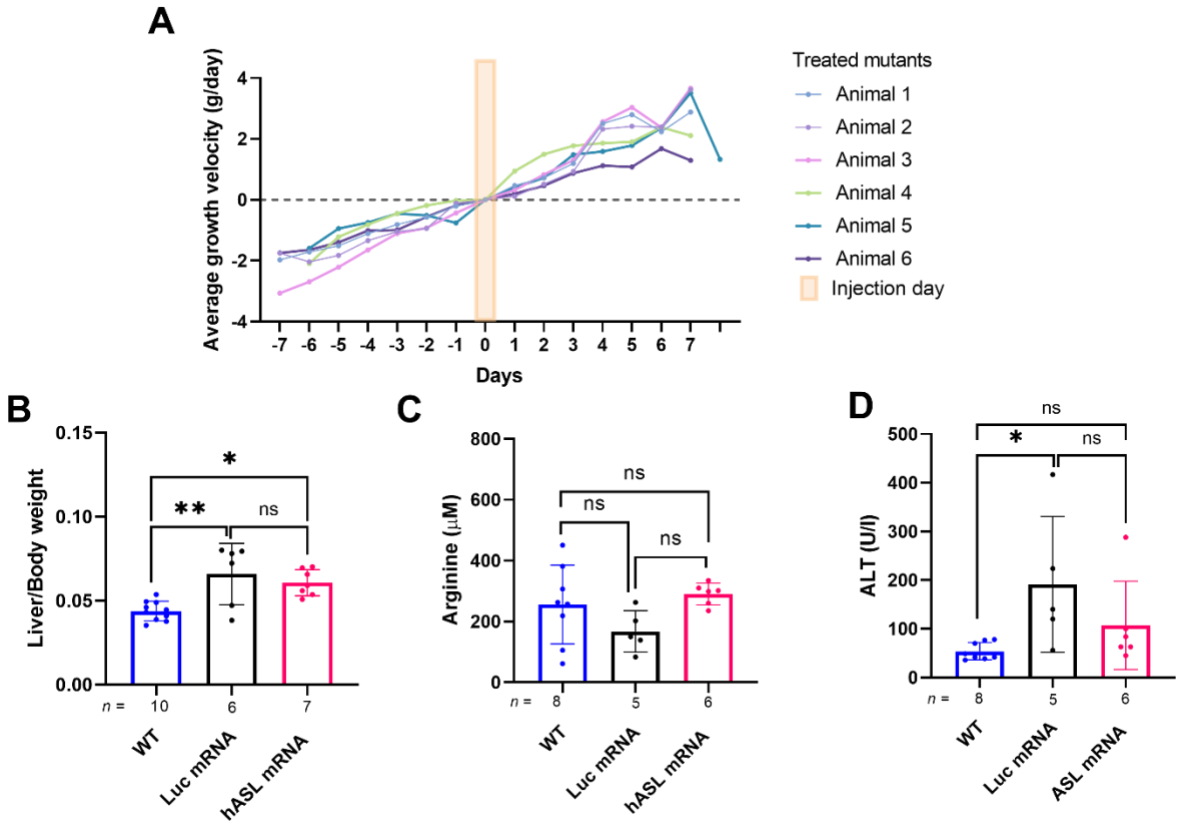

Supplementary Figure 9. *hASL* mRNA therapy partially corrects the adult phenotype in *Asl*$^{Neo/Neo}$ mice

(A) Average mean growth velocity per *hASL* treated animals each week pre- and post-injection. (**B**) Liver to body weight ratio at harvest comparing *Luc* mRNA against *hASL* mRNA treated *Asl*$^{Neo/Neo}$ mice. (**C**) Plasma arginine levels at harvest from dried blood spots comparing WT against *Luc* and *hASL* mRNA treated *Asl*$^{Neo/Neo}$ mice (**D**) Plasma alanine aminotransferase (ALT) levels at harvest comparing WT against *hASL* mRNA treated *Asl*$^{Neo/Neo}$ mice showed no difference. (**A**) Graph shows mean per animal. (**B-D**) One-way ANOVA with Tukey's post-hoc test, ns=not significant, *p<0.05, **p<0.01.

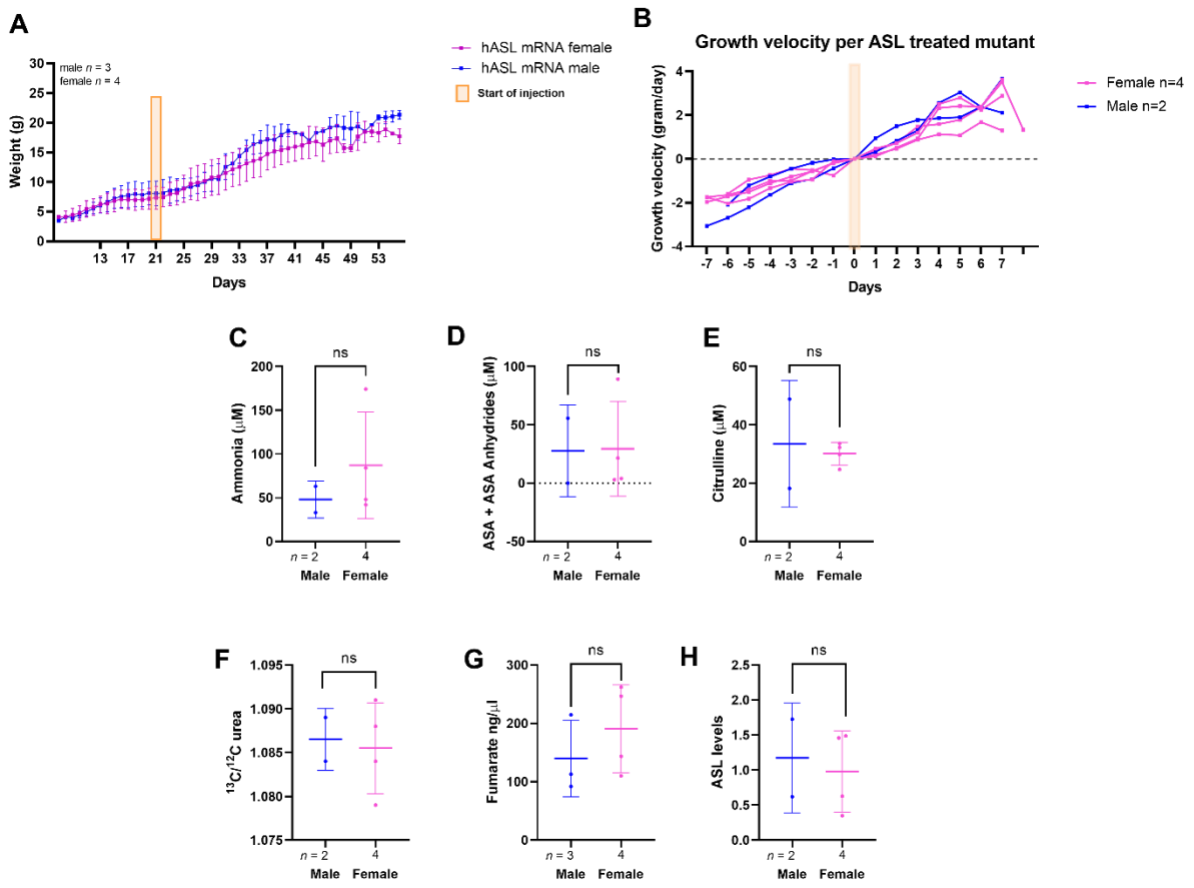

Supplementary Figure 10. Gender effect comparison of *hASL* mRNA treatment in adult treated *Asl*$^{Neo/Neo}$ mice.

(**A**) Average growth curve of adult *hASL*-mRNA treated *Asl*$^{Neo/Neo}$ mice separated by sex. (**B**) Individual growth velocity per *hASL* treated animals each week pre- and post-injection (pink) female, (blue) male. Average (**C**) plasma ammonia levels of *hASL*-mRNA treated *Asl*$^{Neo/Neo}$ mice separated by sex. Average (**D**) ASA (**E**) citrulline levels from dried blood spots (**F**) C13 ureagenesis from adult *hASL*-mRNA treated *Asl*$^{Neo/Neo}$ mice separated by sex. Average liver (**G**) ASL activity indicated by fumarate levels and (**H**) ASL levels from western blot analysis of *hASL*-mRNA treated *Asl*$^{Neo/Neo}$ mice separated by sex. (**B**) Graph shows mean per animal. (**C-H**) Unpaired two-tailed t-test per timepoint, ns= not significant. ASA: argininosuccinic acid. ASL: argininosuccinate lyase. Graph shows mean ±SD.

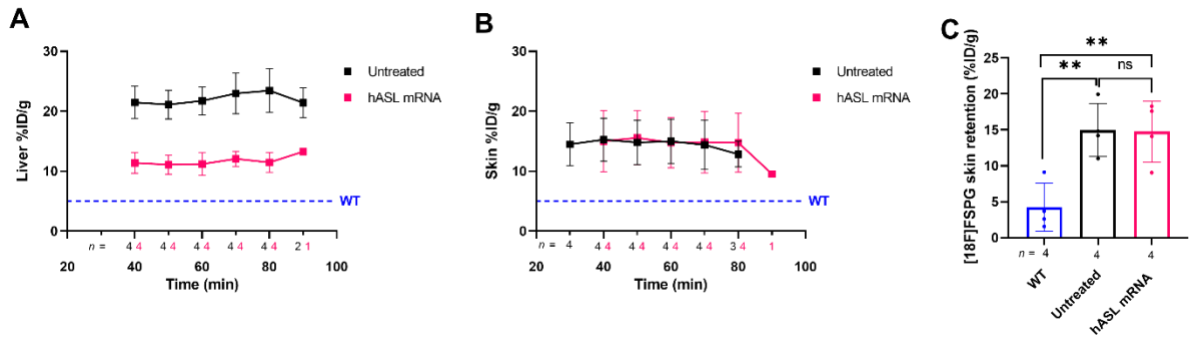

Supplementary Figure 11. *hASL* mRNA therapy corrects the dysfunction of glutathione metabolism in *Asl*$^{Neo/Neo}$ mice

Similarly, to Asl$^{Neo/Neo}$ and WT mice, [^{18}F] FSPG concentration (%ID/g) in mRNA treated *Asl*$^{Neo/Neo}$ [^{18}F] FSPG concentration (%ID/g) was constant between 40-90 minutes post injection in liver (**A**) and skin (**B**). (**C**) [^{18}F] FSPG retention in untreated *Asl*$^{Neo/Neo}$ and *hASL* mRNA treated *Asl*$^{Neo/Neo}$ mice was threefold higher than that of WT mice. One-way ANOVA with Tukey's post-hoc test, ns=not significant, **p<0.01.

Supplementary Tables

Metabolite		**Homocysteine**		**Glutamate**		**Glycine**	
Data analysed		Average	Individual sampling	Average	Individual sampling	Average	Individual sampling
ASLD	Male	14.9 (6.3)	15.6 (11.4)	124 (40)	110 (54)	309 (73)	311 (119)
	Female	14.3 (2.7)	12.6 (3.8)	137 (34)	151 (93)	336 (92)	365 (142)
p value		0.99	0.28	0.89	<0.0001	0.89	<0.0001

Metabolite		**Homocysteine**		**Glutamate**		**Glycine**	
Data analysed		Average	Individual sampling	Average	Individual sampling	Average	Individual sampling
ASSD	Male	9.7 (2.6)	9.9 (4.3)	106 (27)	112 (64)	226 (59)	221 (86)
	Female	7.9 (0)	7.9 (2.5)	159 (0)	159 (63)	221 (0)	221 (66)
p value		0.97	0.89	0.39	0.15	0.99	0.99

Metabolite		**Homocysteine**		**Glutamate**		**Glycine**	
Data analysed		Average	Individual sampling	Average	Individual sampling	Average	Individual sampling
OTCD	Male	13.8 (8.8)	13.5 (8.2)	77 (1.4)	76 (35)	263 (113)	228 (87)
	Female	8.6 (2.7)	9.1 (2.7)	112 (34)	126 (91)	254 (54)	256 (83)
p value		0.38	0.24	0.5	<0.0001	0.99	0.29

Supplementary Table 1: Sex analysis of plasma homocysteine, glutamate and glycine levels in urea cycle deficient patients. ASLD: argininosuccinate lyase deficiency, ASSD: argininosuccinate synthase deficiency, OTCD: ornithine transcarbamylase deficiency. 2 way ANOVA with Šídák's post-hoc test: significance: $p<0.05$.

	ID	Gender	Age-onset	Age at last follow up	Genotyping	Metabolic control	Chronic liver disease (ALT or AST >2N without hyperammonaemia)	Daily protein allowance (g/kg/d)	Number of scavenger drugs	Dosage of scavenger at last follow-up			Dosage of arginine mg/kg/day	Mean plasma homocysteine levels (N 5-15 µmol/L)	Mean plasma glutamate levels (N 25-130 µmol/L)	Mean plasma glycine levels (N 100-330 µmol/L)
						Number of hyperammonaemic decompensations over the last 5 years				Na benzoate (mg/kg/d)	Na phenylbutyrate (mg/kg/d)	Glycerol phenylbutyrate (g/m2/d)				
ASLD	1	F	Early	18y	NA	0	Y	0.85	1	/	250	/	340	14	138	468
	2	M	Late	21y	NA	0	N	0.74	0	/	/	/	180	19.6	66	262
	3	M	Early	12y	c.1045-1057del; c.1045-1057del	0	Y	1.2	1	235	/	/	140	15.3	139	289
	4	F	Late	12y	c.1154G>A; c.1154G>A	2	Y	1.1	1	195	/		100	11.5	170	269
	5	F	Early	11y	c.349-1G>A; 532G>A	0	Y	1.3	1	190	/	/	190	13.7	157	333
	6	M	Early	17y	c.719-2A>G; c.857A>G	0	Y	1.09	1	235	/	/	150	29	96	256
	7	M	Early	18y	NA	0	Y	1.09	1	185	/	/	200	11.4	133	432
	8	M	Early	17y	c.437G>A; c.437G>A	0	Y	1	1	235	/	/	185	13.5	112	404
	9	M	Late	11y	NA	0	N	0.9	0	/	/	/	175	11.2	103	370
	10	M	Early	10y	c.919-2A>G; c.925G>A	1	N	0.9	1	/	/	10	100	15.4	127	273
	11	F	Late	9y	c.1153C>T	0	N	1	1	41	/	/	82	18	84	276
	12	M	Early	2.5y	c.280C>T; c.283C>T	1	Y	1	1	/	/	11.9	205	7.5	212	233
	13	M	Early	8.5y	c.749T>A	4	Y	0.9	1	350	/	/	200	11.3	128	265
ASSD	14	M	Early	7y	c.1168G>A; c.1168G>A	2	N	1	1	/	/	12.2	124	10.1	104	194
	15	M	Early	16y	NA (*)	0	N	vegetarian	2	160	100	/	100	13.8	87	204
	16	M	Early	17y	c.1168G>A; c.1168G>A	2	N	0.8	2	205	/	12.3	100	11.6	137	247
	17	M	Early	5y	c.905T>G; 1030C>T	11	N	1	1	/	/	12.8	263	10.7	119	154
	18	F	Early	2.5y	c.605C>A; deletion of exons 11 and 12	1	N	1.4	1	/	/	8.6	88	7.9	159	221
	19	M	NBS	7y	c.991T>C; c.1173C>A	0	N	no restriction	0	/	/	/	/	8.2	68	234
	20	M	Early	10d	c.1168G>A; c.1168G>A	1	N	1.5	2	500	500	/	400	7	131	280
	21	M	Late	13y	c.773+1G>T; ?	0	N	vegetarian	0	/	/	/	/	11	73	329
	22	M	Late	4y	c.1168G>A; c.1168G>A	5	N	1.2	1	/	/	12.5	96	5.2	100	146
	23	M	Early	3y	c.1168G>A; c.1168G>A	5	N	1.4	1	/	/	12.4	190	9.7	139	243
OTCD	24	M	Late	9.5y	c.367G>A	0	N	0.8	0	/	/	/	153	7.6	78	343
	25	F	FH	17y	c.867G>A	0	N	no restriction	0	/	/	/	/	13.7	71	256
	26	M	Late	17y	c.222G>T	6	N	1	2	232	/	9.5	115.8	20	76	183
	27	F	Late	18y	c.173G>A	0	N	0.7	2	269	266	/	85	9	141	255
	28	F	FH	13y	c.595A>G p.(Asn199Asp)	0	N	0.6	2	57.8		8.2	45	6	156	245
	29	F	Late	3y	c.540+265G>A	0	N	1	2	287	232	/	85	9.1	103	329
	30	F	Late	17y	c.595A>G p.(Asn199Asp)	0	N	0.8	2	148	153	/	50	7	104	241
	31	F	Late	16y	c.170T>A	1	N	0.8	1	/	360	/	80	5	58	291
	32	F	FH	10y	c.170T>A	1	N	1.1	1	/	/	3	67	9	134	141
	33	F	Late	18y	c.44delG	0	N	0.7	1	280	/	/	67	10	128	272

Supplementary Table 2: Information about urea cycle deficient patients regarding genotype, phenotype, therapeutic management and metabolite levels. ASLD n=13, ASSD n=10, OTCD n=10. ASLD: argininosuccinate lyase deficiency, ASSD: argininosuccinate synthase deficiency, OTCD: ornithine transcarbamylase deficiency, RFLP: Restriction fragment length polymorphism. (*) Reduced ASS1 activity in fibroblasts 8.7 patom/6h/mg prot (N: 511-5,632)

Supplementary Table 3: Liver untargeted proteomic dataset from *Asl*$^{Neo/Neo}$ mice and WT littermates

See relevant excel file

Metabolite	**Ammonia**			**ASA**		
Data analysed	Average	STD	n	Average	STD	n
Male	63.5	29.5	4	15.7	1.1	4
Female	41	n/a	1	15.7	n/a	1
Metabolite	**Citrulline**			**C13**		
Data analysed	Average	STD	n	Average	STD	n
Male	9.8	2.2	4	1.07	0.002	3
Female	12.4	n/a	1	1.075	n/a	1
Metabolite	**Orotate**			**ASL levels**		
Data analysed	Average	STD	n	Average	STD	n
Male	0.0006	0.0002	4	91.4	0.9	4
Female	0.0004	n/a	1	89.8	n/a	1
Metabolite	**ASL activity**			**Liver to body weight**		
Data analysed	Average	STD	n	Average	STD	n
Male	310.2	33.8	4	0.05	0.006	4
Female	310.2	n/a	1	0.06	n/a	1
Metabolite	**ALT**			**Arginine**		
Data analysed	Average	STD	n	Average	STD	n
Male	40.7	26.4	4	129	150.7	4
Female	27	n/a	1	60.9	n/a	1

Supplementary Table 4: Gender effect analysis on neonatal *hASL* mRNA treated *Asl*$^{Neo/Neo}$ mice.

Metabolite	**Ammonia**			**ASA**		
Data analysed	Average	STD	n	Average	STD	n
Male	48	21.2	2	27.8	39.4	2
Female	87	60.9	4	29.5	40.78	4
p value	0.31			0.96		
Metabolite	**Citrulline**			**C13**		
Data analysed	Average	STD	n	Average	STD	n
Male	33.5	21.7	2	1.08	0.0035	2
Female	30.1	3.9	4	1.08	0.0052	4
p value	0.86			0.79		
Metabolite	**Orotate**			**ASL levels**		
Data analysed	Average	STD	n	Average	STD	n
Male	8.7	11.5	2	1.17	0.78	2
Female	0.45	0.53	4	0.98	0.580	4
p value	0.49			0.79		
	ASL activity			**Arginine**		
Data analysed	Average	STD	n	Average	STD	n
Male	139.75	65.75	3	268.7	46.8	2
Female	190.67	75.12	4	301.1	30.9	4
p value	0.38			0.47		
	Liver to body weight			**ALT**		
Data analysed	Average	STD	n	Average	STD	n
Male	0.063	0.011	3	45	n/a	1
Female	0.058	0.0052	4	133.75	103.94	4
p value	0.53			n/a		

Supplementary Table 5: Gender effect analysis on adult *hASL* mRNA treated *Asl*$^{Neo/Neo}$ mice.

	Gene		Protein function	TPM		Log2 (fold change)	*p* adjusted value
				Wild-type	hASL mRNA treated Asl Neo/Neo		
Upregulated	*Hist1h1b*	Histone 1.5	Nuclear protein regulating gene transcription through chromatin remodelling, nucleosome spacing and DNA methylation.	1	42	4.9	6.96E-06
Downregulated	*Krt20*	Keratin type I cytoskeletal 20	Intermediate filament protein.	42	0	-21.0	4.88E-08
	Stfa1	Stefin-1	Intracellular thiol proteinase inhibitor involved in protein turnover and antigen processing.	15	0	-19.5	1.05E-08
	Ngp	Neutrophilic granule protein	Inhibitor of cathepsin B activity and negative regulator of tumor vascular development , cell invasion and metastasis.	248	2	-6.7	8.31E-03
	Igf2	Insulin like growth factor II	Member of insulin family of polypeptide growth factors, involved in development and growth.	4004	18	-7.8	2.06E-02
	Asl	Argininosuccinic Lyase	Cytosolic enzyme involved in urea and citrulline-nitric oxide cycles	3006	548	-2.4	7.66E-07
	Ccbl2	Cysteine conjugate beta-lyase 2	Aminotransferase degrading L-kynureinic acid into kynurenic acid, an enzymatic step of tryptophan catabolism.	1552	265	-2.5	4.58E-02

Supplementary Table 6: Significantly differentially expressed genes in WT vs neonatally treated *hASL* mRNA treated $Asl^{Neo/Neo}$ mice liver

TPM: transcripts per million

Supplementary Table 7A: Descriptive summary of statistical results for Figure 1.

Figure 1			
Patient plasma			
	Panel B		
Metabolite	**Total homocysteine**		
Data Analysed	**OTCD**	**ASSD**	**ASLD**
Mean	9.8	9.4	14.9
Median	9	9.7	14.1
SD	3.9	2.6	5.5
SEM	1.2	0.9	1.6
Lower 95% CI	7.2	7.4	11.4
Upper 95% CI	12.5	11.4	18.4
N number	11	9	13
P value			
OTCD vs ASSD	0.9		
OTCD vs ASLD	0.02		
ASSD vs ASLD	0.02		
Plasma (mice)			

	Panel C		**Panel D**		**Panel E**		**Panel F**	
Metabolite	**Total homocysteine (mice) µM**		**Total Cysteine µM**		**Total glutamyl cysteine**		**Total glutathione**	
Data Analysed	**WT**	**Asl$^{Neo/Neo}$**	**WT**	**Asl$^{Neo/Neo}$**	**WT**	**Asl$^{Neo/Neo}$**	**WT**	**Asl$^{Neo/Neo}$**
Mean	0.2	1.2	161.3	224.9	4.4	9.2	106.4	84.5
Median	0.2	1.1	151	231	4.9	8.8	103	85.6
SD	0.1	0.5	24.9	18.3	1.8	4.8	17.7	16.1
SEM	0.05	0.2	10.2	6.9	0.7	1.8	7.2	6.1
Lower 95% CI of mean	0.08	0.7	135.1	208	2.5	4.7	87.8	69.7
Upper 95% CI of mean	0.3	1.7	187.5	241.8	6.3	13.7	125	99.4
N number	6	7	6	7	6	7	6	7
P value	0.0002		0.0003		0.1248		0.0395	
Liver (mice)								
	Panel G		**Panel H**		**Panel I**		**Panel J**	
Metabolite	**Total homocysteine**		**Total cysteine**		**Total glutamyl cysteine**		**Total glutathione**	
Data Analysed	**WT**	**Asl$^{Neo/Neo}$**	**WT**	**Asl$^{Neo/Neo}$**	**WT**	**Asl$^{Neo/Neo}$**	**WT**	**Asl$^{Neo/Neo}$**
Mean	0.05	0.1	0.4	0.7	0.05	0.09	0.2	0.07
Median	0.05	0.1	0.4	0.6	0.04	0.09	0.2	0.06
SD	0.02	0.04	0.07	0.2	0.02	0.03	0.06	0.03

SEM	0.007	0.02	0.03	0.06	0.008	0.01	0.02	0.01
Lower 95% CI of mean	0.03	0.1	0.3	0.5	0.03	0.06	0.1	0.05
Upper 95% CI of mean	0.07	0.2	0.4	0.8	0.07	0.1	0.2	0.1
N number	6	7	6	7	6	7	6	7
P value	0.0004		0.001		0.0213		0.0001	
Liver (mice)								
	Panel K		**Panel L**		**Panel M**		**Panel N**	
Metabolite	**GGT activity**		**MDA**		**Nitrate+Nitrite**		**Nitrotyrosine/GAPDH**	
Data Analysed	**WT**	**Asl$^{Neo/Neo}$**	**WT**	**Asl$^{Neo/Neo}$**	**WT**	**Asl$^{Neo/Neo}$**	**WT**	**Asl$^{Neo/Neo}$**
Mean	3,205	15,851	0.03	0.05	0.2	0.1	0.07	0.09
Median	2,068	14,432	0.03	0.05	0.2	0.1	0.08	0.1
SD	3,158	4,957	0.009	0.02	0.1	0.03	0.03	0.03
SEM	1,579	2,479	0.003	0.009	0.04	0.01	0.01	0.01
Lower 95% CI of mean	-1,820	7,962	0.02	0.03	0.1	0.09	0.02	0.05
Upper 95% CI of mean	8,230	23,739	0.04	0.07	0.3	0.1	0.1	0.1
N number	4	4	6	7	9	7	4	4
P value	0.0051		0.1091		0.0417		0.3811	
Liver (mice)								

	Panel O		**Panel P**		**Panel Q**	
Metabolite	**GCLC**		**GCLM**		**GS**	
Data Analysed	**WT**	**Asl$^{Neo/Neo}$**	**WT**	**Asl$^{Neo/Neo}$**	**WT**	**Asl$^{Neo/Neo}$**
Mean	3.4	1.2	4.5	1.1	1.8	1.0
Median	3.5	1.2	4.6	1.3	1.6	1.0
SD	0.8	0.7	1.9	0.5	0.9	0.2
SEM	0.4	0.3	0.9	0.2	0.4	0.1
Lower 95% CI of mean	2.0	0.1	1.4	0.3	0.3	0.6
Upper 95% CI of mean	4.7	2.2	7.7	1.9	3.3	1.4
N number	4	4	4	4	4	4
P value	0.006		0.01		0.1	

Supplementary Table 7B: Descriptive summary of statistical results for Figure 2.

Figure 2				
	Panel C		**Panel D**	
	FSPG liver retention		**FSPG liver retention**	
Data Analysed	**WT**	**Asl$^{Neo/Neo}$**	**WT**	**Asl$^{Neo/Neo}$**
Mean	5.2	13.6	5.3	13.4
Median	4.9	12.5	5.2	14.1
SD	1.5	3.9	2.3	1.7
SEM	0.5	1.9	0.7	0.9
Lower 95% CI of mean	4.1	7.4	3.7	10.6
Upper 95% CI of mean	6.3	19.7	7.0	16.2
N number	10	4	10	4
P value	<0.0001		<0.0001	

Supplementary Table 7C: Descriptive summary of statistical results for Figure 3.

Figure 3									
	Panel A: Ammonia								
Timepoint	**2h**		**24h**		**72h**		**7 days**		
Treatment	Luc mRNA	hASL mRNA	Luc mRNA	hASL mRNA	Luc mRNA	hASL mRNA	Luc mRNA	hASL mRNA	WT
Mean	224	511	251	106	461	88	497	101	61
Median	198	609	282	81	417	87	475	99	57
SD	175	393	99	76	181	28	192	48	12
SEM	101	227	44	29	104	16	96	28	7
Lower 95% CI of mean	-211	-465	128	36	11	17	192	-18	30
Upper 95% CI of mean	659	1,488	375	177	911	159	803	220	92
N number	3	3	5	7	3	3	4	3	3
P value	0.1		0.5		0.04		0.02		
	Panel B: ASA								
Timepoint	**2h**		**24h**		**72h**		**7 days**		
Treatment	Luc mRNA	hASL mRNA	Luc mRNA	hASL mRNA	Luc mRNA	hASL mRNA	Luc mRNA	hASL mRNA	WT
Mean	118.8	1839	143.6	54.58	172.1	22.66	125.3	49.09	57

Median	109.7	235.5	137.3	41.74	180.8	23.34	113.7	53.25	61
SD	58.8	2824	41.64	24.3	79.35	1.181	26.08	16.22	12.49
SEM	33.95	1631	18.62	10.87	45.81	0.6817	13.04	8.11	7.211
Lower 95% CI of mean	-27.31	-5177	91.93	24.4	-24.99	19.72	83.83	23.28	29.97
Upper 95% CI of mean	264.9	8855	195.3	84.75	369.2	25.59	166.8	74.9	92.03
N number	3	3	5	5	3	3	4	4	3
P value	0.0178		0.0941		0.0063		0.1834		
	Panel C: Citrulline								
Timepoint	**2h**		**24h**		**72h**		**7 days**		
Treatment	Luc mRNA	hASL mRNA	Luc mRNA	hASL mRNA	Luc mRNA	hASL mRNA	Luc mRNA	hASL mRNA	WT
Mean	254.8	407.1	300	198.1	340.6	166.7	336.8	228.1	173.8
Median	239.6	418.7	278	182.8	380.4	164.3	336.3	238.9	170.7
SD	73.68	53.9	63.11	25.15	122.2	5.382	11.71	42.46	6.604
SEM	42.54	31.12	28.22	11.25	70.57	3.107	5.857	21.23	3.813
Lower 95% CI of mean	71.77	273.2	221.7	166.9	36.91	153.3	318.2	160.5	157.4
Upper 95% CI of mean	437.8	541	378.4	229.3	644.2	180	355.5	295.6	190.2
N number	3	3	5	5	3	3	4	4	3
P value	0.0134		0.0377		0.0044		0.0503		

	Panel E			**Panel I**					
Metabolite	**Orotate**			**Histology**					
Treatment	Luc mRNA	hASL mRNA	WT	Luc mRNA	hASL mRNA	WT			
Mean	128.2	0.994	3.433	5.024	46.15	51.11			
Median	95.67	0.7074	2.33	4.719	59.19	51.35			
SD	121.3	0.9655	3.272	1.041	23.23	5.447			
SEM	54.27	0.4318	1.463	0.6008	13.41	3.145			
Lower 95% CI of mean	-22.48	-0.2049	-0.6298	2.439	-11.55	37.58			
Upper 95% CI of mean	278.8	2.193	7.495	7.609	103.9	64.65			
N number	5	5	5	3	3	3			
P value									
WT vs. hASL mRNA	0.3314			0.9002					
WT vs. Luc mRNA	0.0031			0.0151					
hASL mRNA vs. Luc mRNA	0.0003			0.0248					
	Panel G: ASL levels								
Timepoint	**2h**		**24h**		**72h**		**7 days**		
Treatment	Luc mRNA	hASL mRNA	Luc mRNA	hASL mRNA	Luc mRNA	hASL mRNA	Luc mRNA	hASL mRNA	WT

Mean	0.08528	0.1513	0.03525	0.9559	0.1966	0.5688	0.2257	0.5704	1
Median	0.08866	0.1503	0.04496	0.9521	0.1517	0.5777	0.1724	0.4879	0.9836
SD	0.01071	0.09662	0.01865	0.08316	0.1424	0.2259	0.1325	0.2158	0.3977
SEM	0.006185	0.05578	0.01077	0.04801	0.08223	0.1304	0.07647	0.1246	0.2296
Lower 95% CI of mean	0.05867	-0.08871	-0.01107	0.7494	-0.1572	0.007577	-0.1033	0.03422	0.01201
Upper 95% CI of mean	0.1119	0.3913	0.08157	1.163	0.5504	1.13	0.5547	1.107	1.988
N number	3	3	3	3	3	3	3	3	3
p value	0.9861		<0.0001		0.0112		0.0381		
	Panel J: ASL activity								
Timepoint	**2h**		**24h**		**72h**		**7 days**		
Treatment	Luc mRNA	hASL mRNA	Luc mRNA	hASL mRNA	Luc mRNA	hASL mRNA	Luc mRNA	hASL mRNA	WT
Mean	80.69	83.2	69.82	196.6	90.52	179.3	90.17	125.7	199.2
Median	83.59	81.62	69.84	195.5	87.45	203.3	93.49	121.1	198.2
SD	5.816	8.229	5.931	7.489	16.49	48.22	10.92	35.49	9.997
SEM	3.358	4.751	2.652	3.349	9.522	27.84	5.459	17.75	4.471
Lower 95% CI of mean	66.24	62.76	62.46	187.3	49.55	59.5	72.8	69.2	186.8
Upper 95% CI of mean	95.14	103.6	77.18	205.9	131.5	299.1	107.5	182.1	211.6
N number	3	3	5	5	3	3	4	4	5

P value	0.9998	<0.0001	0.0002	0.1043	

Supplementary Table 7D: Descriptive summary of statistical results for Figure 4.

Figure 4									
	Panel B		**Panel C**						
Parameter	**Survival**		**Growth**						
Treatment	Luc mRNA	hASL mRNA	WT	Luc mRNA	hASL mRNA				
N number	6	5	6	5	4				
P value	0.002		Luc-LNPs vs. ASL-LNPs		<0.0001				
			Luc-LNPs vs. WT		<0.0001				
			ASL-LNPs vs. WT		0.1222				
	Panel E			**Panel F**			**Panel G**		
Metabolite	**Ammonia**			**ASA**			**Citrulline**		
Treatment	WT	Luc mRNA	hASL mRNA	WT	Luc mRNA	hASL mRNA	WT	Luc mRNA	hASL mRNA
Mean	28.75	2954	59	17.21	3123	15.73	13	87.91	72.84
Median	28	3125	49	15.27	347.1	15.68	12.1	67.15	11.28
SD	12.15	2149	27.45	4.364	6885	0.9275	2.5	72.84	2.24
SEM	6.074	877.2	12.28	2.182	2811	0.4148	1.117	27.53	1.002

Lower 95% CI of mean	9.419	699.3	24.92	10.27	-4102	14.58	9.9	20.54	7.552
Upper 95% CI of mean	48.08	5209	93.08	24.15	10348	16.88	16.1	155.3	13.09
N number	4	6	5	4	6	5	4	6	5
P value									
WT vs. hASL mRNA	0.9994			>0.9999			0.9956		
WT vs. Luc mRNA	0.0172			0.5421			0.0444		
hASL mRNA vs. Luc mRNA	0.0124			0.5008			0.0371		
	Panel H			**Panel I**			**Panel K**		
Metabolite	**Orotate**			**C13 urea**			**ASL levels**		
Treatment	WT	Luc mRNA	hASL mRNA	WT	Luc mRNA	hASL mRNA	WT	Luc mRNA	hASL mRNA
Mean	0	1207	0	1.074	1.06	1.072	1	0.01717	1.364
Median	0	1108	0	1.074	1.06	1.071	0.7602	0.01413	1.258
SD	0	622.5	0	0.004681	0.000876	0.002905	0.4207	0.005589	0.2646
SEM	0	254.1	0	0.002341	0.000438	0.001452	0.2429	0.003227	0.1528
Lower 95% CI of mean	0	554.1	0	1.066	1.059	1.067	-0.04516	0.003284	0.7071
Upper 95% CI of mean	0	1861	0	1.081	1.076	1.061	2.045	0.03105	2.022
N number	4	6	5	4	4	4	3	3	3

P value						
WT vs. hASL mRNA	>0.9999			0.6289		0.332
WT vs. Luc mRNA	0.0015			0.0005		0.0135
hASL mRNA vs. Luc mRNA	0.0009			0.0015		0.0029
	Panel M			**Panel N**		
Metabolite	**ASL histology**			**ASL activity**		
Treatment	WT	Luc mRNA	hASL mRNA	WT	Luc mRNA	hASL mRNA
Mean	85.35	12.49	91.12	309.7	77.2	310.2
Median	85.24	15.46	91.33	310.6	69.88	328.7
SD	6	11.51	1.096	7	17.91	29.32
SEM	2.821	5.149	0.4902	3.843	7.312	13.11
Lower 95% CI of mean	76.37	-1.803	89.76	293.2	58.41	273.8
Upper 95% CI of mean	94.32	26.79	92.48	326.2	96	346.6
N number	4	5	5	4	6	5
P value						
WT vs. hASL mRNA	0.513			0.513		
WT vs. Luc mRNA	<0.0001			<0.0001		

hASL mRNA vs. Luc mRNA	<0.0001	<0.0001	

Supplementary Table 7E: Descriptive summary of statistical results for Figure 5.

Figure 5									
	Panel B		**Panel C**						
Parameter	**Survival**		**Growth**						
Treatment	Luc mRNA	hASL mRNA	WT	Luc mRNA	hASL mRNA				
N number	6	7	6	7	6				
p value	0.002		Luc-LNPs vs. ASL-LNPs		<0.0001				
			Luc-LNPs vs. WT		<0.0001				
			ASL-LNPs vs. WT		0.00913				
	Panel E			**Panel F**			**Panel G**		
Metabolite	**Ammonia**			**ASA**			**Citrulline**		
Treatment	WT	Luc mRNA	hASL mRNA	WT	Luc mRNA	hASL mRNA	WT	Luc mRNA	hASL mRNA
Mean	71	338	74	0	192.7	28.9	16.6	224	31.3
Median	48	345	55	0	259.7	12.8	16.9	233	21.1
SD	5	205	52	0	192.7	36.2	2.5	44.8	10.3
SEM	19	92	21	0	86.2	14.8	0.9	20.0	4.2

Lower 95% CI of mean	26	82	19	0	86.3	-8.9	14.5	168.4	20.4
Upper 95% CI of mean	116	593	129	0	564.8	66.9	18.8	279.7	42.1
N number	8	5	6	10	5	6	8	6	5
P value									
WT vs. hASL mRNA	01.0			0.8			0.5		
WT vs. Luc mRNA	0.002			<0.0001			<0.0001		
hASL mRNA vs. Luc mRNA	0.004			0.0001			<0.0001		
	Panel H			**Panel I**			**Panel K**		
Metabolite	**Orotate**			**C13 urea**			**ASL levels**		
Treatment	WT	Luc mRNA	hASL mRNA	WT	Luc mRNA	hASL mRNA	WT	Luc mRNA	hASL mRNA
Mean	0.7	18.8	3.2	1.089	1.077	1.086	1	0.1002	1.045
Median	0.07	9.9	0.7	1.089	1.078	1.086	0.9699	0.8773	1.044
SD	1.2	18.1	6.7	0.004218	0.000957	0.004355	0.1765	0.04394	0.5783
SEM	0.4	8.1	2.7	0.001334	0.000479	0.001778	0.1019	0.01794	0.2361
Lower 95% CI of mean	-0.3	-3.6	-3.8	1.086	1.076	1.081	0.5614	0.0541	0.4383
Upper 95% CI of mean	1.7	41.2	10.2	1.092	1.079	1.09	1.439	0.1463	1.652
N number	8	5	6	10	4	6	3	6	6
P value									

WT vs. hASL mRNA	0.9			0.3	0.9
WT vs. Luc mRNA	0.01			0.0003	0.01
hASL mRNA vs. Luc mRNA	0.04			0.009	0.003
	Panel M				
Metabolite	**ASL activity**				
Treatment					
Mean	246.5	89.1	181.7		
Median	247.3	81.9	179.2		
SD	16	15.8	67.9		
SEM	5.229	7.06	27.7		
Lower 95% CI of mean	234.5	69.5	110.4		
Upper 95% CI of mean	258.6	108.8	253		
N number	9	5	6		
P value					
WT vs. hASL mRNA	0.01				
WT vs. Luc mRNA	<0.0001				
hASL mRNA vs. Luc mRNA	0.003				

Supplementary Table 7F: Descriptive summary of statistical results for Figure 6.

Figure 6									
	Panel B			**Panel C**				**Panel D**	
Metabolite	**FSPG liver retention**			**Total glutathione in liver**				**Total Homocysteine in liver**	
Treatment	WT	Untreated	hASL mRNA	WT	Luc mRNA	hASL mRNA neonatal	hASL mRNA adult	Untreated	hASL mRNA
Mean	5.0	21.7	11.2	0.1	0.03	0.08	0.09	2.7	1.2
Median	4.7	22.4	11.0	0.1	0.03	0.08	0.09	2.4	1.2
SD	2.7	2.3	1.9	0.009	0.02	0.02	0.006	0.8	0.2
SEM	1.4	1.1	0.9	0.005	0.009	0.01	0.003	0.3	0.1
Lower 95% CI of mean	0.6	18.0	8.1	0.1	-0.003	0.05	0.08	1.9	0.9
Upper 95% CI of mean	9.4	25.4	14.2	0.1	0.06	0.1	0.1	3.4	1.5
N number	4	4	4	4	4	4	4	7	5
P value									

WT vs. Untreated	<0.0001	WT vs. Luc mRNA	<0.0001	n/a
WT vs. hASL mRNA	0.005	WT vs. hASL mRNA (Neonatal)	0.06	n/a
Untreated vs. hASL mRNA	0.0003	WT vs. hASL mRNA (Adult)	0.2	0.002
		Luc mRNA vs. hASL mRNA (Neonatal)	0.0007	
		Luc mRNA vs. hASL mRNA (Adult)	0.0002	
		hASL mRNA (Neonatal) vs. hASL mRNA (Adult)	0.8	

Supplementary Table 7G: Descriptive summary of statistical results for Figure 7.

Figure 7				
	Panel F		**Panel G**	
	GCLC Fold difference		**GCLM Fold difference**	
Treatment	**DMSO**	**SNAP**	**DMSO**	**SNAP**
Mean	1	1.7	1	1.6
Median	1	1.7	1	1.6
SD	0	0.3	0	0
SEM	0	0.1	0	0.03
Lower 95% CI of mean	1	1.0	1	1.3
Upper 95% CI of mean	1	2.3	1	1.8
N number	3	3	3	3
P value	0.0004		0.01	

Supplementary Table 7: Summarised statistical results for main figures 1-7. Tables include mean, median, SD, SEM, Lower and upper 95% CI, n numbers and *p*-values post statistical test comparison per groups. SD= standard deviation, SEM= standard error of mean, CI= confidence interval.

Data file S1. Raw, individual-level data for experiments for main text figures 1 to 7 and supplementary figures 1 to 11.